

**Tsunami Design Criteria for Coastal Infrastructure: A Case Study for
Spencer Creek Bridge, Oregon**

by

**Seshu B. Nimmala, Graduate Research Assistant
Solomon C. Yim, Professor**

**Dept. of Civil and Construction Engineering
Oregon State University**

and

**Kwok Fai Cheung, Professor
Yong Wei, Post-Doctoral Researcher**

**Department of Ocean and Resources Engineering
University of Hawaii**

for

Oregon Department of Transportation (ODOT)

Date: Nov 20, 2006

Technical Report Documentation Page

1. Report No. OR-RD-07-03		2. Government Accession No.		3. Recipient's Catalog No.	
4. Title and Subtitle Tsunami Design Criteria for Coastal Infrastructure: A Case Study for Spencer Creek Bridge, Oregon				5. Report Date November 2006	
				6. Performing Organization Code	
7. Author(s) Seshu B. Nimmala, Solomon C. Yim, and Kwok F. Cheung				8. Performing Organization Report No.	
9. Performing Organization Name and Address Oregon State University Dept. of Civil, Construction, and Environmental Engineering 220 Owen Hall Corvallis, OR 97331-3212				10. Work Unit No. (TRAIS)	
				11. Contract or Grant No. IN7400	
12. Sponsoring Agency Name and Address Oregon Department of Transportation Bridge Engineering Section 355 Capitol Street NE Salem, Oregon 97301-3871				13. Type of Report and Period Covered Final Report	
				14. Sponsoring Agency Code	
15. Supplementary Notes					
16. Abstract The load effects on a coastal bridge due to the impact of a tsunami wave were developed. Three Cascadia Fault rupture scenarios were considered using the Cornell model and the FVWAVE model to generate the waves for each scenario. The FVWAVE model for the worst case rupture scenario was used to develop the load effects. Fluid-structure interaction analysis was conducted with the computational mechanics software LS-DYNA to create a time-history of the lateral and uplift pressures on the bridge deck. From the pressure data, a time-history of the lateral and vertical reaction forces on the columns was plotted. The computations were conducted in two dimensions, but work will continue for three dimensional modeling that will incorporate the applied pressures on the columns.					
17. Key Words tsunami, bridge, model, force, wave, structure, simulation				18. Distribution Statement Copies available online at http://egov.oregon.gov/ODOT/TD/TP_RES/	
19. Security Classification (of this report) Unclassified		20. Security Classification (of this page) Unclassified		21. No. of Pages 60	22. Price

Table of Contents

Abstract.....	1
1. Introduction.....	5
2. Tsunamigenic Earthquakes.....	5
3. Tsunami Generation, Propagation, and Inundation	5
<i>3.1 Tsunami Generation.....</i>	<i>5</i>
<i>3.2 Propagation and Inundation.....</i>	<i>6</i>
4. Fluid-Structure Interaction.....	8
5. Case Study	9
<i>5.1 Spencer Creek Bridge</i>	<i>9</i>
<i>5.2 Site Description.....</i>	<i>9</i>
<i>5.3 Cascadia Earthquakes</i>	<i>9</i>
6. Model Setup.....	10
<i>6.1 Tsunami Models.....</i>	<i>10</i>
<i>6.2 Tsunamis and Flow Conditions</i>	<i>11</i>
<i>6.3 Bridge Model</i>	<i>12</i>
<i>6.3.1 General notes.....</i>	<i>13</i>
<i>6.3.2 Two-dimensional model.....</i>	<i>13</i>
<i>6.3.3 Three-dimensional model.....</i>	<i>13</i>
<i>6.3.4 Some constraints on analyses</i>	<i>13</i>
7. Results and Discussion.....	14
<i>7.1 Using Cornell model for 2D analyses.....</i>	<i>14</i>
<i>7.2 Using FVWAVE model for 2D analyses</i>	<i>15</i>
<i>7.3 Using FVWAVE model for 3D analyses</i>	<i>15</i>
<i>7.4 Potential extension to other coastal bridges.....</i>	<i>16</i>

8. Concluding remarks	16
Acknowledgements	17
References.....	18
List of Figures.....	20
Appendix A	56

1. Introduction

This report contains the tsunami design criteria for coastal infrastructure using a case study of the proposed Spencer Creek Bridge on the US Highway-101 at Newport, Oregon. The process outlined herein would generally be applicable to any other coastal infrastructure facility as well. Evolving such a process and applying it to a time-critical real-time project is not only challenging, but also considered as an effort trying to bridge the “gap” between theory and practice. At the same time, it required multi-disciplinary expertise in fields such as structural engineering, ocean and coastal engineering, simulations, supercomputing, etc. and thus involved a fruitful collaboration between Oregon State University and University of Hawaii. This study was initiated on behalf of the Oregon Department of Transportation (ODOT).

2. Tsunamigenic Earthquakes

The earth’s crust is undergoing continuous transformation as a result of tectonic plate movements. Subduction zones exist along boundaries where tectonic plates converge and deep trenches develop. Slippage of locked joints releases stress build-up and generates earthquakes. For submarine earthquakes, the seafloor deformation displaces the ocean water and may generate a tsunami.

Figure 1 shows the locations of tsunamigenic earthquakes during 1900-2005 along with the major subduction zones in the Pacific Basin. During the last century, there were several great tsunamis generated at the Japan-Kuril-Kamchatka, Aleutian-Alaska, and South America subduction zones that impacted the entire Pacific Basin. The New Britain Solomon Vanuatu and Toga-Komadec subduction zones were active, but did not generate far-reaching destructive tsunamis because of the relatively shallow waters in the region. The Cascadia subduction zone was relatively inactive during the last three centuries. However, geological and sedimentary evidence has suggested intense, but infrequent paleoseismological activities in the subduction zone.

Long-term records of seismic activities exist at most of the subduction zones and allow evaluation of occurrence probabilities for engineering design and risk assessment. The Cascadia subduction zone, however, lacks long-term seismological data. Previous studies on tsunami hazards in the Pacific Northwest have been mostly based on assumed earthquake scenarios. In particular, the National Tsunami Hazard Mitigation Program recommended the use of a *credible worst-case* scenario in the development of tsunami inundation maps (González et al., 2005).

3. Tsunami Generation, Propagation, and Inundation

3.1 Tsunami Generation

Earth surface deformation due to internal faulting is generally modeled using elastic theory of dislocation in which the earth is treated as a homogeneous, isotropic, and elastic material (Steketee, 1958). Figure 2 provides a schematic of an idealized faulting mechanism. The

rectangular fault plane is located at the focal depth below the seafloor and its orientation is defined by the strike and dip angles. The rake angle indicates the direction of fault movement and the slip is the amount of that movement. With L and W denoting the length and width of the fault and Δu_j the fault displacement, the deformation can be described by an integral over the fault plane as

$$u_i = \int_{x_1}^{x_1-L} \int_p^{p-W} \Delta u_j \left[\lambda \delta_{jk} \frac{\partial u_i^n}{\partial \xi_n} + \mu \left(\frac{\partial u_i^j}{\partial \xi_k} + \frac{\partial u_i^k}{\partial \xi_j} \right) \right] v_k d\xi_1 d\xi_2, \quad (1)$$

in which λ and μ are Lamé's constants, δ_{jk} is the Kronecker delta, v_k is the direction cosine of the normal, the superscripts indicate the deformation due to the respective components of a unit point force at the fault plane, and

$$p = x_2 \cos \delta + d \sin \delta \quad (2)$$

where δ is the dip angle, d is the focal depth, and (ξ_1, ξ_2, ξ_3) and (x_1, x_2, x_3) are coordinate systems on the fault plane and seafloor respectively.

Researchers have developed various analytical and numerical solutions to (1). The algorithm of Okada (1985) is commonly used to describe the earth surface deformation in tsunami modeling. The displacement of the seafloor is simplified into the strike-slip and dip-slip components in terms of the input seismic source parameters in Figure 1. Equation (1) is rewritten into

$$u_i = u_i(x_1, p) - u_i(x_1, p - W) - u_i(x_1 - L, p) + u_i(x_1 - L, p - W) \quad (3)$$

The analytical expressions derived from the integrals define the surface deformation due to shear and tensile failure of a fault. The resulting surface deformation includes uplift, subsidence, and offset. The surface deformation is a linear function of the slip and its horizontal dimensions are linearly proportional to those of the fault.

The uplift and subsidence of the seafloor displace the ocean water and generate a tsunami. The determination of the initial tsunami waveform is not trivial and depends on a number of factors. The most important is the rupture time, which affects the transfer of energy from the seafloor deformation to the water. Earthquakes typically have rupture durations of minutes, which can be considered as instantaneous when compared to the time scale of the subsequent tsunamis. Kajiura (1970) suggested for tsunami modeling the initial surface wave be treated as identical to the vertical component of the seafloor deformation due to faulting. Abe (1973) showed the general resemblance and direct correlation between the seafloor deformation due to faulting and the initial tsunami wave. Due the lack of more detailed information, the initial tsunami waveform is typically assumed to be exactly the same as the vertical component of the seafloor deformation due to faulting.

3.2 Propagation and Inundation

Modeling of tsunami propagation across the ocean and inundation at coastlines requires a suite of numerical models to account for the pertinent characteristics of different time and length scales. Based on the long-wave assumptions, these processes can be described by various forms of the depth-integrated shallow-water equations, which include a continuity equation and two momentum equations in two orthogonal directions defined on the ocean surface.

Let t denotes time and g the gravitational acceleration. The linear Boussinesq equations in the spherical longitude and latitude (ψ , φ) coordinates describe the variation of the water surface elevation ζ and the flow velocity (u , v) in the open ocean as

$$\frac{\partial \zeta}{\partial t} + \frac{h}{R \cos \varphi} \left[\frac{\partial u}{\partial \psi} + \frac{\partial}{\partial \varphi} (v \cos \varphi) \right] = 0 \quad (4)$$

$$h \frac{\partial u}{\partial t} + \frac{gh}{R \cos \varphi} \frac{\partial \zeta}{\partial \psi} - fhv = \frac{h^3}{3R^2 \cos \varphi} \frac{\partial}{\partial \psi} \left[\frac{1}{\cos \varphi} \frac{\partial}{\partial t} \left\{ \frac{\partial u}{\partial \psi} + \frac{\partial (v \cos \varphi)}{\partial \varphi} \right\} \right] \quad (5)$$

$$h \frac{\partial v}{\partial t} + \frac{gh}{R} \frac{\partial \zeta}{\partial \varphi} - fhu = \frac{h^3}{3R^2} \frac{\partial}{\partial \varphi} \left[\frac{1}{\cos \varphi} \frac{\partial}{\partial t} \left\{ \frac{\partial u}{\partial \psi} + \frac{\partial (v \cos \varphi)}{\partial \varphi} \right\} \right] \quad (6)$$

where h is the water depth, R the earth radius, and f the Coriolis force. The linear Boussinesq model is coupled with a nonlinear shallow-water model, which describes nearshore transformation of the tsunami. The governing equations in the Cartesian coordinates (x , y) are

$$\frac{\partial \zeta}{\partial t} + \frac{\partial}{\partial x} (Hu) + \frac{\partial}{\partial y} (Hv) = 0 \quad (7)$$

$$\frac{\partial}{\partial t} (Hu) + \frac{\partial}{\partial x} (Hu^2) + \frac{\partial}{\partial y} (Huv) + gH \frac{\partial \zeta}{\partial x} + \frac{\tau_x}{\rho} = 0 \quad (8)$$

$$\frac{\partial}{\partial t} (Hv) + \frac{\partial}{\partial x} (Huv) + \frac{\partial}{\partial y} (Hv^2) + gH \frac{\partial \zeta}{\partial y} + \frac{\tau_y}{\rho} = 0 \quad (9)$$

in which $H = h + \zeta$ is the flow depth, ρ is water density, and

$$\tau_x = \frac{gn^2}{H^{1/3}} u(u^2 + v^2) \quad (10a)$$

$$\tau_y = \frac{gn^2}{H^{1/3}} v(u^2 + v^2) \quad (10b)$$

are bottom shear stress components with n denoting the Manning number (e.g., Kowalik and Murty, 1993; Liu et al., 1995; and Titov and Synolakis, 1998). The solutions to (4) to (9) can be obtained simultaneously through an explicit finite-difference scheme with up to four levels of nested grids. Wei et al. (2003) and Yamazaki et al. (2006) used this coupled model to pre-compute mareograms for real-time tsunami forecasting and obtained very favorable predictions of coastal tsunami heights.

When dealing with discontinuities, volume conservation becomes an issue for the two sets of governing equations (4) to (9). The finite-difference solution is not intended for situations, when the seabed slope is steep or discontinuous or when a bore develops. An alternative approach is to describe the flow using the conservative form of the nonlinear shallow water equations, which expresses the two momentum equations as

$$\frac{\partial}{\partial t}(Hu) + \frac{\partial}{\partial x}\left(Hu^2 + \frac{gH^2}{2}\right) + \frac{\partial}{\partial y}(Huv) = gH \frac{\partial h}{\partial x} - \frac{\tau_x}{\rho} \quad (11)$$

$$\frac{\partial}{\partial t}(Hv) + \frac{\partial}{\partial x}(Huv) + \frac{\partial}{\partial y}\left(Hv^2 + \frac{gH^2}{2}\right) = gH \frac{\partial h}{\partial y} - \frac{\tau_y}{\rho} \quad (12)$$

The right-hand sides of the equations are known as the source terms in the finite-volume method, which solves the governing equations in integral form to provide a fully conservative scheme. Wei et al. (2006) makes use of the surface-gradient method of Zhou et al. (2001) and a Godunov-type scheme with an exact Riemann solver to track the moving waterline and to capture flow discontinuities associated with breaking waves, which are essential for runup calculations. The scheme is second order in space and time and provides an accurate description of small flow-depth perturbations near the moving waterline. The computed surface elevation, flow velocity, and runup show very good agreement with previous asymptotic and analytical solutions as well as laboratory data.

The coupled finite difference model efficiently provides the boundary conditions for the computationally more intensive finite volume model of Wei et al. (2006) to determine runup of nonbreaking and breaking tsunami waves. Finite difference solutions of the nonlinear shallow water equations generally provide accurate descriptions of tsunami propagation across the ocean and transformation around land masses. The finite-volume runup model, which mimics breaking waves as bores and conserves volume across flow and bathymetry discontinuities in the nearshore region, complements the finite-difference propagation model in providing a complete description of a tsunami event.

4. Fluid-Structure Interaction

This has been an area under intense research. Traditionally, fluids are modeled using Eulerian formulation (wherein the material flows in a fixed/undeformed mesh), whereas solids/structures are modeled using Lagrangian formulation (wherein the mesh deforms and moves along with the material). Recent developments include Arbitrary Lagrangian Eulerian (ALE) formulation that permits arbitrary (or user-defined) motion of the mesh that has both Eulerian as well as Lagrangian formulations as its special cases. Also, fluids are generally simulated using finite difference (FD) or finite volume (FV) techniques. Most commercial computational fluid dynamics (CFD) codes are based on either of these two techniques. This is in contrast to the structural analysis codes which are almost always based on the finite element method (FEM). On the other hand, FV is not used much beyond the fluid domain. The relative merits of FEM when compared to the FD or FV are discussed in Gresho and Sani (1998). GFEM (Galerkin finite element method) is a generalized finite volume method with rigorous mathematical analysis and forms the ideal framework for performing the fully-coupled fluid-structure interaction.

LS-DYNA, a state-of-the-art computational mechanics software, uses FEM and has several capabilities to do the fluid-structure interaction. This software has several hundreds of constitutive models. It has both explicit and implicit integration schemes and is used in high-

speed impact situations. So the software lends itself naturally to the analysis of the tsunami impact on the structure (a bridge in this case).

5. Case Study

5.1 Spencer Creek Bridge

This bridge was proposed as a replacement of the temporary bridge across the Spencer Creek on the Highway-101, 10 miles south of Depoe Bay and six miles north of Newport, Oregon. The original Spencer Creek Bridge, built in 1947, has deteriorated to the point that it has been determined unsafe and closed to traffic. A temporary bridge was constructed in 1999 adjacent to the old bridge and has a design service life of five to eight years. Thus, the proposed bridge is of extreme importance to the public in order to continue to have US-101 as the lifeline highway on the Oregon Coast. The plans and elevations of the new bridge are enclosed in Appendix A.

5.2 Site Description

The OSU research group has visited the site of the proposed bridge to understand the topographical features and took several digital pictures of the original bridge and the temporary bridge along with the surrounding areas. The location is in close proximity to the Pacific Ocean. There is a creek underneath the bridges that is quite shallow. The bridge site has a wide area of a recreation park on the side away from the Ocean that is full of trees. More importantly, the bridge is very close to the Cascadia subduction zone. Newport city has several warning signs indicating the possible hazard of tsunamis for the safety of general public.

5.3 Cascadia Earthquakes

The Cascadia subduction zone, which extends 1,100 km along the Pacific coast from Northern California to British Columbia, is only 80 km from the bridge site. Great Cascadia earthquakes have an average recurrence interval of 500 to 600 years (Clague, 1997; and Goldfinger et al., 2003). Evidences from North America and Japan show that the most recent Cascadia event occurred in 1700 (e.g., Satake et al., 1996; and Jacoby et al., 1997).

Satake et al. (2003) examined the magnitude and rupture zone of the 1700 Cascadia earthquake through tsunami records in Japan and paleoseismological evidence along the Cascadia coast. A linear shallow-water model reproduced 18 possible tsunami events based on six rupture configurations with different lengths, widths, and down-dip slip distributions. Comparison of the computed coastal wave heights with records of flooding and damage at three locations in Japan yields a rupture 1,100 km long with moment magnitude M_w 9.0 as the most likely 1700 Cascadia earthquake scenario.

The lack of historical records negates a rigorous statistical analysis to determine a design tsunami event for the Spencer Creek Bridge. A rational approach is to establish the tsunami design criteria based on the 1700 earthquake with M_w 9.0. Geist (2005) concluded the most likely rupture will occur along the entire 1,100 km of the subduction zone. However, this long rupture covers a large area and is less critical to the project site as compared to the short-north and short

central ruptures considered by Satake et al. (2003). This study considers all three ruptures as possible design events for the bridge. While Satake et al. (2003) did not provide details of the 1700 Cascadia events, the fault geometry and seismic source parameters along the Cascadia subduction zone are obtained from Kirby et al. (2006).

Figure 3 shows the three rupture configurations and the initial tsunami waveforms. The long, short-north, and short-central ruptures are respectively divided into 4, 3, and 2 rectangular faults for the implementation of the Okada (1985) formula. The specific dip angle of the subduction zone gives rise to a skewed surface deformation that is significantly higher on the ocean side. The maximum amplitudes of the initial waveforms are 4.7, 6.7, and 12.2 m for the long, short-north, and short-central ruptures respectively. A large area of subsidence extends all the way to the coastlines. The predicted subsidence values for the long, short-north, and short-central rupture scenarios at the bridge site are 2.76m, 3.41m, and 6.73m, respectively. These values are taken into account in the calculations for tsunami runup, inundation and wave loads on the bridge.

The present deterministic approach uses three specific events to determine the tsunami loading on the structure. It can be replaced by the probabilistic approach proposed by Geist and Parsons (2006) with a greater level of effort.

6. Model Setup

6.1 Tsunami Models

The computation involves three levels of nested grids with increasing resolution of 0.5' (~1,000 m), 3'' (~100 m), and 0.3'' (~10 m). Fig. 4a shows the level-1 grid over the eastern Pacific Ocean around the Cascadia subduction zone. The bathymetry is obtained from Marks and Smith (2006), who blended the original data of Smith and Sandwell (1997) with the General Bathymetric Chart of the Oceans from the British Oceanographic Data Center to produce a 1' (~2,000 m) bathymetry dataset. The water is deep and the bathymetry varies gradually over most of the region. A linear solution to the Boussinesq equations with a grid size of 0.5' is sufficient to model tsunami propagation in this region.

Nonlinear effects become important and finer computational grids are necessary as tsunamis approach land masses. Figure 4b shows the level-2 grid that provides more a detailed description of tsunami transformation over the continental shelf around the site. The grid resolution of 3'' (~100 m) is sufficient to resolve large-scale bathymetric features and provides the boundary conditions for the nearshore runup calculation. The bathymetry is based on the 3'' US Coastal Relief Model from the National Geophysical Data Center (NGDC). The moving waterline is computed at this level to avoid the need to impose a minimum water depth and a vertical wall along the coastline.

The finite volume model of Wei et al. (2006) provides the runup in the level-3 grid at the site. Fig. 4c shows the bathymetry and topography in the computational grid. The 0.6'' (~10 m) grid resolution is needed to resolve the topographic features and to describe the inflow and outflow through Spencer Creek at the site. The bathymetry and topography is blended from a mix of

datasets. The 3" NGDC US Coastal Relief data provides the bathymetry in the grid. The NOAA LiDAR data with resolution of approximately 2 m defines the topography over a 300 m by 150 m area, which provides reasonable coverage of the site. The remaining areas are covered by the USGS Digital Elevation Model data at 10-m resolution.

The time steps of the computation are determined by the CFL criterion to be 0.4, 0.2, and 0.05 sec for the three levels of grids. The level-1 and level-2 grids are dynamically coupled in the finite difference model. The computed surface elevation and flow velocity are interpolated in time and space to define the boundary conditions of the level-3 grid used in the finite volume model. Despite the use of a second-order scheme, the finite-volume runup model generates stable results over the rugged bathymetry and topography without artificial damping mechanisms or smoothing.

6.2 Tsunamis and Flow Conditions

The finite difference and finite volume models provide a complete description of the tsunamis generated by the three possible rupture configurations of the 500-year Cascadia earthquake. The rupture is assumed to occur simultaneously over the entire fault. This is not necessarily the case for ruptures over long and narrow faults. In the absence of more detailed information, the assumption leads to more conservative tsunami events for the bridge design.

Figure 5 shows the wave amplitude distributions generated by the long rupture over the 1,100-km fault. This is the most likely scenario to occur and is also the least severe of the three. Tsunami energy is known to propagate perpendicularly to the fault. As shown in Figure 5a, the concave shape of the northern part of the fault focuses the energy toward the open ocean. Figure 5b shows that the tsunami propagating toward the coast is focused over a number of shoals before reaching the continental shelf. The tsunami approaches the coastline from the northwest due to refraction and the wave height reaches catastrophic levels at several locations.

The short-north rupture covers 670 km of the fault. The resulting wave fields as shown in Figure 6 are very similar to those of the long rupture, but with higher amplitudes. Both tsunamis primarily affect the shoreline adjacent to the fault and have only minor impacts to the rest of the coast. The short-central rupture covers 360 km of the fault and produces the most severe tsunami as shown in Figure 7. Even though the rupture is significantly shorter, the wave field on either side of the fault is very similar to those of the other two events. The inundation of all three scenarios is general small because of the steep mountain slopes along the coastline, but may extend deep into valleys and basins between mountain ridges. In particular, the floodwater of the short-central tsunami extends more than 1.4 km from the coastline into the Spencer Creek basin.

Modeling of the three tsunami scenarios provides the flow conditions at the site for structural and scour designs of the bridge. Figure 8 shows the flow depth and velocity at the centerline of Spencer Creek Bridge. The flow depth is measured from the bottom of the creek including effects of subsidence, the velocity is depth-averaged, and time zero is when the earthquake occurs. The initial wave energy distribution has a significant effect on the arrival time. The short-central tsunami arrives at 900 sec after the earthquake as compared to 1900 sec for the long event. The arrival of the peak wave varies slightly between the events due to nonlinear effects associated with the wave height and land subsidence over the shallow part of the continental

shelf. The floodwater of the short-central event rises to 17-m above the creek bottom and overtops the bridge embankment. The peak elevation of the long event is substantially lower at 3.6 m.

The u and v components of the flow velocity in Figure 8 are positive in the east and north direction, respectively. The alignment of the bridge is north-south. The u component, which is perpendicular to the bridge, is critical to the bridge design and scour evaluation. The flow speed increases with the arrival of the floodwater and continues to increase until the peak arrives. The tsunami generated by the long rupture only floods the low-lying part of the creek basin and the floodwater cannot immediately return to the ocean. For the short-north and short-central events, the flooding in the creek basin is extensive and flow reverses after the peak flow as the floodwater recedes and drains back to the ocean. The flow in the north-south direction corresponds to the refracted and reflected waves along the coast and has minor roles in the design of the bridge.

Plots of the time-history of three scenarios using Cornell and FVWAVE models are in Figures 9 and 10 respectively. Time-history of Short-central fault configuration using both FVWAVE and Cornell models is shown in Figure 11 for comparison. While flow depths are comparable in either model, velocity u is higher in case of FVWAVE model. Also, the peaks of flow depth and u occur at different points of time. Hence results from both models are considered as input to the bridge models. Out of the three scenarios, Short-Central fault configuration is the most critical (using both Cornell and FVWAVE models) in terms of both the peak flow depth and velocity u in exerting the maximum impact on the bridge. Hence this configuration is considered for performing the analysis.

6.3 Bridge Model

A schematic showing the orientation of the bridge model and the direction of tsunami is provided in Figure 12.

Two finite element models are prepared for performing the fluid-structure (i.e., tsunami and bridge) interaction, one for two-dimensional analysis, and another for three-dimensional analysis. The 2D model has just the deck (a thin slice of it perpendicular to span) modeled at the center of the bridge. The cross-section is based on the section of bent-4 (at the center of the span) in drawing 13-20198BT4_sc.pdf (also enclosed in the Appendix-A). The tsunami acts in the plane of the model, i.e., perpendicular to the span of the bridge. This model, while being simpler, is expected to provide quick results of the pressure on the bridge deck besides giving an idea of the computational efforts required for the more complicated 3D analysis. While the 2D model may satisfy the general requirements of the scope of the work specified in the contract, a later discussion of Dr. Yim with the ODOT engineers indicated that the column/pier design is also of interest to them. So it was decided to add the more involved and complicated 3D analysis task to the extent allowed in the time scope of the work.

The analysis is conducted using LS-DYNA, a state-of-the-art computational mechanics software for analyzing complex fluid-structure interaction problems. Also a Supercomputing facility with over 1,000 nodes is used for performing the simulations.

6.3.1 General notes

The units used in the generation of the Tsunami wave have been in metric system. However, the ODOT drawings are in English system. As such, the FE models along with the input parameters, velocities, etc. are prepared in English system so as to make the results readily accessible and easier to interpret for design engineers.

6.3.2 Two-dimensional model

The model has about 74,000 nodes and 36,000 elements. The 2D bridge deck models are shown in Figures 13-15. The deck is provided with three intermediate supports corresponding to the arches running along the span. Boundary conditions at the supports are specified such that the translations are restrained in all three directions. The primary model extends in X & Y directions, while thickness in Z direction is 3 inches (i.e., the model is a thin slice of 3 inches thickness). The six node numbers corresponding to the support reactions (three each on faces $Z = 0, 3$ in) are shown in Figures 16-17. Thus the nodes 70297, 71086 and 71884 are at $Z = 0$ in whereas nodes 72185, 72973 and 73770 are at $Z = 3$ in. It may be noted that the plots of support reactions show three curves on account of symmetry of the arrangement of three nodes on either face. That is, nodes 70297 and 72185 have the same reaction as an example. Location of the elements on the front and bottom faces (as referred in the pressure plots) of the bridge deck is shown in Figure 18.

6.3.3 Three-dimensional model

Symmetry of the bridge about the line through the middle of the span is exploited in creating the 3D model to reduce the computation time. Thus the model contains the three arches, columns and the deck (without all the internal details) over half the span. The base of the columns is fixed at the bottom of the arch backstop. This model has about 754,000 nodes and 707,000 solid elements. Some of the views of the 3D –model are provided in Figures 19-23.

6.3.4 Some constraints on analyses

As is evident from the tsunami hydrograph, the total duration of action-time is well over 2,500 sec. However, it is decided to be practical by picking only the “area of interest” from the graph and conduct the analyses (more justification for this choice follows later).

The “preliminary” analyses that were taken assumed that the bridge is linearly elastic. More elaborate analyses would require considerably larger magnitude of efforts and time from both modeling and computational points of view. Analysis of 5 sec tsunami run (using 3D model) consumed 36 hours on 60 CPUs, resulting in 2,160 CPU-hours. An obvious suggestion would be that more CPUs could make it run faster. However, as our previous investigations have shown, inter-processor communication overhead as well as the availability of the licenses would be the limiting factors. As the bridge material is deformed under the impact of tsunami, the time-step for performing the integration is found to be coming down as it is based on the smallest element size at the point of time. Since the idea is to obtain the pressures acting on the column, use of a stiffer (close to “rigid”) material is expected to yield the desired results for the purposes of the design office. The area of the hydrograph is selected to contain the peak velocity and the peak height for 2D analyses, whereas the peak velocity is considered to occur simultaneously with the

peak height for 3D analyses (this is found to lead to conservative results and more feasible computational times).

7. Results and Discussion

7.1 Using Cornell model for 2D analyses

The simulation is performed for 60 sec duration (the part of the hydrograph corresponding to the level that reached the bridge deck). It took 29 hours on 36 CPUs. Gravity is applied quasi-statically during the first 5 sec. The actual hydrograph starts from $t = 10$ sec. A screenshot of the applied velocity 'u' (units: in/sec) in the input file is in Figure 24. It can be seen that the peak velocity exists within the first 60 sec duration.

Confirmation of the velocity from the post-processing of results (appears to be the same as the above except that the abscissa is for the run duration specified, $T = 60$ sec, where T is the total duration) is shown in Figure 25. A few screenshots of the results at different time-steps are given in Figures 26-28.

The pressures (in psi) near the face (toward the tsunami) of the deck are plotted in Figure 29. It can be seen that the peak occurs at about $t = 50$ sec (which also corresponds to the maximum velocity) with a value of 26 psi.

The plot of the pressures including both the front (as in above plot) and bottom face of the bridge deck is in Figure 30. It can be seen that maximum pressure on the bottom face is 55psi which is way higher than that on the front and is increasing steadily.

A "closer" examination of the pressures (same as above) in between $t = 50$ and 60 sec is in Figure 31. The white line in Figures 30 & 31 is due to several elements on the bottom face having the same magnitude of pressure and thus staggered together.

The time-histories of the support reactions (units: lb(f) per 3 inch sectional thickness) in both X and Y directions are plotted in Figures 32-33. Maxima in X and Y directions are -3,500 (this is at the far end support node) & -2,500 (this is at the middle support node) units, respectively. Since there are two support nodes each at the near end, far end and the middle support (i.e., a total of six nodes), these nodal reactions are to be multiplied by two to get the forces on the supports. Hence, maximum lateral force on any support = 2,333 lb(f) per 1 inch thickness, vertical force = 1,667 lb(f) per 1 inch thickness.

The tsunami forces (in kips/ft along the span) on the deck in both horizontal & vertical directions are shown in Figure 34. These are computed by the algebraic summation of the nodal reactions and are intended for design purposes. Maximum horizontal force is 13.3 kips/ft, whereas maximum vertical force magnitude is 35.9 kips/ft.

7.2 Using FVWAVE model for 2D analyses

The simulation is performed for 60 sec duration (the part of the hydrograph corresponding to the level that reached the bridge deck). It took 29 hours on 36 CPUs. Gravity is applied quasi-statically during the first 5 sec. The actual hydrograph starts from $t = 10$ sec. A screenshot of the applied velocity 'u' (units: in/sec) in the input file is shown in Figure 35. It can be seen that the peak velocity exists within the first 60 sec duration.

Confirmation of the velocity from the post-processing of results (appears to be the same as the above except that the abscissa is for the run duration specified, $T = 60$ sec, where T is the total duration) is in Figure 36. A few screenshots of the results at different time-steps are given in Figures 37-39.

The pressures (in psi) near the face (toward the tsunami) of the deck are plotted in Figure 40. It can be seen that the peak occurs at about $t = 20$ sec (which also corresponds to the maximum velocity) with a value of 55 psi.

The plot of the pressures including both the front (as in above plot) and bottom face of the bridge deck is given in Figure 41. It can be seen that maximum pressure on the bottom face is 120 psi which is way higher than that on the front face. The pressure spike marked as 'FP' is found to occur at the element located at the bottom face of the far end (away from the ocean) of the bridge deck. This peak occurs for a very short duration and falls down rapidly below 120 psi which is the value that most elements have.

The time-histories of the support reactions (units: lb(f) per 3 inch sectional thickness) in both X and Y directions are plotted in Figures 42-43. Maxima in X and Y directions are -6,500 (this is at the far end support node) & -3,900 (this is at the middle support node) units, respectively. Since there are two support nodes each at the near end, far end and the middle support (i.e., a total of six nodes), these nodal reactions are to be multiplied by two to get the forces on the supports. Hence, maximum lateral force on any support = 4,333 lb(f) per 1 inch thickness, vertical force = 2,600 lb(f) per 1 inch thickness.

The tsunami forces (in kips/ft along the span) on the deck in both horizontal & vertical directions are shown in Figure 44. These are computed by the algebraic summation of the nodal reactions and are intended for design purposes. Maximum horizontal force is 23.9 kips/ft (c.f. 13.3 kips/ft for corresponding valued obtained from the Cornell model), whereas maximum vertical force magnitude is 37.9 kips/ft (c.f. 35.9 kips/ft for the Cornell model).

7.3 Using FVWAVE model for 3D analyses

From the 2D results, it can be seen that the FVWAVE model gave more conservative results and as such the peak velocity and height corresponding to this model are used for the 3D analysis.

The simulation is performed using rigid material for the bridge for 10 sec duration. It took 28 hours on 36 CPUs. Gravity is applied quasi-statically during the first 1 sec. The actual hydrograph starts from $t = 1$ sec. A screenshot of the applied velocity 'u' (units: in/sec) in the input file is in Figure 45. Confirmation of the velocity from the post-processing of results is shown in Figure 46. A few screenshots of the results at different time-steps are provided in

Figures 47-53.

The pressures (in psi) near the face (toward the tsunami) of the bridge are plotted but these are not presented in this report as these are being studied at this point of time.

7.4 Potential extension to other bridges

This is an interesting issue that was discussed during one of the recent meetings among ODOT engineers and the authors. The process outlined in this report is sufficiently general to be used for any other bridges/infrastructure as well. However, the specific end results could vary based on the location. For instance the velocities and heights of the tsunami (even if the source is essentially the same) are necessarily dependent on the bathymetry, proximity of the site, etc. As discussed in the meeting, one way could be to generate contour maps of total horizontal or vertical forces and overturning moments as a function of velocity and height of tsunami at critical locations. Nevertheless, the ideas are going to be the same as in this report.

8. Concluding remarks

This report provided tsunami design criteria for coastal infrastructure using a case study of the proposed Spencer Creek Bridge on the US Highway-101 at Newport, Oregon. The process outlined herein is quite general and is applicable to any other facility under wave-body impact situations.

University of Hawaii's Department of Ocean and Resource Engineering have developed the expertise with the state-of-the-art of the tsunami generation in the Pacific Ocean, thus the resulting data pertains to "Ocean scale". The results so obtained have to be applied on manmade structures such as bridges on a much smaller scale, which can be called as "Structure scale" in order to perform the detailed structural analyses and arrive at the forces of tsunami impact on the structures as required by a bridge design engineer. Some of the experiences gained in this work are summarized below:

The efforts of analyses on the Structure scale are primarily distributed in the model preparation, getting the model up and running (including debugging time), computational time and post-processing. As the model goes to the level of detail of 3D, the data files to be managed are found to be getting bigger (over 100 MB of input file and several Gigabytes of output) thereby slowing down the process of interpretation. Without the fineness of the mesh, results are going to be less accurate. At the same time, with a very fine mesh, the runs are found to be extremely slow even on supercomputer. Since the goal is to arrive at the best-possible results for use in the design of the proposed bridge at the earliest date, different practical ways to meet the goal are investigated. One way is to use rigid material for the bridge, but this run can give only the pressures on the face of the bridge but doesn't result in the reactions. On the other hand, assumptions of the linear elastic material make the run a lot slower, but one can get the reactions. At the time of writing this report, 3D analysis with rigid body material has been run and the results are being examined. Since there are several elements that have high pressures, it might be more useful to get some reactions as well. However, it requires more time and efforts (to run and to interpret) than that available before the deadline of the project. The project team at OSU will continue to make

progress in this direction. As of now, the results (2D) are derived using the FVWAVE model are recommended for the design purposes. It might be of interest to understand some of the background information in making this choice. FVWAVE model is a recently developed second generation wave model (and an improvement over the more widely employed first generation Cornell model) due to its superior mass conservation and energy dissipation properties. The Tsunami waves have been generated using both models to provide calibration against each other and determine how these model predictions vary with numerical modeling difference. The results of FVWAVE model have generally been more conservative than the Cornell model in this case study. The height of tsunami and the corresponding velocity (which are different in either model) have a bearing in resulting in the different forces on the 2D model.

It may be noted that an issue such as scour is also of practical importance but not considered in this report. It is an area that is still in the research arena and hence appropriate for future investigations.

In this report, while base-shear forces induced by wave loads on the typical cross-section of the bridge deck are provided, no wave loads on the columns are presented. This is due to the fact that the 2-D model cannot reasonably simulate the effects of fluid forces of the flow around the columns, which are necessarily three dimensional. We are continuing to perform 3D fluid-structure analysis to examine the wave loads on the columns. However, 3D analysis is outside the scope of this study and due to time constraints, the results are not available at reporting time.

The knowledge and experience gained in this project is expected to result in significant cost savings in any such future endeavors. Besides, designing infrastructure such as bridges using some of the more conventional tools (formulae) that tend to be more conservative could result in more expensive construction as compared to the more accurate and rational analyses. As such this report can be considered as amongst the first steps made in this direction.

Finally, we caution the readers concerning interpretation of the numerical predictions of the fluid loads on the bridge structure. While we are confident that the numerical results of the highly nonlinear fluid loads obtained in this study are based on state-of-the-art computational mechanics models and are of high quality, it is well known that numerical simulations of nonlinear systems with this level of complexity need to be calibrated with experimental data. In general, when the complex numerical model of a particular physical structure is fully calibrated and its prediction accuracy determined, it can then be used confidently to perform parametric studies within a reasonable range of variations of the original system parameters. Numerical simulations, without experimental calibration, may only be considered qualitative and used as design guidance.

Acknowledgements

This study was initiated by the Oregon Department of Transportation (ODOT) under Work Order No. 06-09 to Oregon State University. The authors would like to thank the ODOT staff for their cooperation, willingness to share information, prompt review and feedback during the course of the project.

References

- Abe, K. (1979). Size of great earthquakes of 1873-1974 inferred from tsunami data. *Journal of Geophysical Research*, 84(B4), 1561-1568.
- Clague, J.J. (1997). Evidence for large earthquakes at the Cascadia subduction zone. *Reviews of Geophysics*, 35(4), 439-460.
- Geist, E.L. (2005). Local tsunami hazards in the Pacific Northwest from Cascadia subduction zone earthquakes. US Geological Survey Professional Paper 1661-B, Reston, Virginia.
- Geist, E.L. and Parsons, T. (2006). Probabilistic analysis of tsunami hazards. *Natural Hazards*, 37(3), 277-314.
- Goldfinger, C., Nelson, C.H., Johnson, J.E., and The Shipboard Scientific Party. (2003). Holocene earthquake records from the Cascadia subduction zone and northern San Andreas Fault based on precise dating of offshore turbidites. *Annual Review of Earth and Planetary Sciences*, 31, 555-577.
- González, F.I., Titov, V.V., Mofjeld, H., Venturato, A., Simmons, S., Hansen, R., Combellick, R., Eisner, R., Hoirup, D., Yanagi, B., Yong, S., Darienzo, M., Priest, G., Crawford, G., and Walsh, T. (2005). Progress in NTHMP hazard assessment. *Natural Hazards*, 35(1), 89-110.
- Gresho, P.M., Sani, R.L. (1998). Incompressible flow and the Finite Element method, Advection-Diffusion and Isothermal Laminar Flow, *John Wiley and sons*.
- Jacoby, G.C., Bunker, D.E., and Benson, B.E. (1997). Tree-ring evidence for an AD 1700 Cascadia earthquake in Washington and northern Oregon. *Geology*, 25(11), 999-1002.
- Kajiura, K. (1970). Tsunami source, energy and the directivity of wave radiation. *Bulletin of the Earthquake Research Institute*, University of Tokyo, 48, 835-869.
- Kirby, S., Geist, E.L., Lee, W.H.K., Scholl, D., and Blakely, R. (2006). Tsunami Source Characterization for Western Pacific Subduction Zone, US Geological Survey Report, in review.
- Kowalik, Z. and Murty, T.S. (1993). Numerical simulation of two-dimensional tsunami runup. *Marine Geodesy*, 16(*), 87-100.
- Liu, P.L.-F., Cho, Y.-S., Briggs, M.J., Kanoglu, U. and Synolakis, C.E. (1995). Runup of solitary waves on a circular island. *Journal of Fluid Mechanics*, 302, 259-285.
- Marks, K.M. and Smith, W.H.F. (2006). An evaluation of publicly available global bathymetry grids. *Marine Geophysical Researches*, 27(1), 19-34.
- Oregon Department of Transportation's (ODOT) drawings of Spencer Creek bridge in PDF format.
- Okada, Y. (1985). Surface deformation due to shear and tensile faults in a half space. *Bulletin of the Seismological Society of America*, 75, 1135-1154.
- Satake, K., Shimazaki, K., Tsuji, Y., and Ueda, K. (1996). Time and size of a giant earthquake in Cascadia inferred from Japanese tsunami records of January 1700. *Nature*, 379, 246-249.
- Satake, K., Wang, K., and Atwater, B.F. (2003). Fault slip and seismic moment of the 1700 Cascadia earthquake inferred from Japanese tsunami descriptions. *Journal of Geophysical Research*, 108(B11), 2535, doi:10.1029/2003JB002521.
- Smith, W.H.F. and Sandwell, D.T. (1997). Global sea floor topography from satellite altimetry and ship depth soundings. *Science*, 227(5334), 1956-1962.
- Steketee, J.A. (1958). On Volterra's Dislocation in a semi-infinite elastic medium. *Canadian Journal of Physics*, 36, 192-205.

- Titov, V.V. and Synolakis, C.E. (1998). Numerical modeling of tidal wave runup. *Journal of Waterway, Port, Coastal and Ocean Engineering*, 124(4), 157-171.
- Wei, Y., Cheung, K.F., Curtis, G.D., and McCreery, C.S. (2003). Inverse algorithm for tsunami forecasts. *Journal of Waterway, Port, Coastal, and Ocean Engineering*, 129(2), 60-69.
- Wei, Y., Mao, X.Z., and Cheung, K.F. (2006). Well-balanced finite volume model for long-wave runup. *Journal of Waterway, Port, Coastal, and Ocean Engineering*, 132(2), 114-124.
- Yamazaki, Y., Wei, Y., Cheung, K.F., and Curtis, C.D. (2006). Forecast of tsunamis generated at the Japan-Kuril-Kamchatka source region. *Natural Hazards*, 38(3), 411-435.
- Zhou, J.G., Causon, D.M., Mingham, C.G., and Ingram, D.M. (2001). The surface gradient method for the treatment of source terms in the shallow-water equations. *Journal of Computational Physics*, 168(1), 1-25.

List of Figures

1. Major subduction zones in the Pacific and tsunamigenic earthquakes during 1900-2005. —, subduction zone; •, tsunamigenic earthquakes.
2. Schematic of faulting mechanism.
3. Three potential rupture configurations and seafloor deformation of the 500-year Cascadia earthquake. (a) Long. (b) Short-north. (c) Short-central.
4. Bathymetry and topography in computational grids. (a) Level-1 eastern Pacific. (b) Level-2 continental shelf. (c) Level-3 study site. •, Bridge site.
5. Tsunami wave amplitude of the 500-year Cascadia earthquake with the long rupture configuration. (a) Eastern Pacific. (b) Continental shelf. (c) Study site.
6. Tsunami wave amplitude of the 500-year Cascadia earthquake with the short-north rupture configuration. (a) Eastern Pacific. (b) Continental shelf. (c) Study site.
7. Tsunami wave amplitude of the 500-year Cascadia earthquake with the short-central rupture configuration. (a) Eastern Pacific. (b) Continental shelf. (c) Study site.
8. Flow depth and velocity of the 500-year Cascadia earthquake at bridge site. —, long rupture configuration; ----, short-north configuration; ·····, short-central configuration.
9. Comparison of computed tsunami waves from Cornell model for all three fault configurations.
10. Comparison of computed tsunami waves from FVWAVE for all three fault configurations.
11. Comparison of computed tsunami waves from FVWAVE and Cornell model based on short-central fault configuration.
12. Schematic showing the location of 2D model and the direction of tsunami
13. 2D model of the bridge and tsunami. Pink color of the surrounding box corresponds to air, blue color corresponds to tsunami wave.
14. 2D model of the bridge and tsunami. FE mesh of bridge is also shown.
15. 2D model of the bridge and tsunami (oblique view).
16. Node numbers indicating the support reactions (on the face of the 2D model at $Z=0$ in)
17. Node numbers indicating the support reactions (on the face of the 2D model at $Z=3$ in)
18. Schematic showing the location of the elements at the front face and the bottom face of the bridge deck for referencing the pressure plots.

19. 3D model of the bridge.
20. 3D model of the bridge (another view).
21. 3D model of the bridge with the FE mesh.
22. 3D model of the bridge; the box enclosing the bridge is rendered transparent; the box itself contains two parts: one with dark green color is air, one with light blue color has water for introducing the tsunami.
23. 3D model of the bridge; the box enclosing the bridge is rendered transparent and the FE mesh is shown.
24. Cornell model: Time history of the input velocity (u in inches/sec versus t in sec).
25. Cornell model: Confirmation of the input velocity u from post-processing.
26. Cornell model: screen shot at t=49.8 sec.
27. Cornell model: screen shot at t=53.5 sec.
28. Cornell model: screen shot at t=60 sec.
29. Cornell model: pressures (in psi) near the face (toward the tsunami) of the deck.
30. Cornell model: The plot of the pressures (in psi) including both the front and bottom face of the bridge deck.
31. Cornell model: A “closer” examination of the pressures between t = 50 and 60 sec.
32. Cornell model: Support reactions in X-direction.
33. Cornell model: Support reactions in Y-direction.
34. Cornell model: Tsunami forces on the deck in both horizontal & vertical directions
35. FVWAVE model: Time history of the input velocity (u in inches/sec versus t in sec).
36. FVWAVE model: Confirmation of the input velocity u from post-processing.
37. FVWAVE model: screen shot at t=17.8 sec.
38. FVWAVE model: screen shot at t=33.6 sec..
39. FVWAVE model: screen shot at t=53.7 sec.
40. FVWAVE model: pressures (in psi) near the face (toward the tsunami) of the deck.

41. FVWAVE model: The plot of the pressures (in psi) including both the front and bottom face of the bridge deck.
42. FVWAVE model: Support reactions in X-direction.
43. FVWAVE model: Support reactions in Y-direction.
44. FVWAVE model: Tsunami forces on the deck in both horizontal & vertical directions
45. FVWAVE model (3D): Time history of the input velocity (u in in/sec versus t in sec).
46. FVWAVE model (3D): Confirmation of the input velocity u from post-processing.
47. FVWAVE model: screen shot at t=1.9 sec.
48. FVWAVE model: screen shot at t=2.2 sec.
49. FVWAVE model: screen shot at t=3 sec.
50. FVWAVE model: screen shot at t=3.8 sec.
51. FVWAVE model: screen shot at t=4.7 sec.
52. FVWAVE model: screen shot at t=7 sec.
53. FVWAVE model: screen shot at t=10 sec.

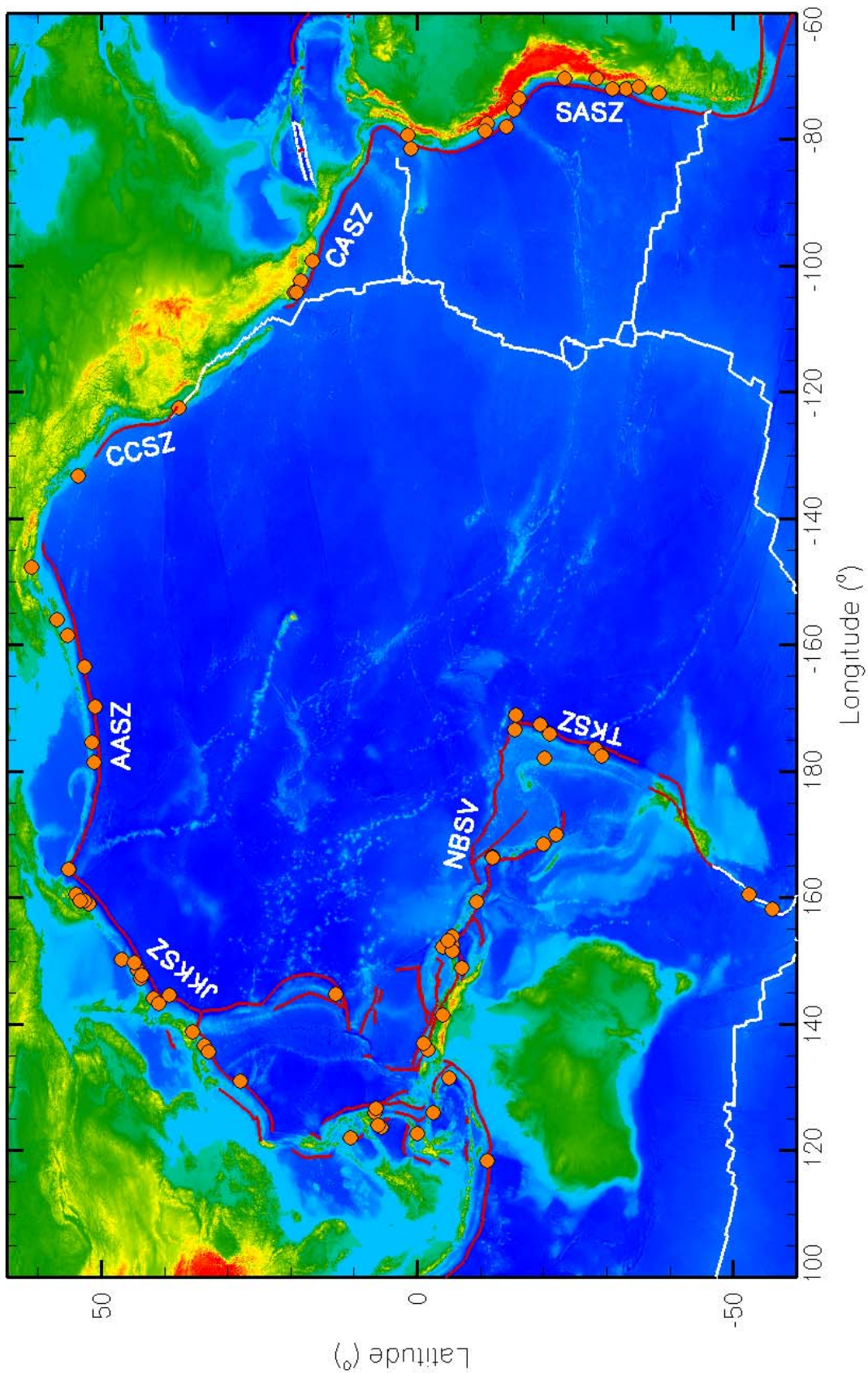


Fig. 1 Major subduction zones in the Pacific and tsunamigenic earthquakes during 1900-2005. —, subduction zone. •, tsunamigenic earthquakes.

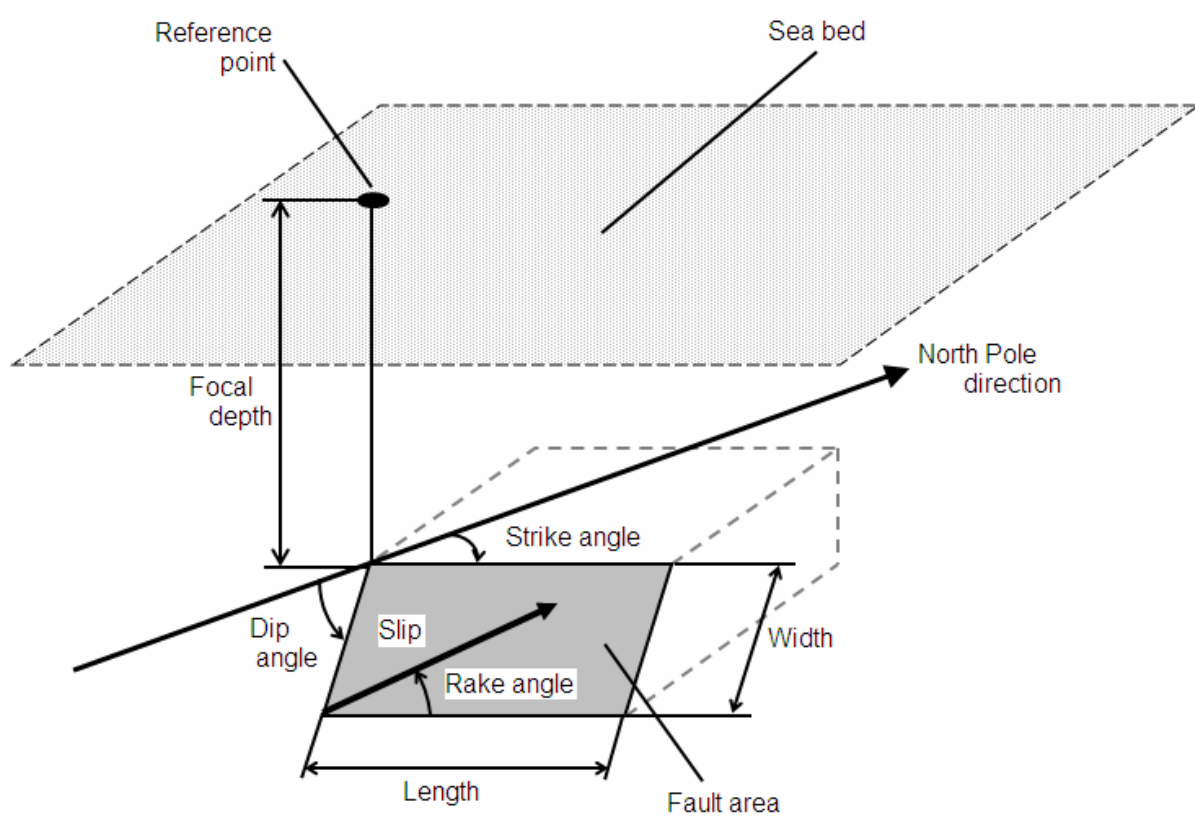


Fig. 2 Schematic of faulting mechanism.

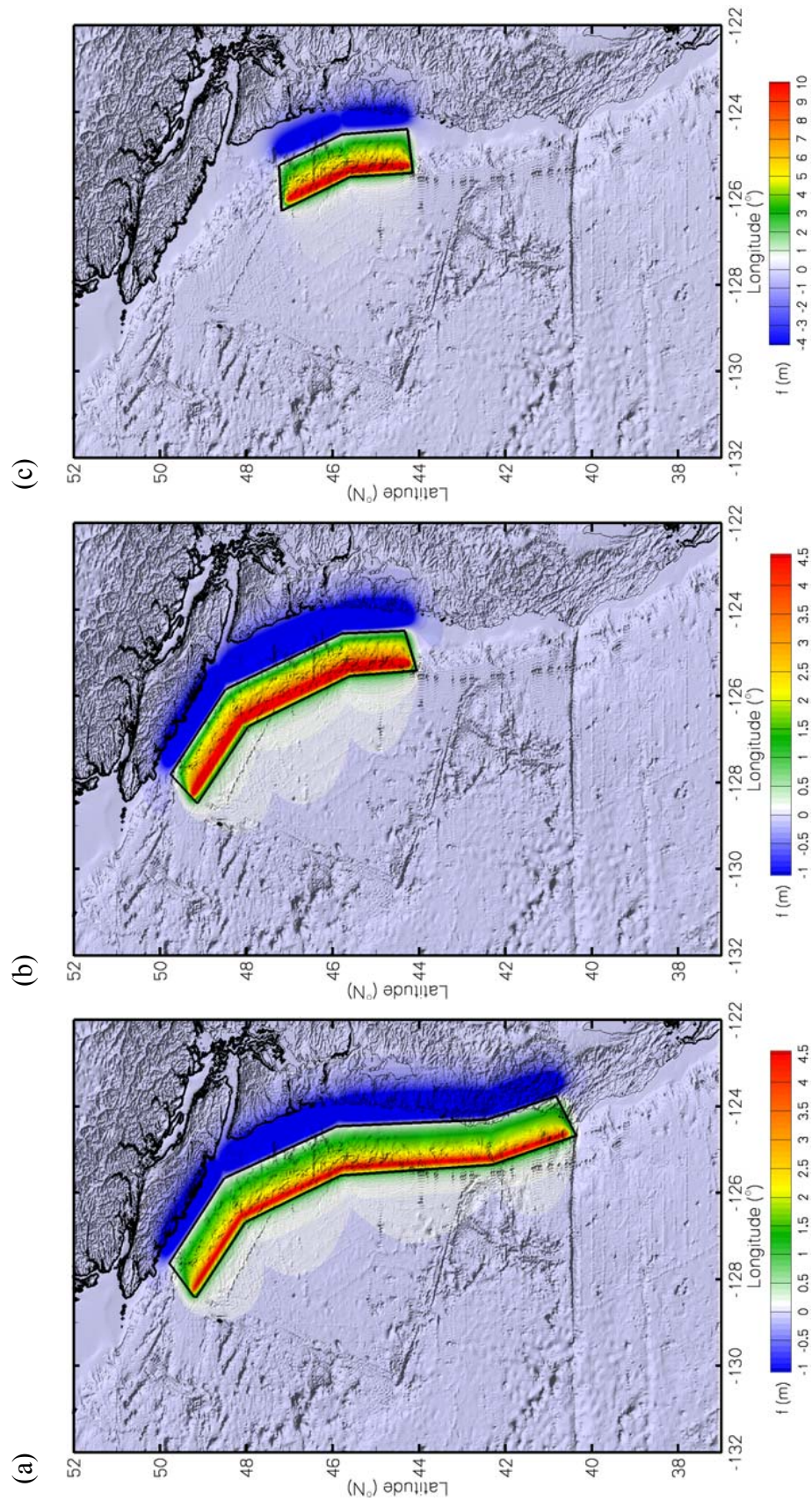


Fig. 3 Three potential rupture configurations and seafloor deformation of the 500-year Cascadia earthquake. (a) Long. (b) Short-north. (c) Short-central.

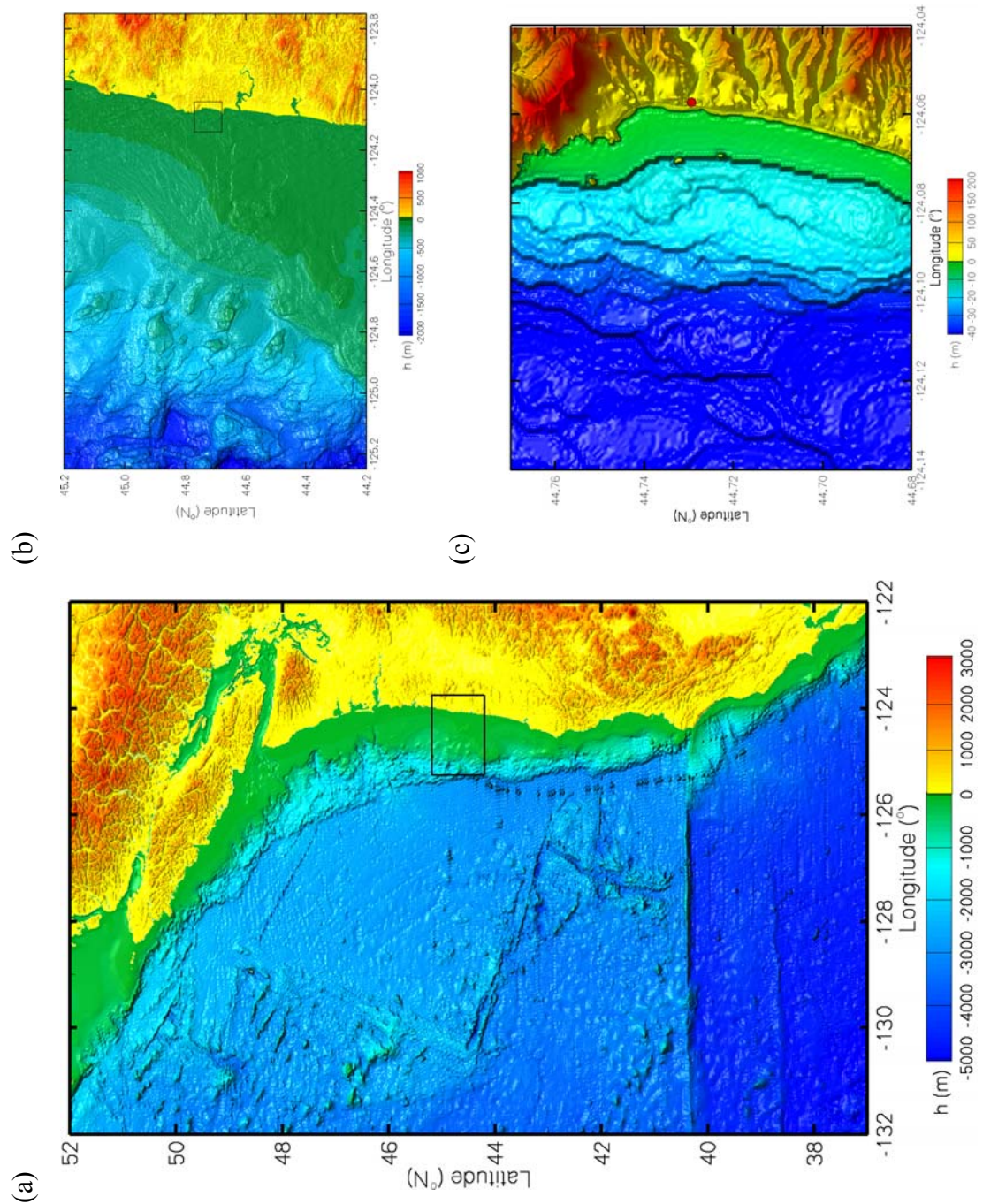


Fig. 4 Bathymetry and topography in computational grids. (a) Level-1 eastern Pacific. (b) Level-2 continental shelf. (c) Level-3 study site. •, Bridge site.

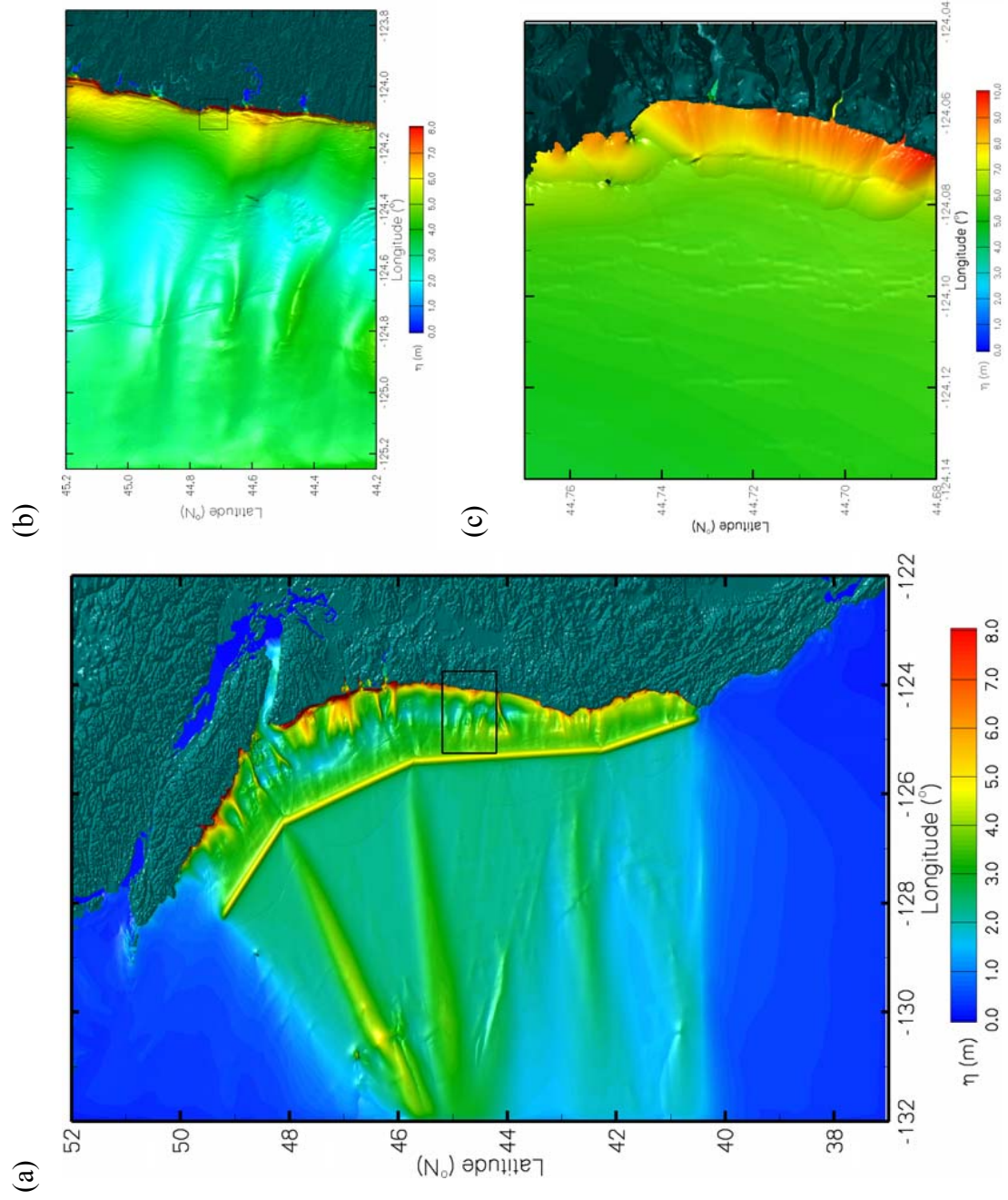


Fig.5 Tsunami wave amplitude of the 500-year Cascadia earthquake with the long rupture configuration. (a) Eastern Pacific. (b) Continental shelf. (c) Study site.

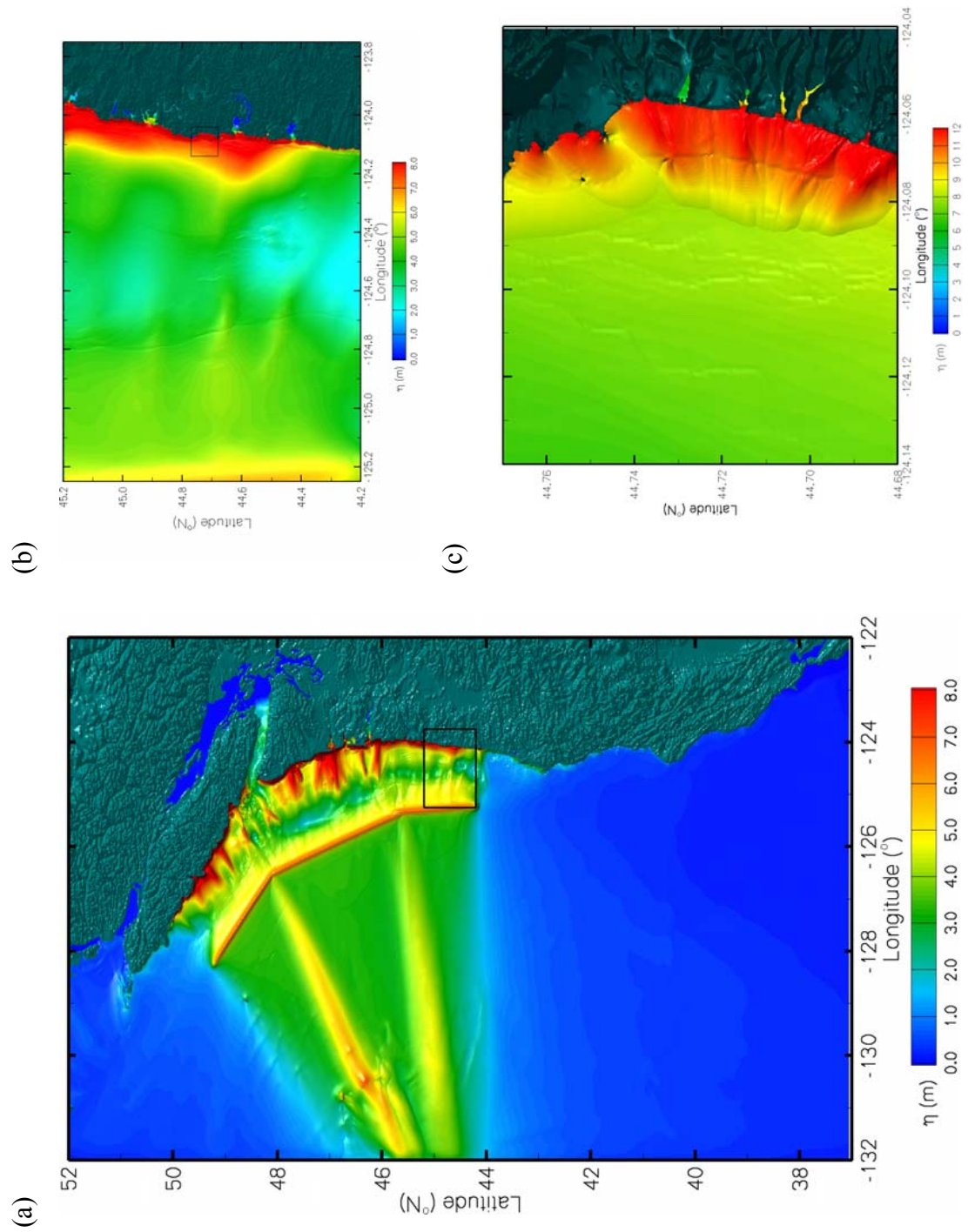


Fig 6 Tsunami wave amplitude of the 500-year Cascadia earthquake with the short-north rupture configuration. (a) Eastern Pacific. (b) Continental shelf. (c) Study site.

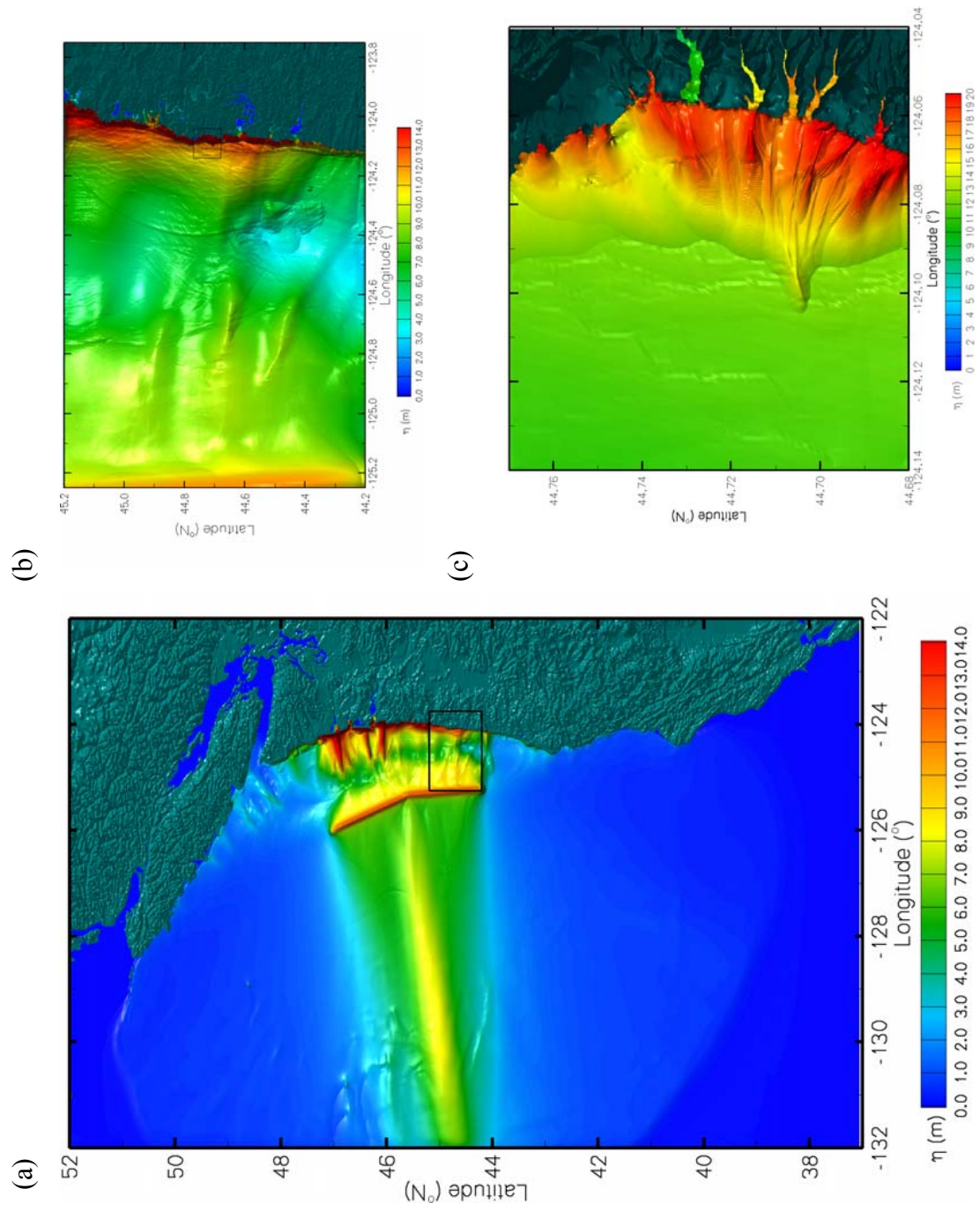


Fig. 7 Tsunami wave amplitude of the 500-year Cascadia earthquake with the short-central rupture configuration. (a) Eastern Pacific. (b) Continental shelf. (c) Study site.

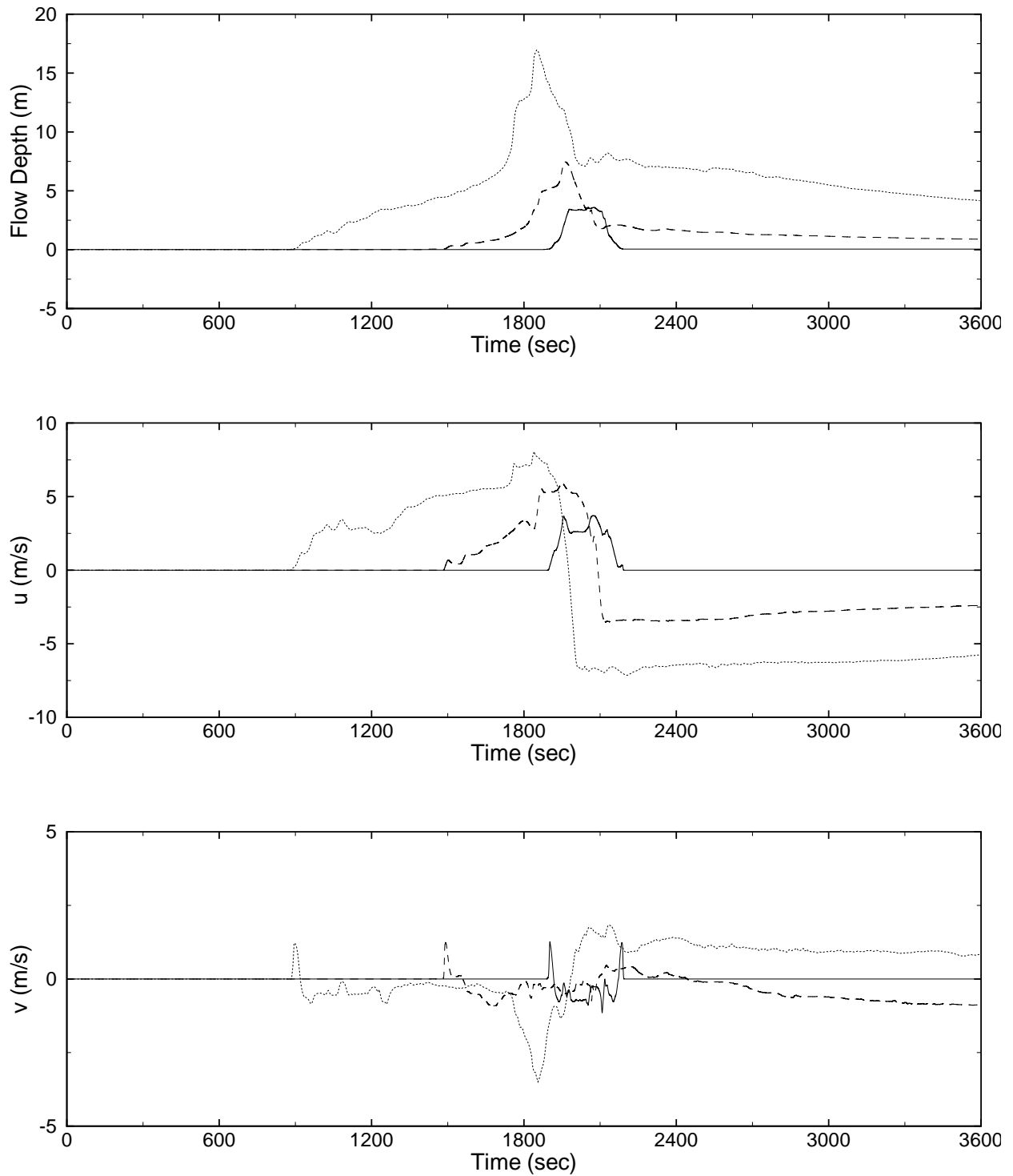


Fig. 8 Flow depth and velocity of the 500-year Cascadia earthquake at bridge site. —, long rupture configuration; ---, short-north configuration; ····, short-central configuration, the velocity directions are u (west to east) and v (south to north).

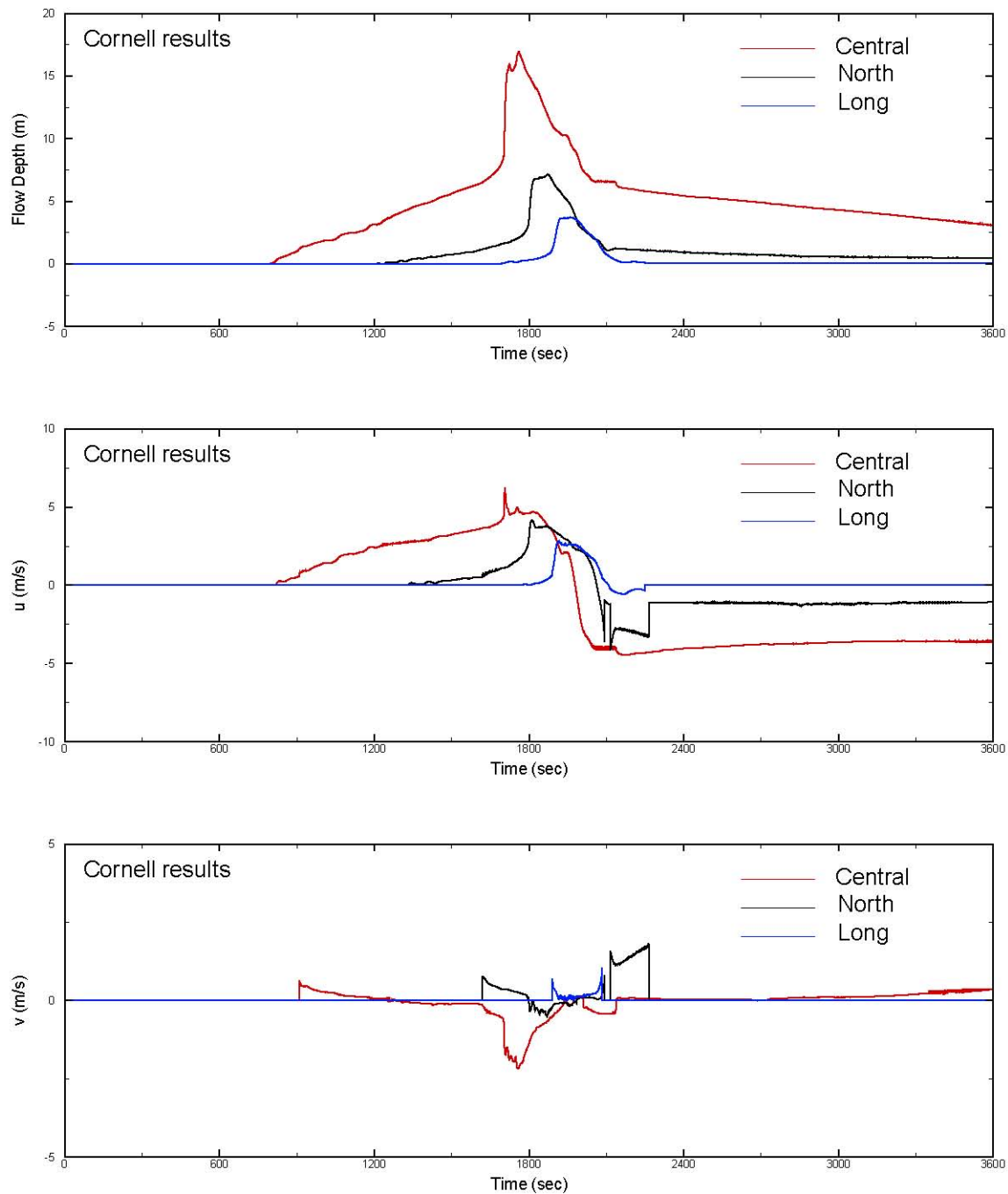


Figure 9. Comparison of computed tsunami waves from Cornell model for all three fault configurations; the velocity directions are u (west to east) and v (south to north).

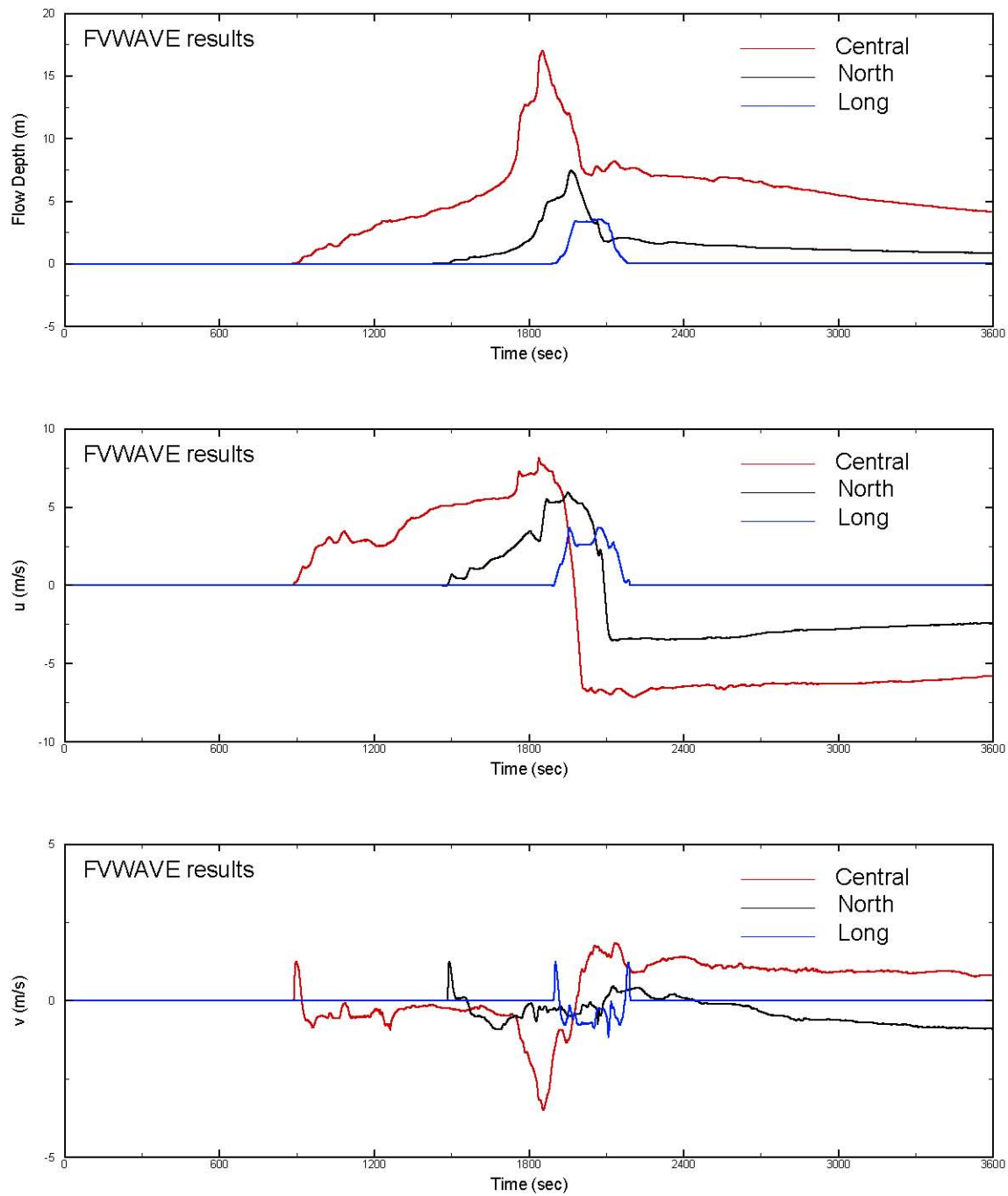


Figure 10. Comparison of computed tsunami waves from FVWAVE for all three fault configurations; the velocity directions are u (west to east) and v (south to north).

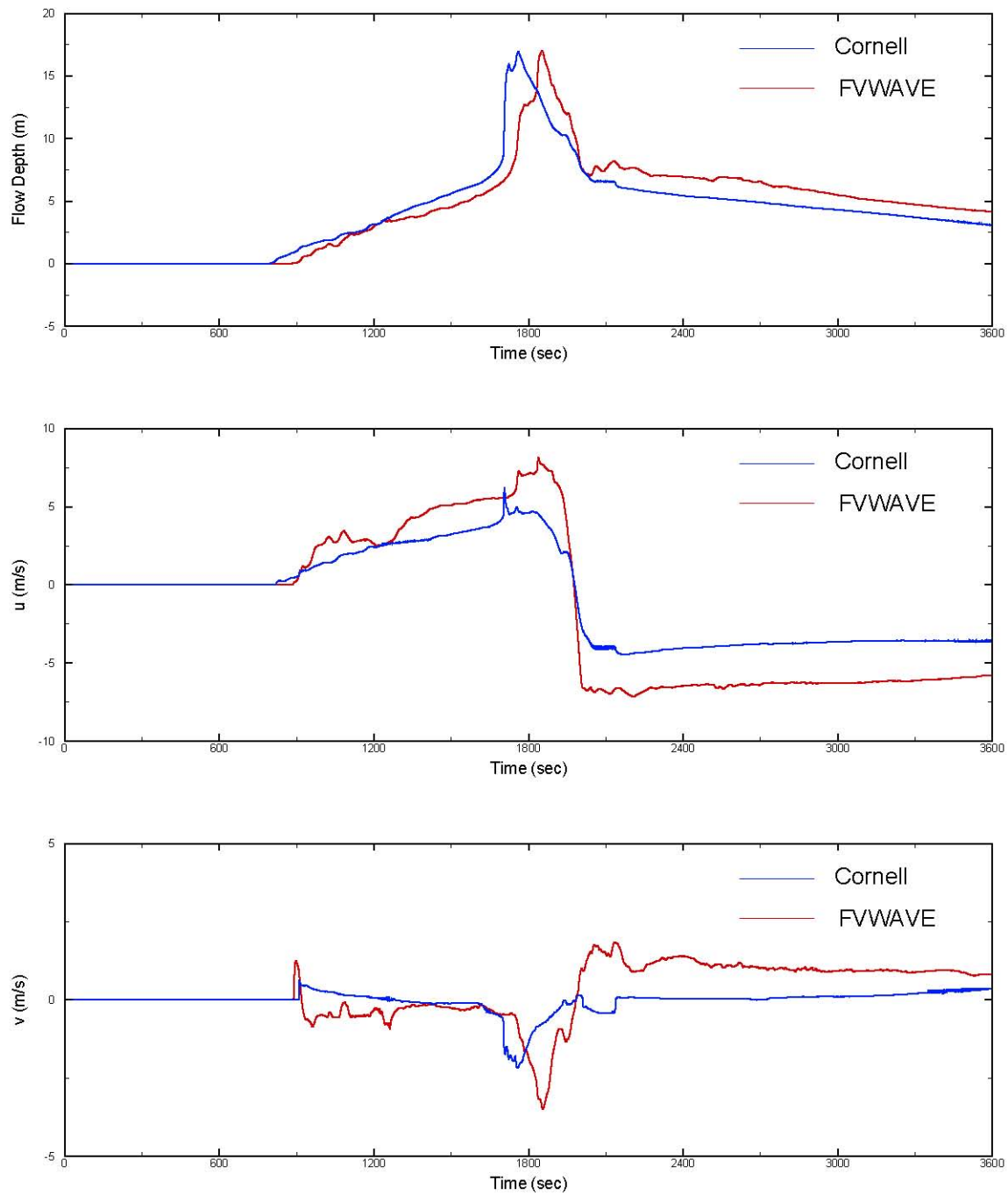
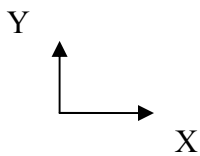
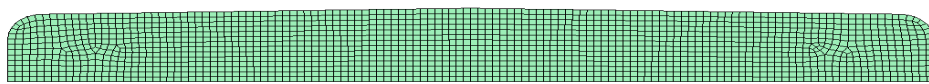
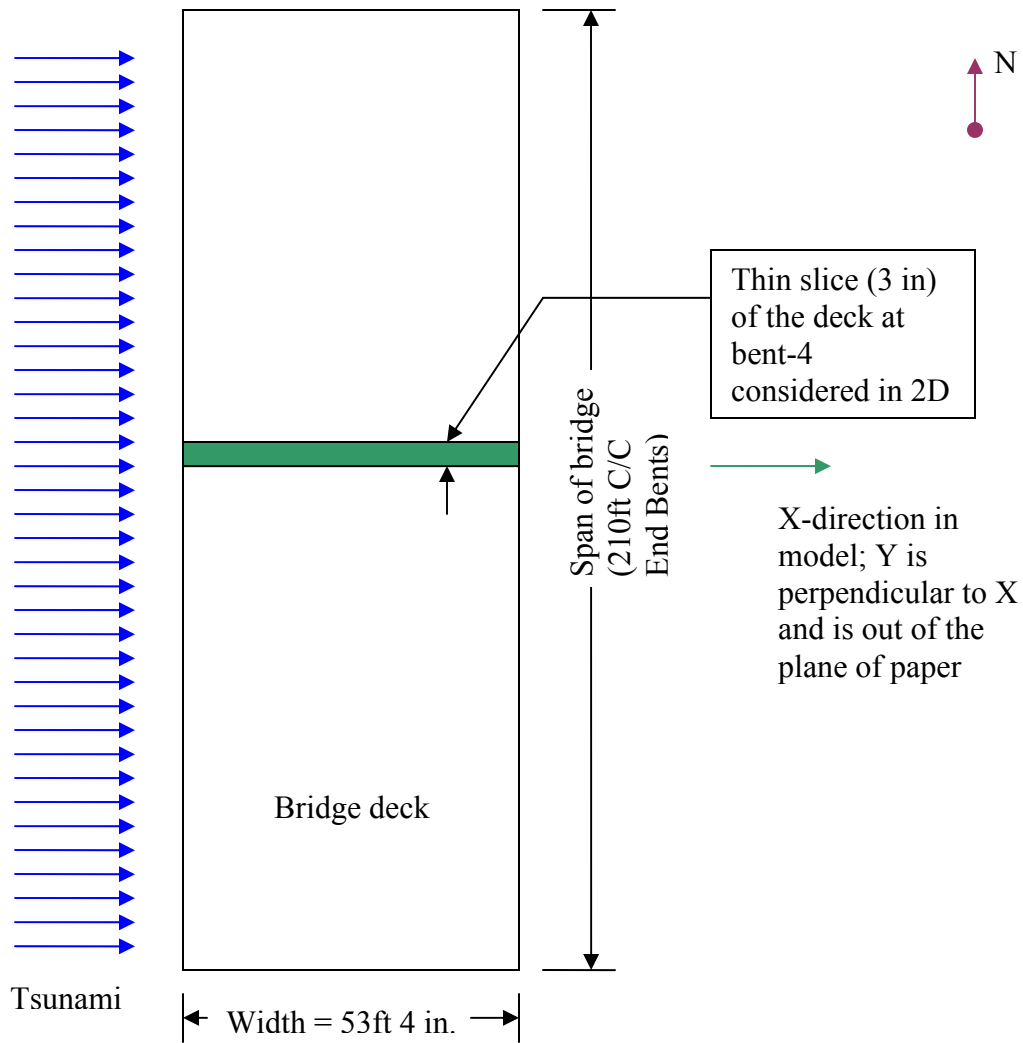


Figure 11. Comparison of computed tsunami waves from FVWAVE and Cornell model based on short-central fault configuration.



Cross-section of bridge deck (Bent-4) (depth at ends~5.5 ft)

Figure 12: Schematic showing the location of 2D model and the direction of tsunami (refer the drawings enclosed in Appendix-A for more details; the cross-section is based on elevation at bent-4)

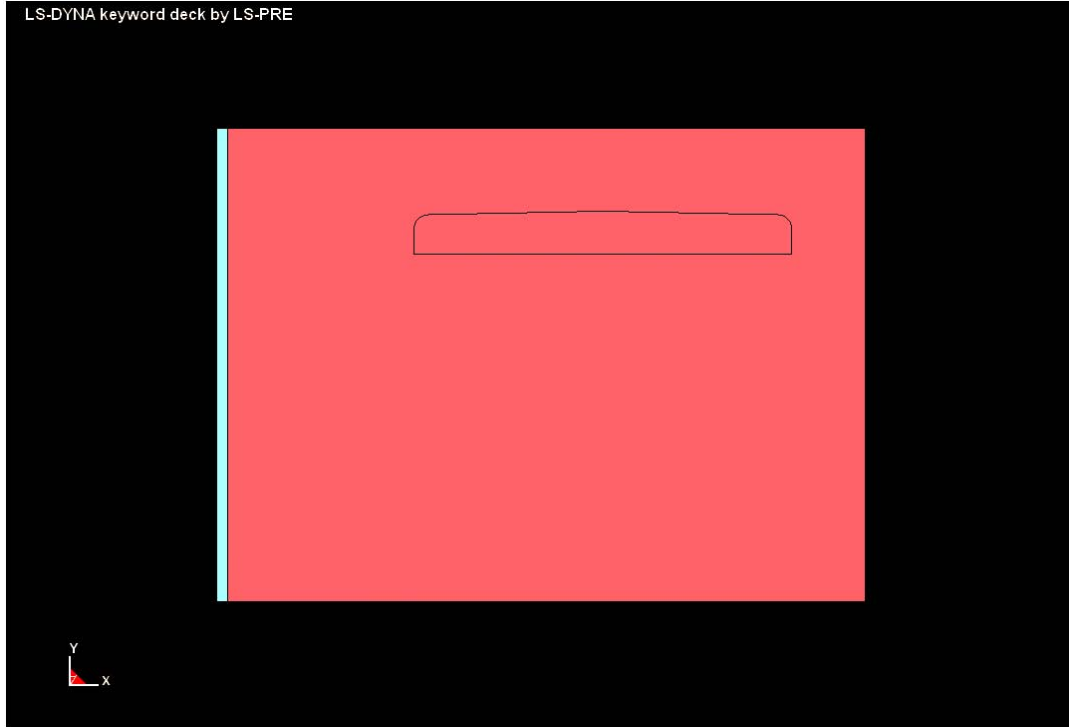


Figure 13. 2D model of the bridge and tsunami. Pink color of the surrounding box corresponds to air, blue color corresponds to tsunami wave.

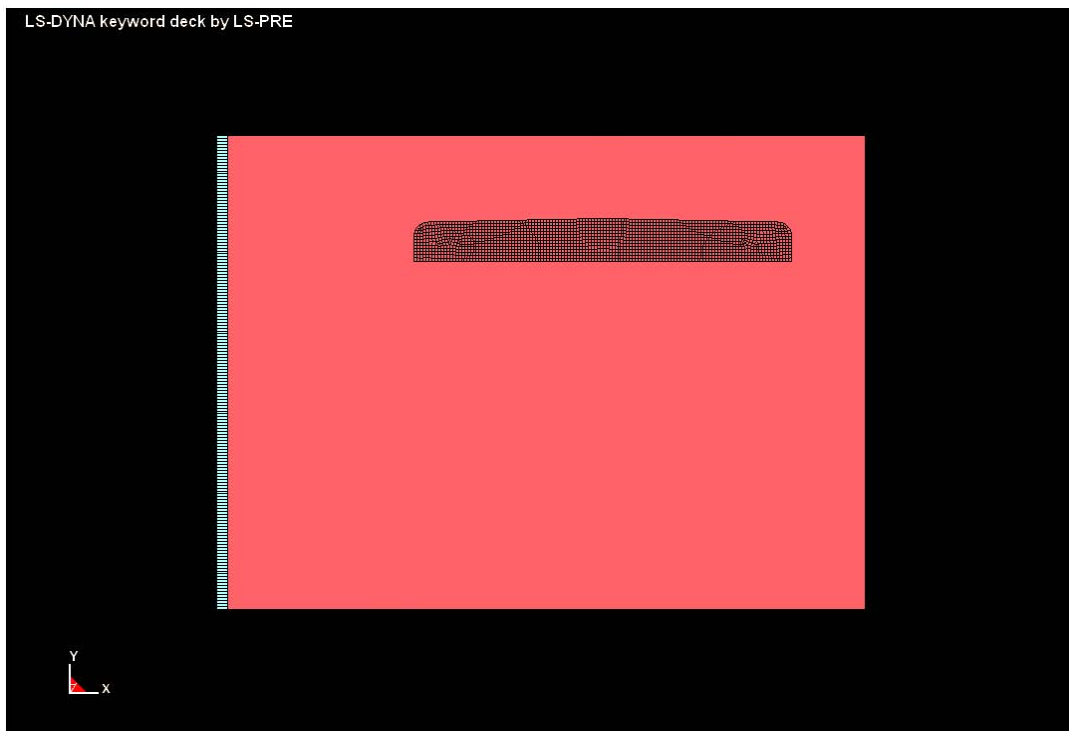


Figure 14. 2D model of the bridge and tsunami. FE mesh of bridge is also shown.

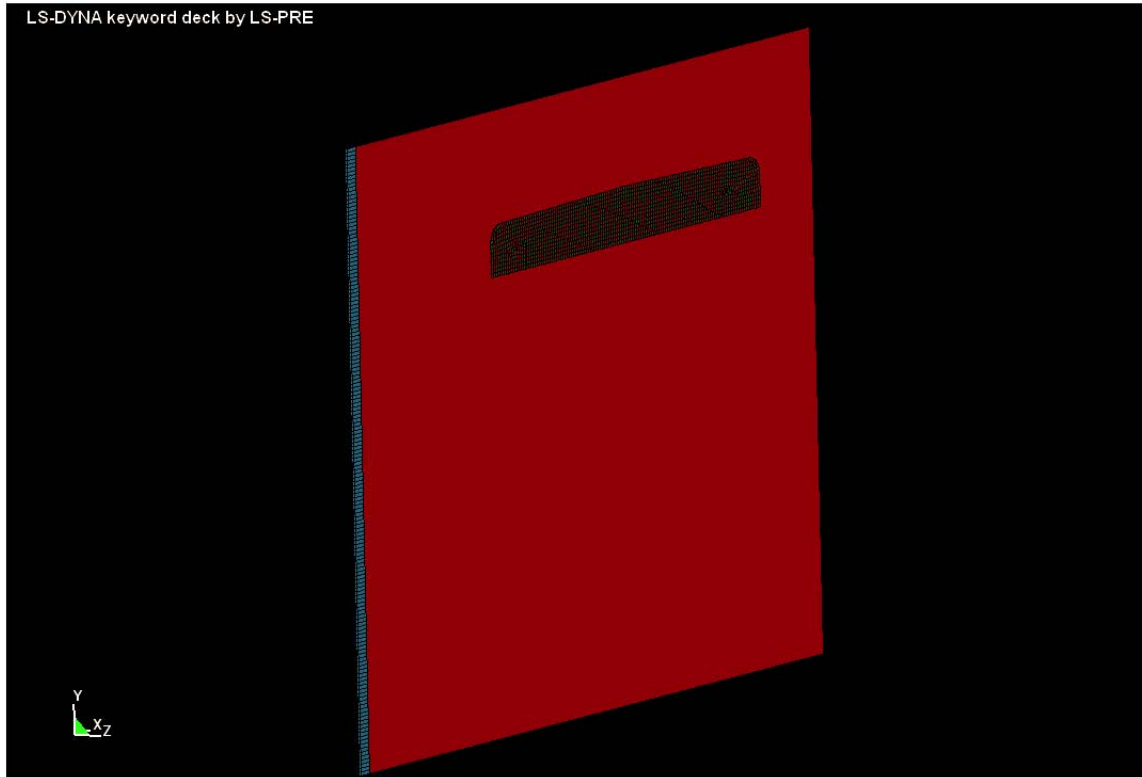


Figure 15. 2D model of the bridge and tsunami (oblique view).

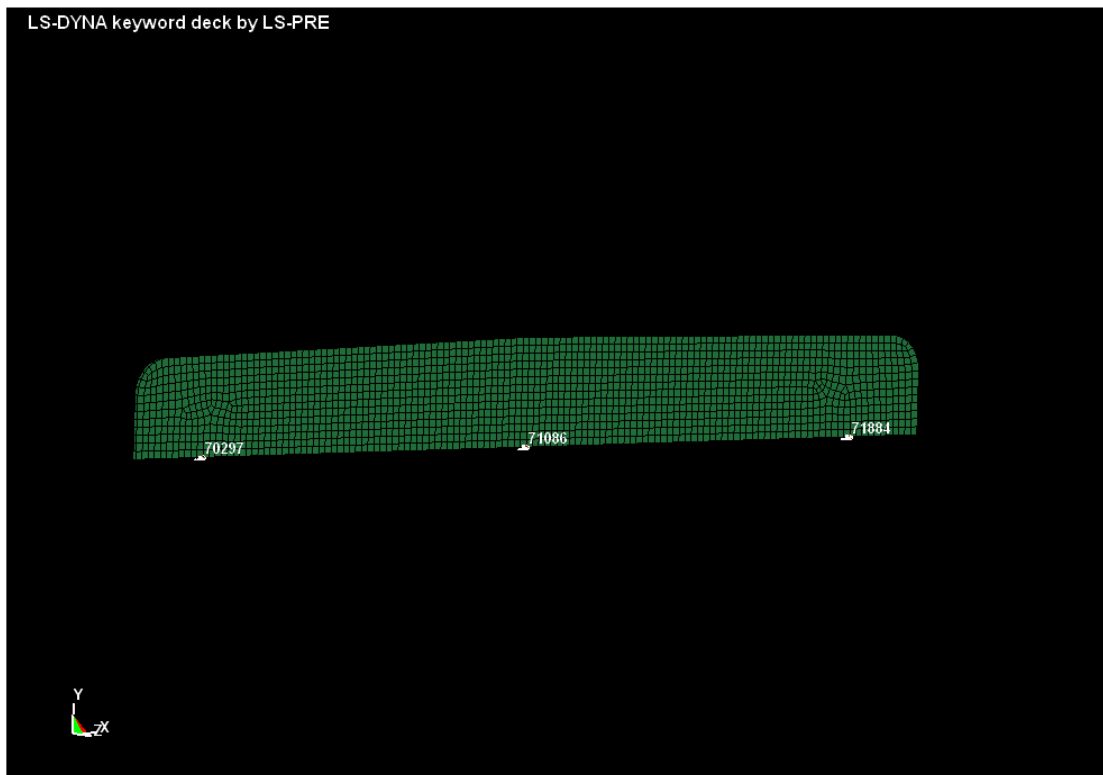


Figure 16. Node numbers indicating the support reactions (on the face of the 2D model at $Z=0$ in)

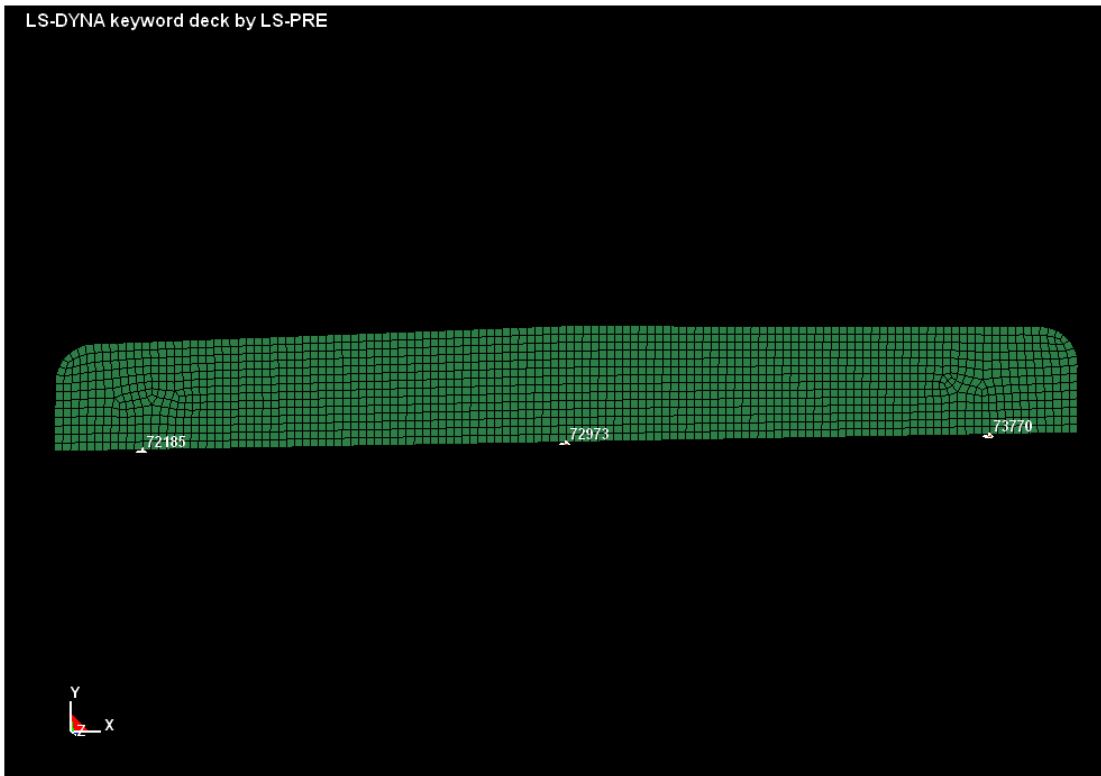


Figure 17. Node numbers indicating the support reactions (on the face of the 2D model at Z =3 in)

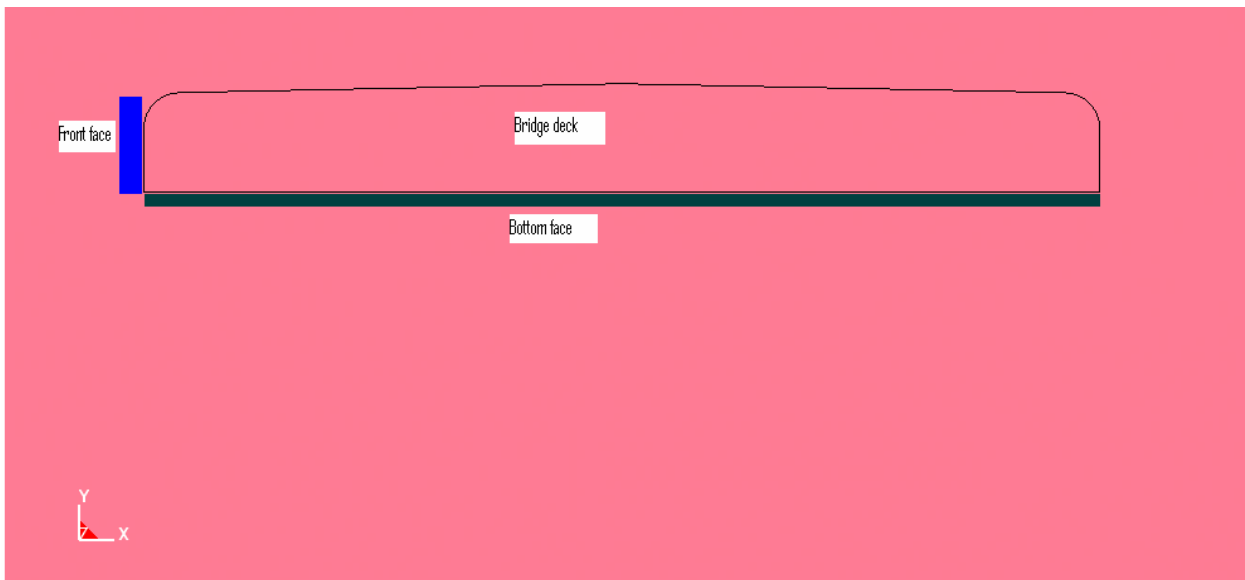


Figure 18. Schematic showing the location of the elements at the front face and the bottom face of the bridge deck for referencing the pressure plots.



Figure 19. 3D model of the bridge.

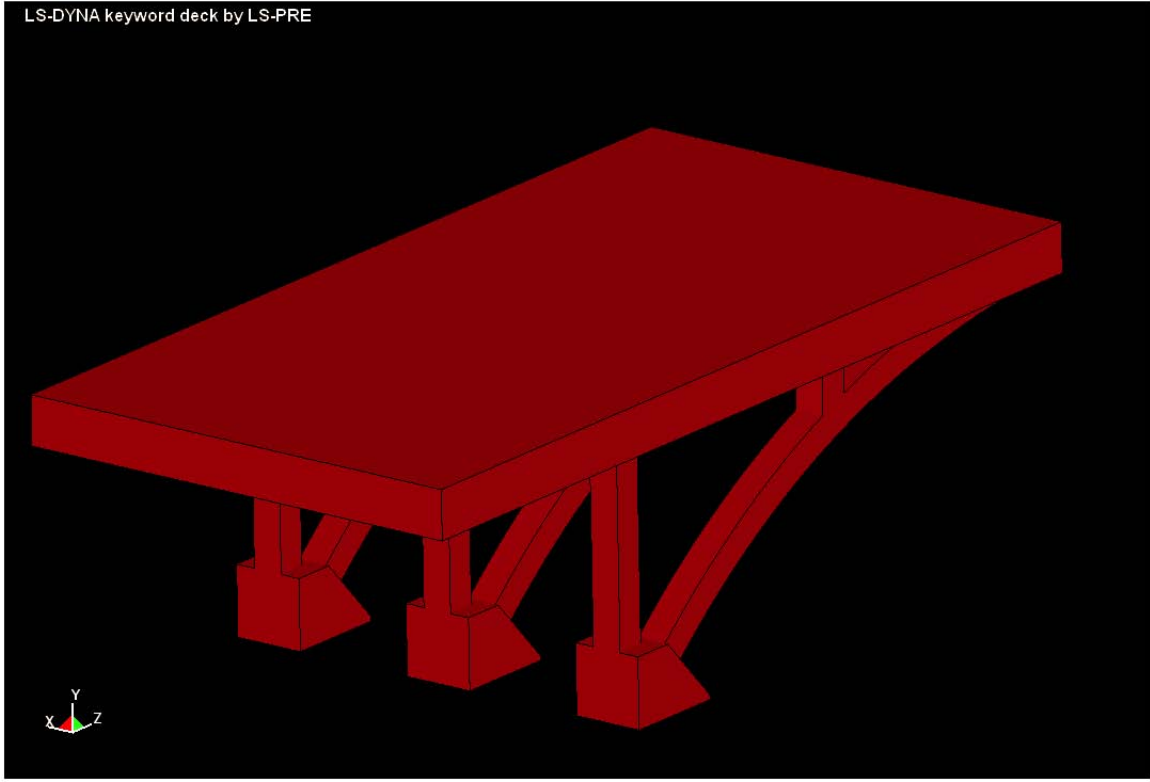


Figure 20. 3D model of the bridge (another view).

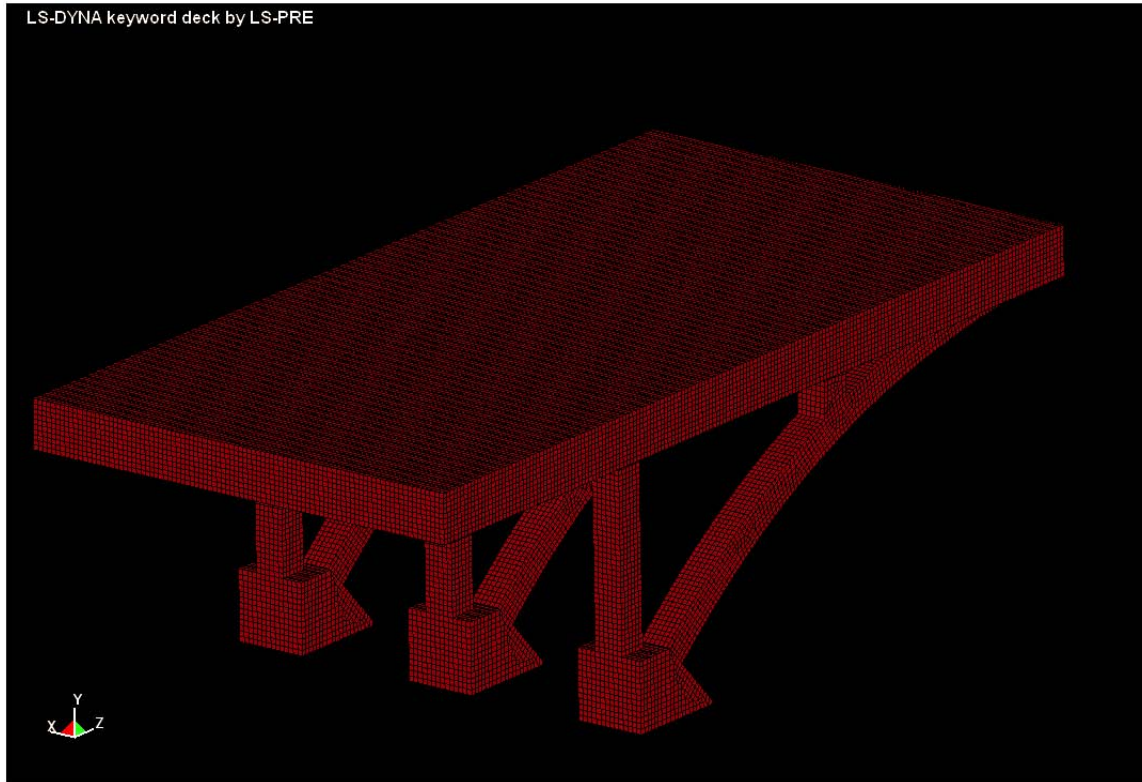


Figure 21. 3D model of the bridge with the FE mesh.



Figure 22. 3D model of the bridge; the box enclosing the bridge is rendered transparent; the box itself contains two parts: one with dark green color is air, one with light blue color has water for introducing the tsunami.

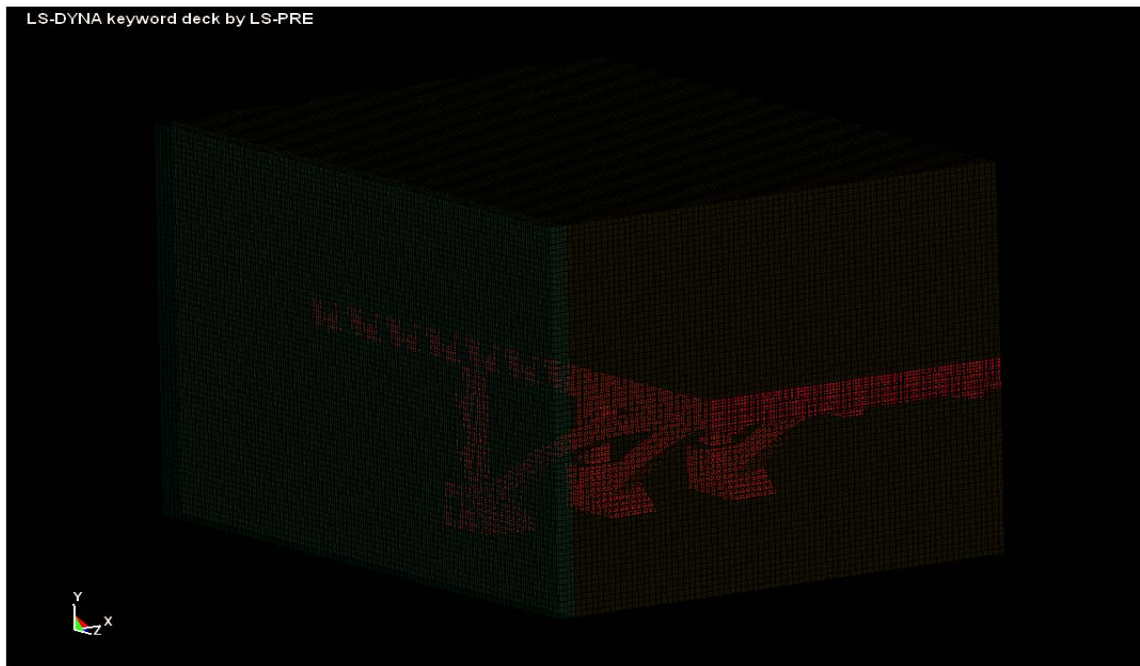


Figure 23. 3D model of the bridge; the box enclosing the bridge is rendered transparent and the FE mesh is shown.

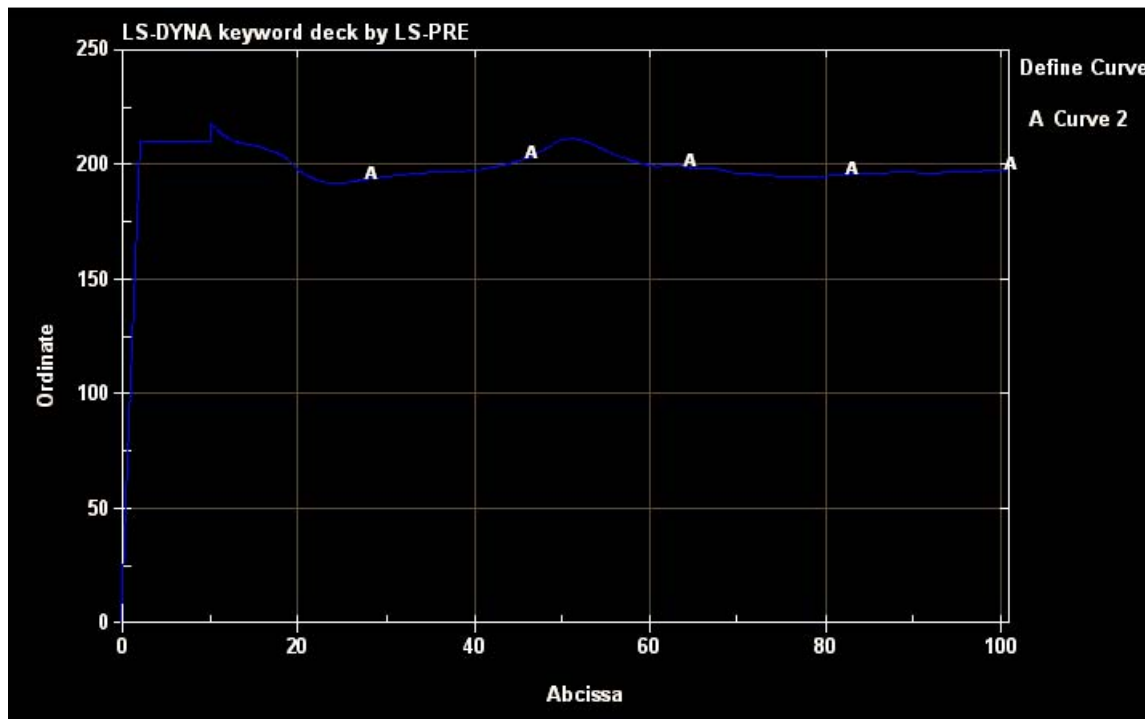


Figure 24. Cornell model: Time history of the input velocity (ordinate is u in inches/sec, abscissa is time t in sec).

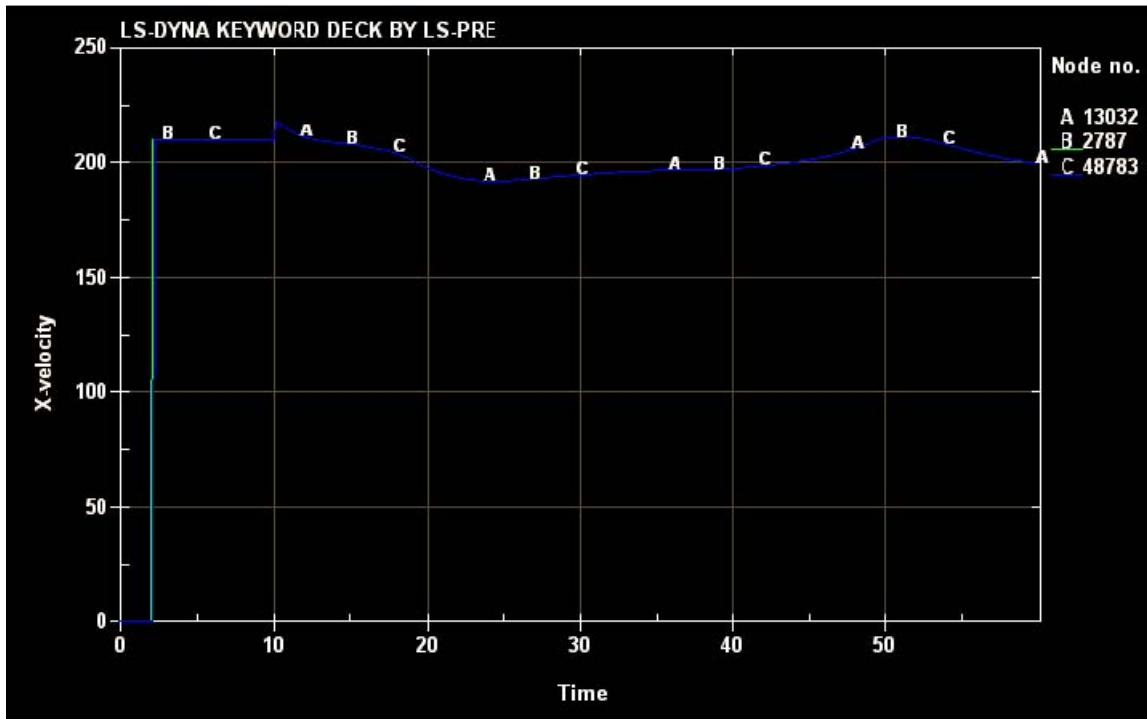


Figure 25. Cornell model: Confirmation of the input velocity u from post-processing (ordinate is u in inches/sec, abscissa is time t in sec).

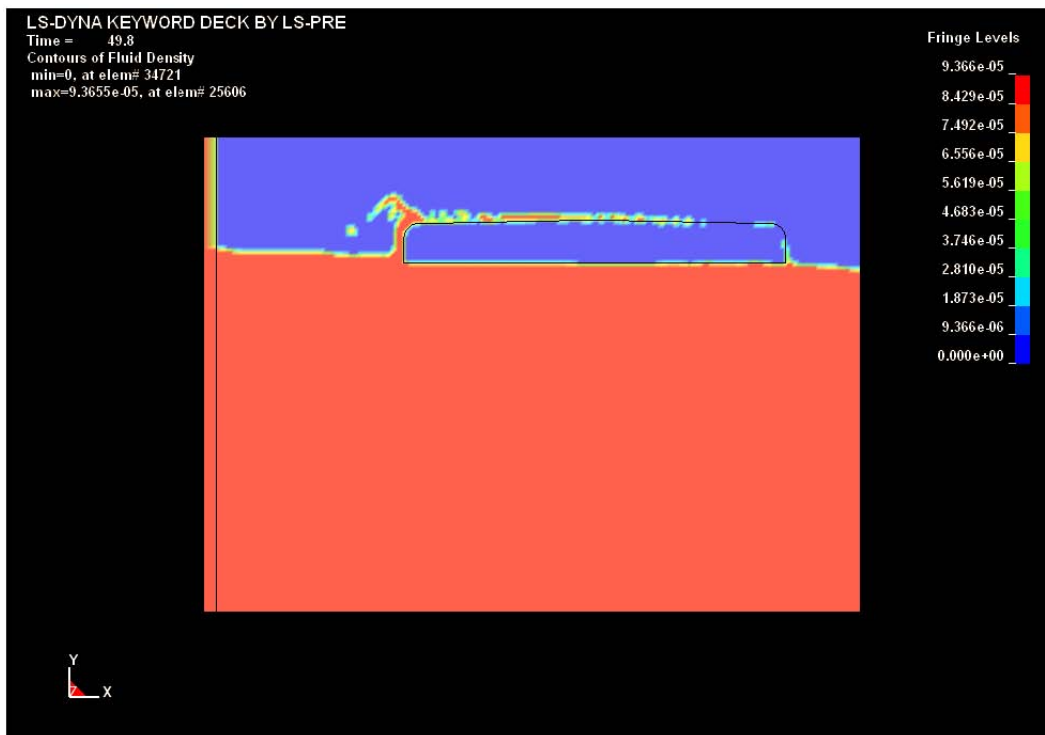


Figure 26. Cornell model: screen shot at $t=49.8$ sec.

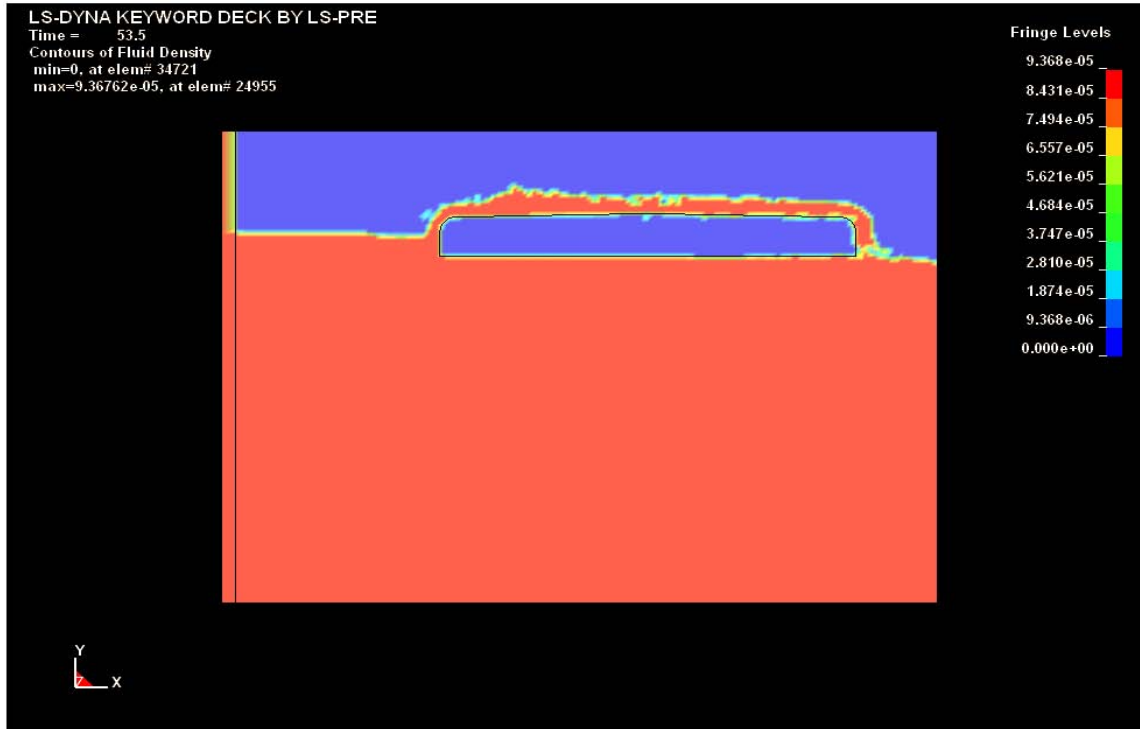


Figure 27. Cornell model: screen shot at t=53.5 sec.

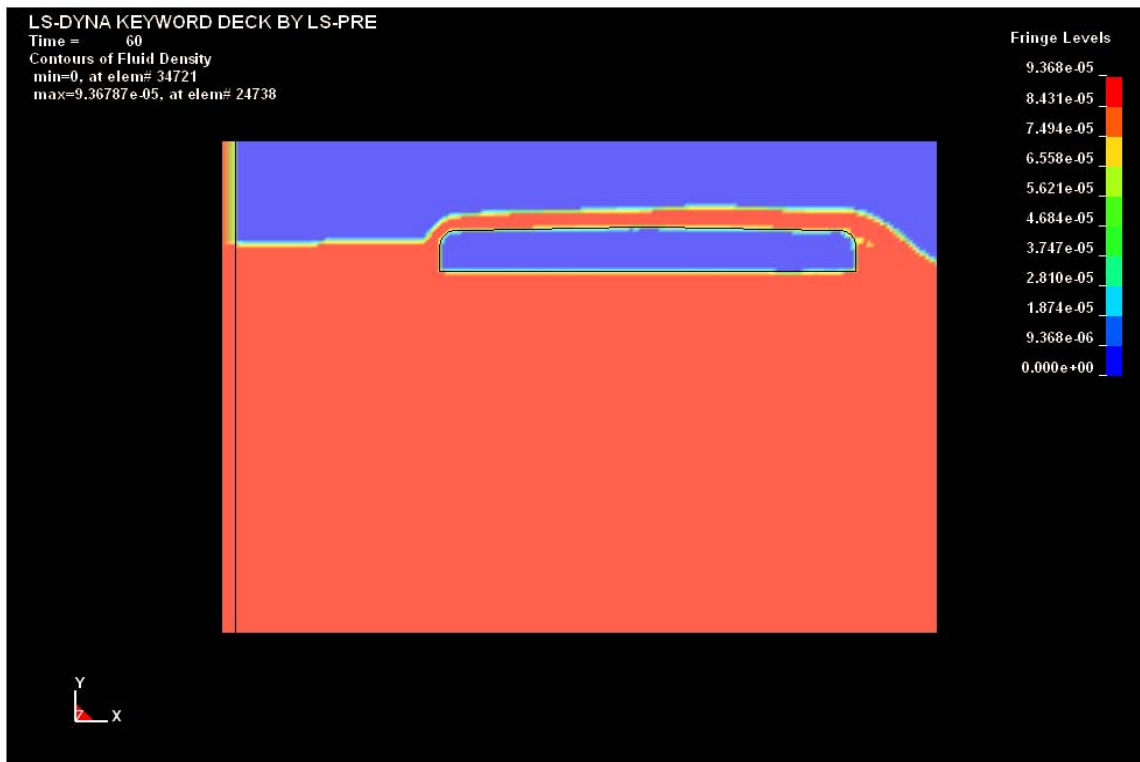


Figure 28. Cornell model: screen shot at t=60 sec.

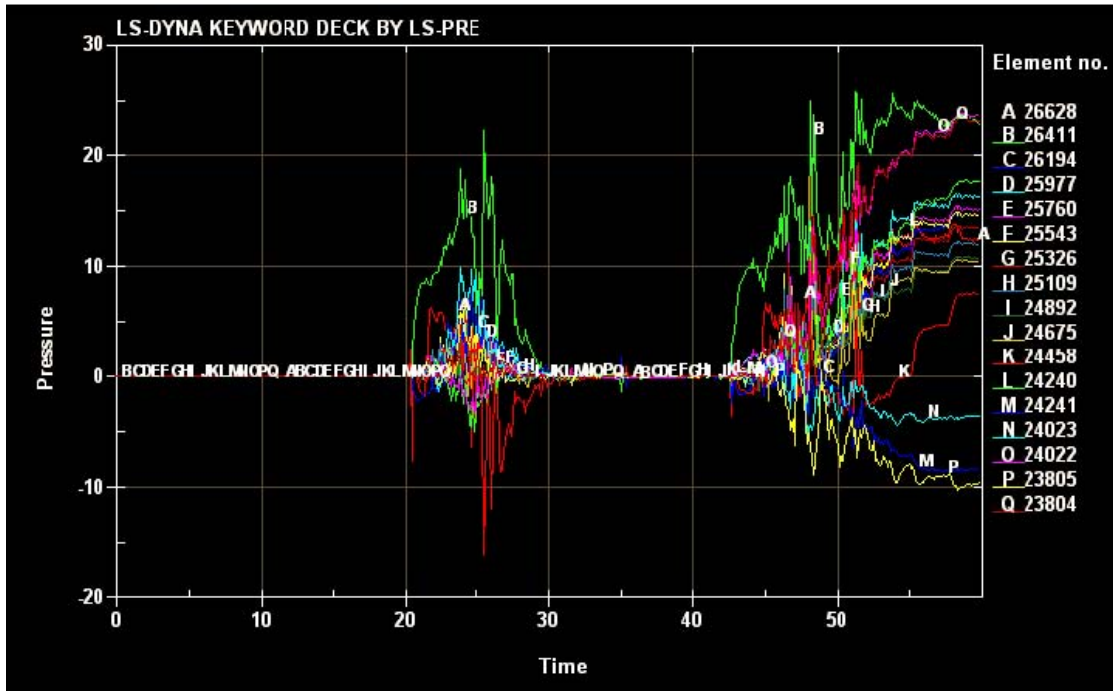


Figure 29. Cornell model: pressures (in psi) near the face (toward the tsunami) of the deck.

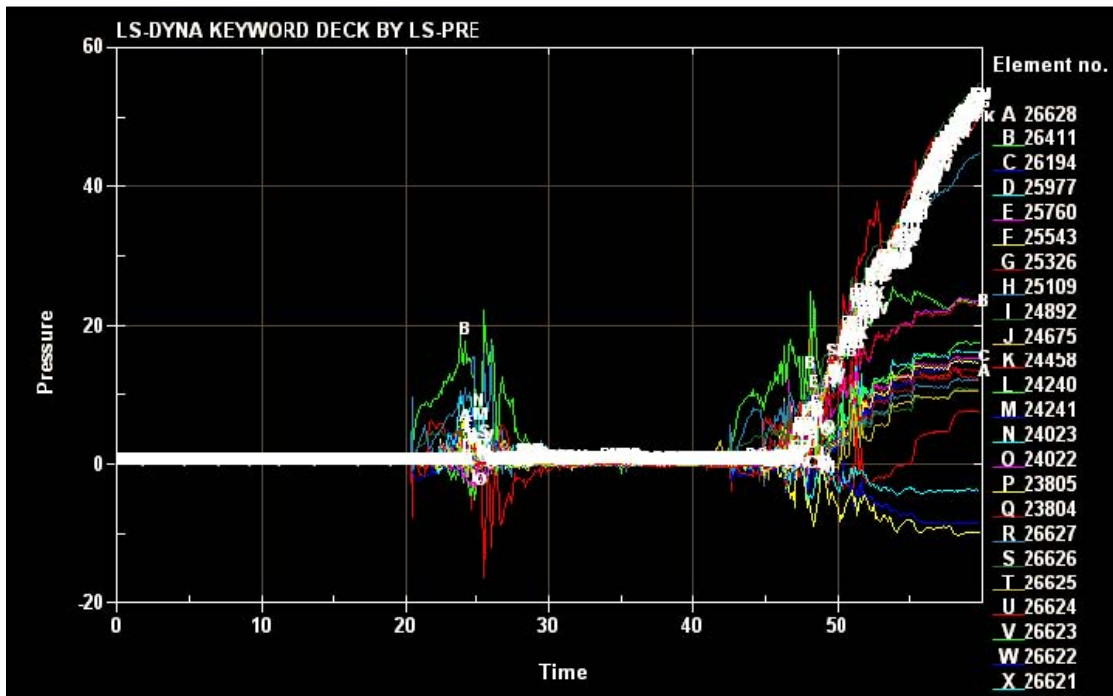


Figure 30. Cornell model: The plot of the pressures (in psi) including both the front and bottom faces of the bridge deck; the white line corresponds to several elements on bottom face having same magnitude of pressure.

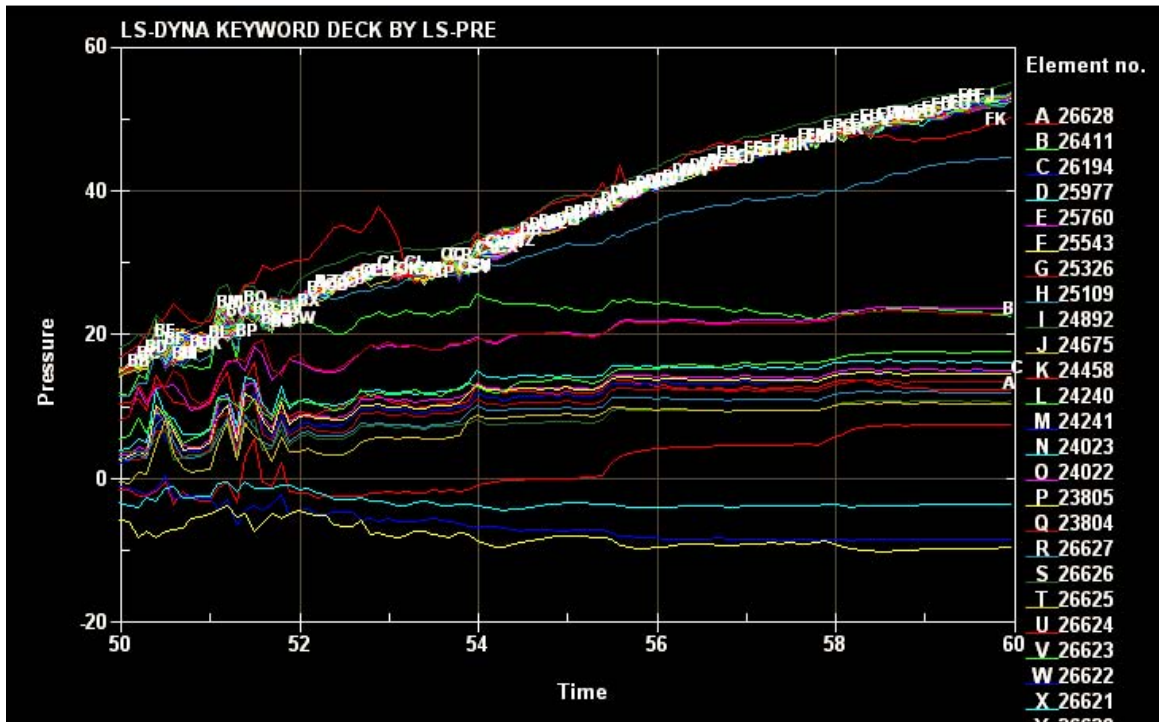


Figure 31. Cornell model: A “closer” examination of the pressures (in psi) between $t = 50$ and 60 sec; the white line corresponds to several elements on bottom face having same magnitude of pressure.

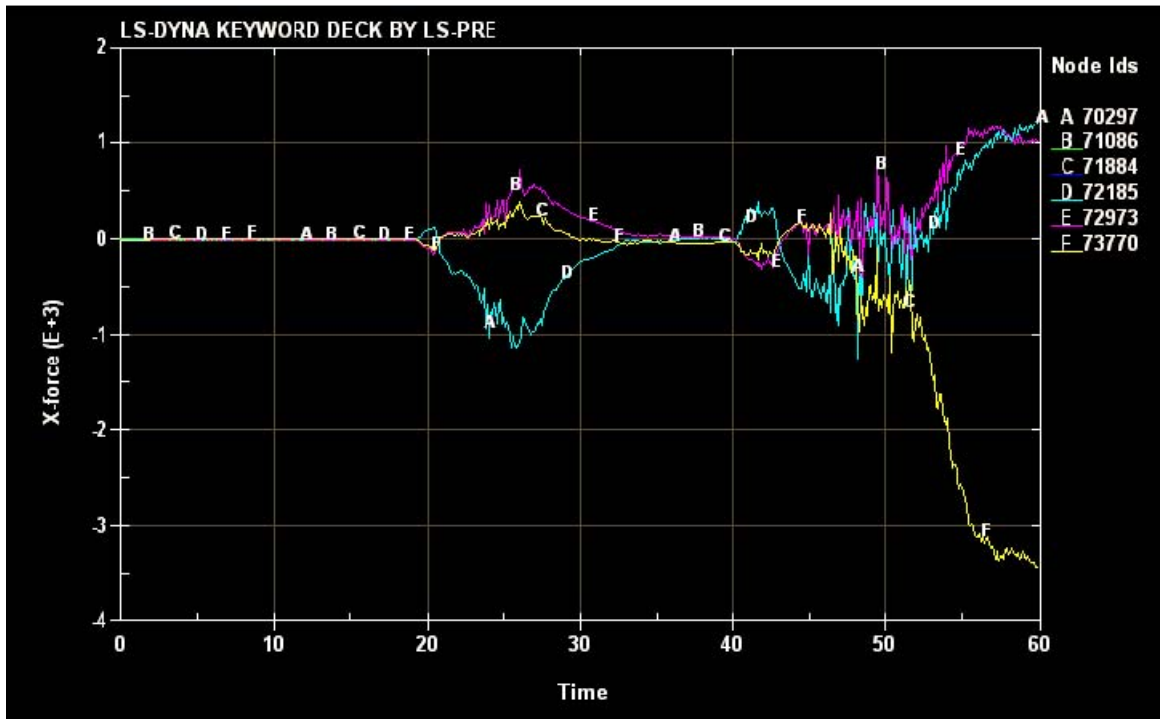


Figure 32. Cornell model: Support reactions (lb(f) per 3 inch sectional thickness) in X-direction (node numbers are labeled in Figures 16-17).

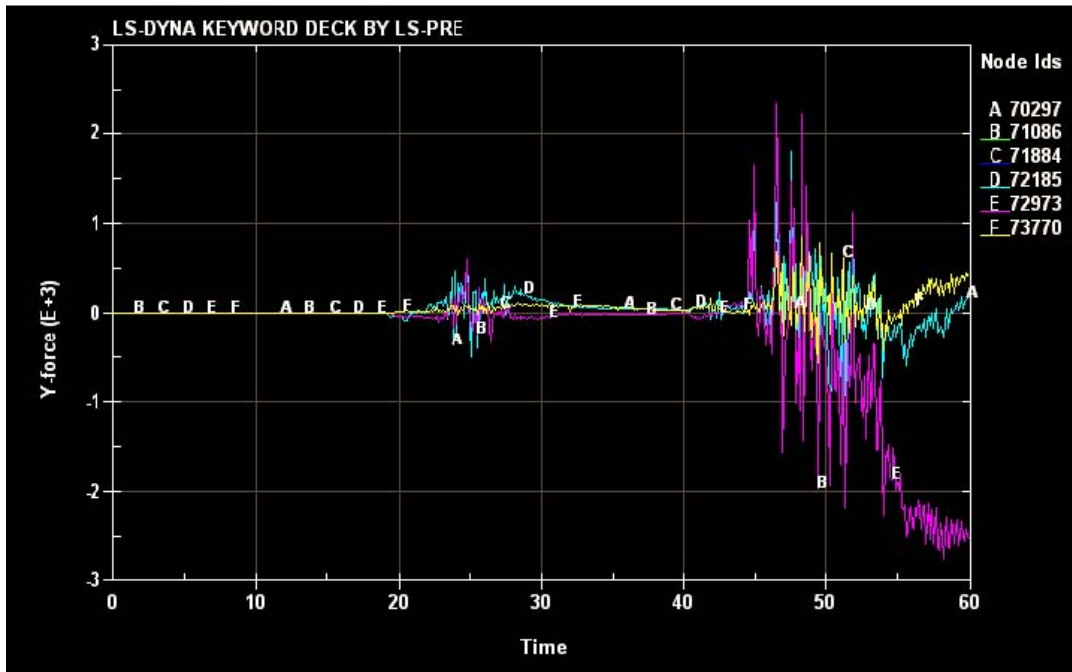


Figure 33. Cornell model: Support reactions (lb(f) per 3 inch sectional thickness) in Y-direction (node numbers are labeled in Figures 16-17).

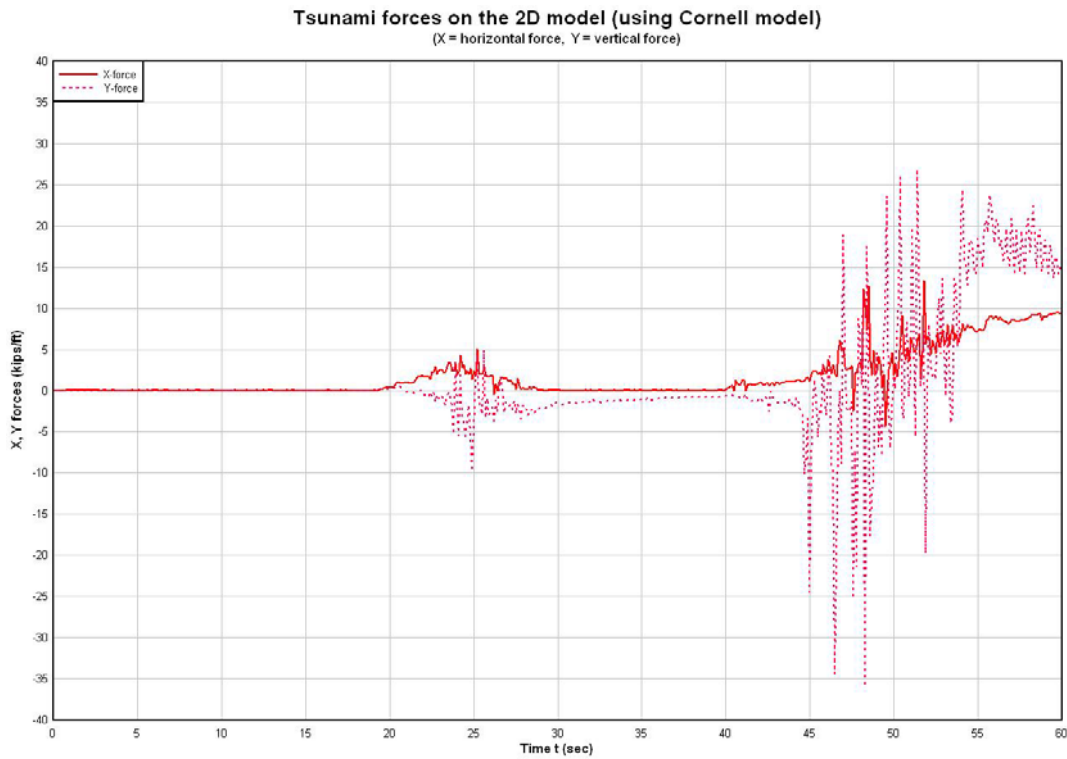


Figure 34. Cornell model: Tsunami forces (kips/ft) on the deck in both horizontal & vertical directions

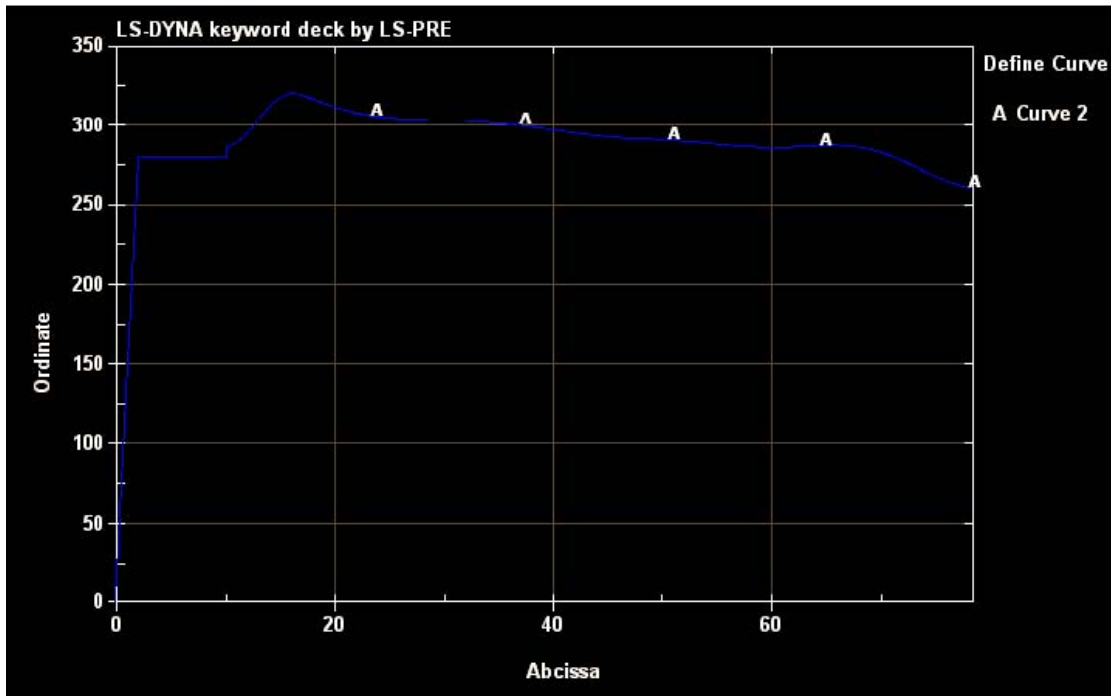


Figure 35. FVWAVE model: Time history of the input velocity (ordinate is u in inches/sec, abscissa is time t in sec)).

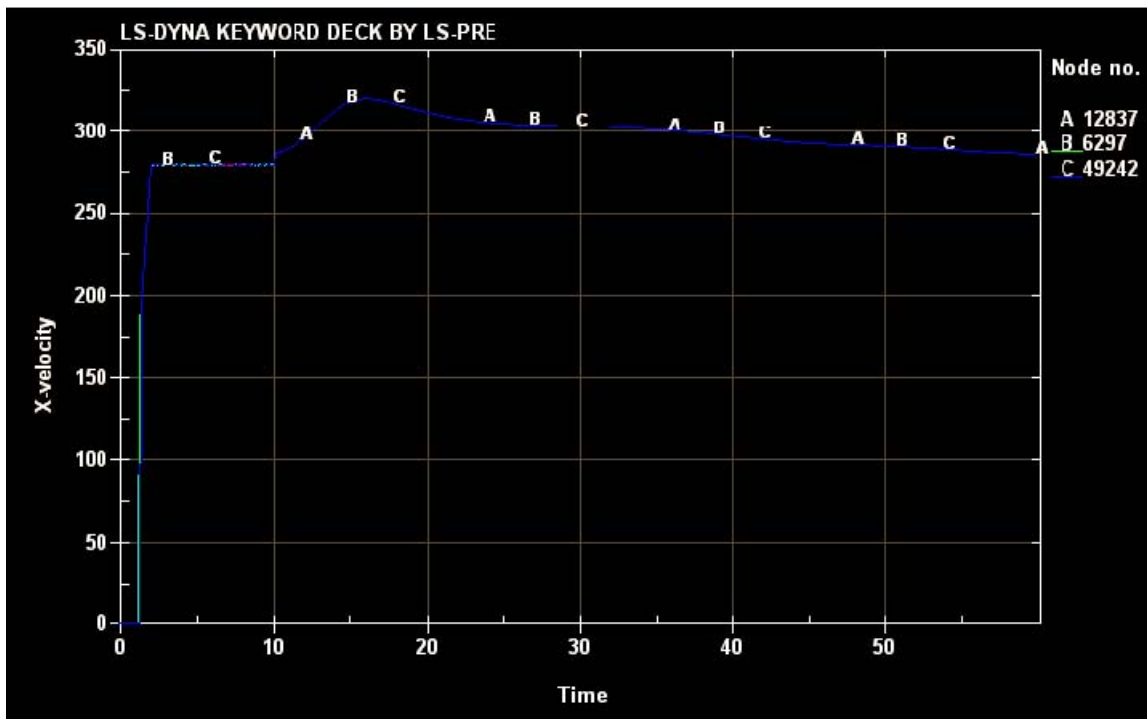


Figure 36. FVWAVE model: Confirmation of the input velocity u from post-processing (ordinate is u in inches/sec, abscissa is time t in sec).

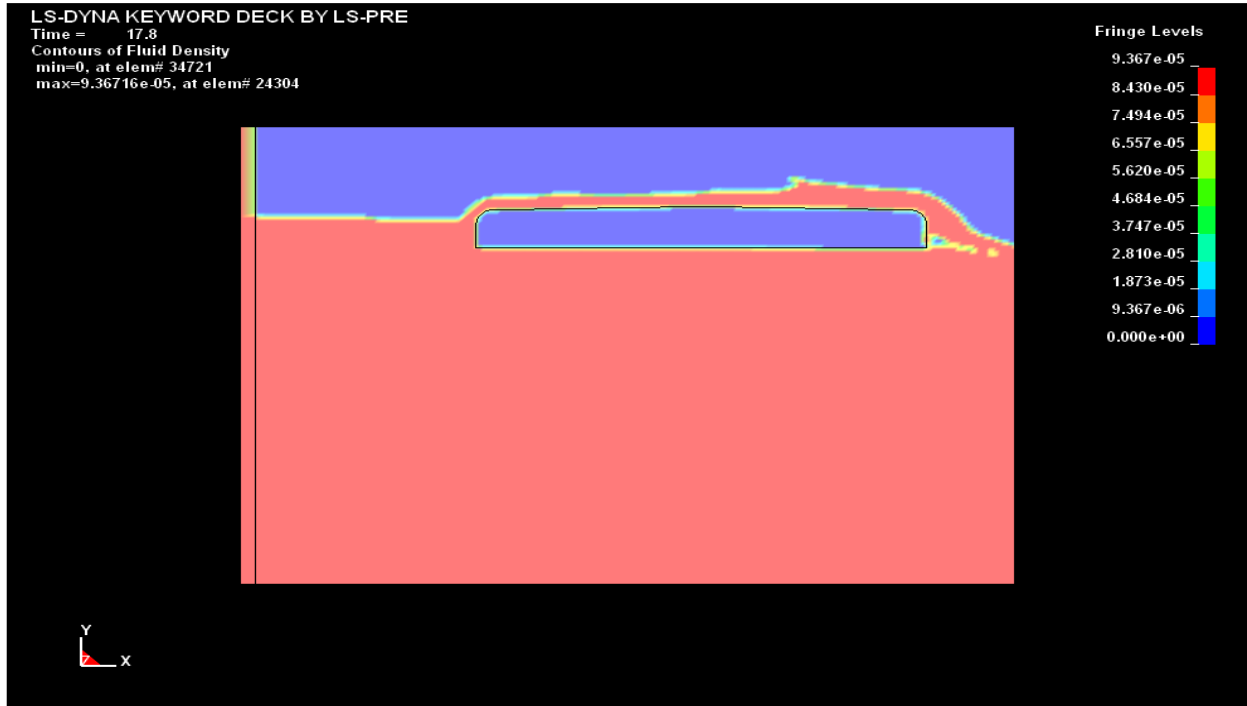


Figure 37. FVWAVE model: screen shot at t=17.8 sec.

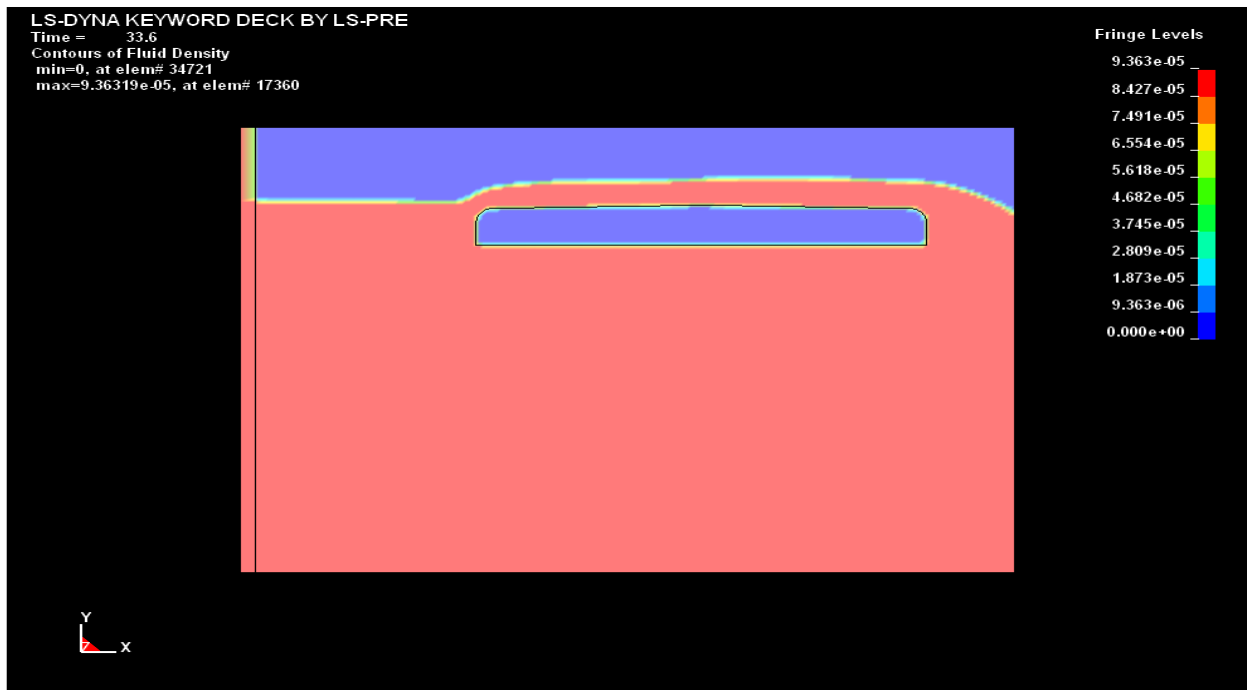


Figure 38. FVWAVE model: screen shot at t=33.6 sec.

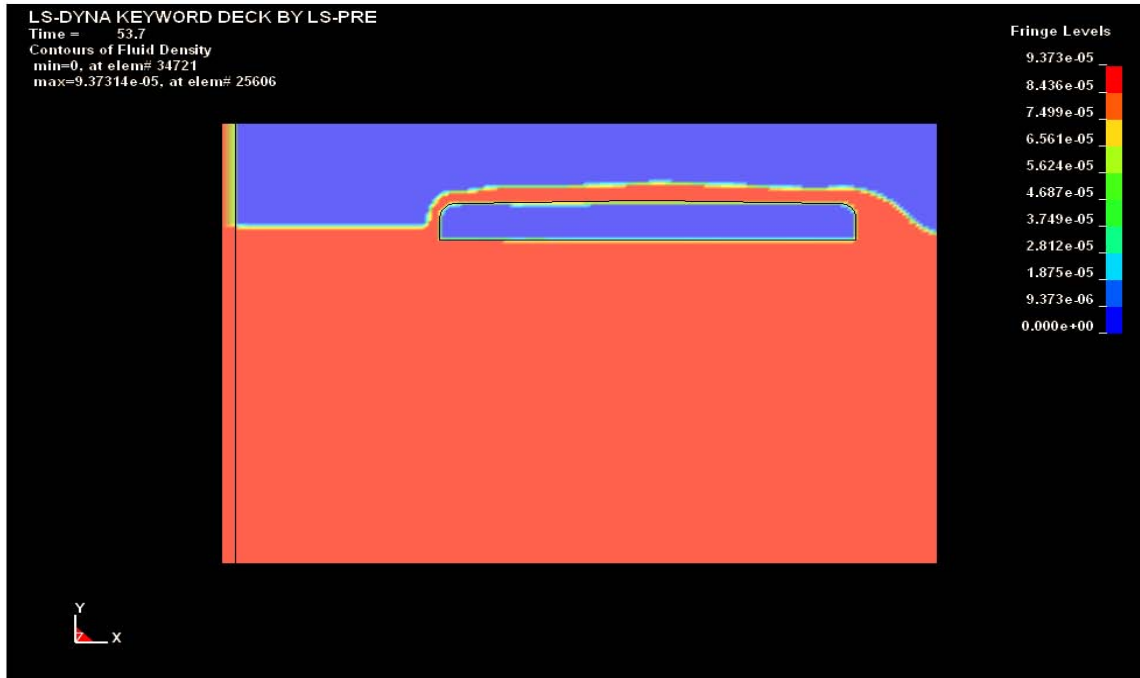


Figure 39. FVWAVE model: screen shot at t=53.7 sec.

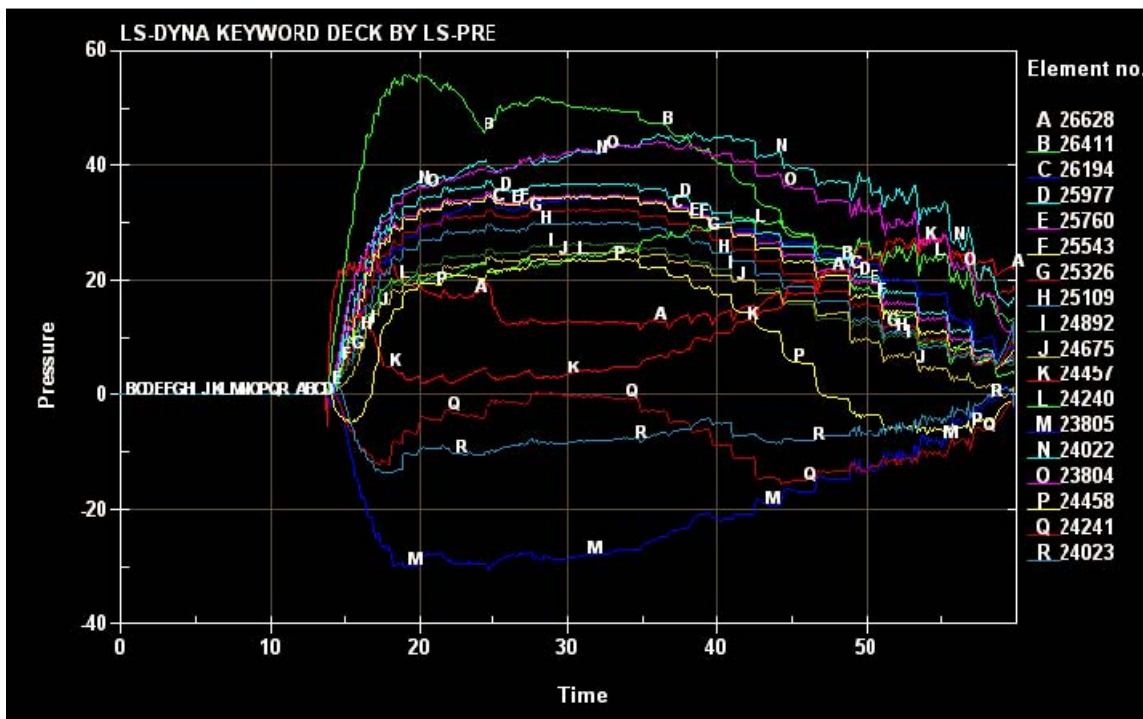


Figure 40. FVWAVE model: pressures (in psi) near the face (toward the tsunami) of the deck.

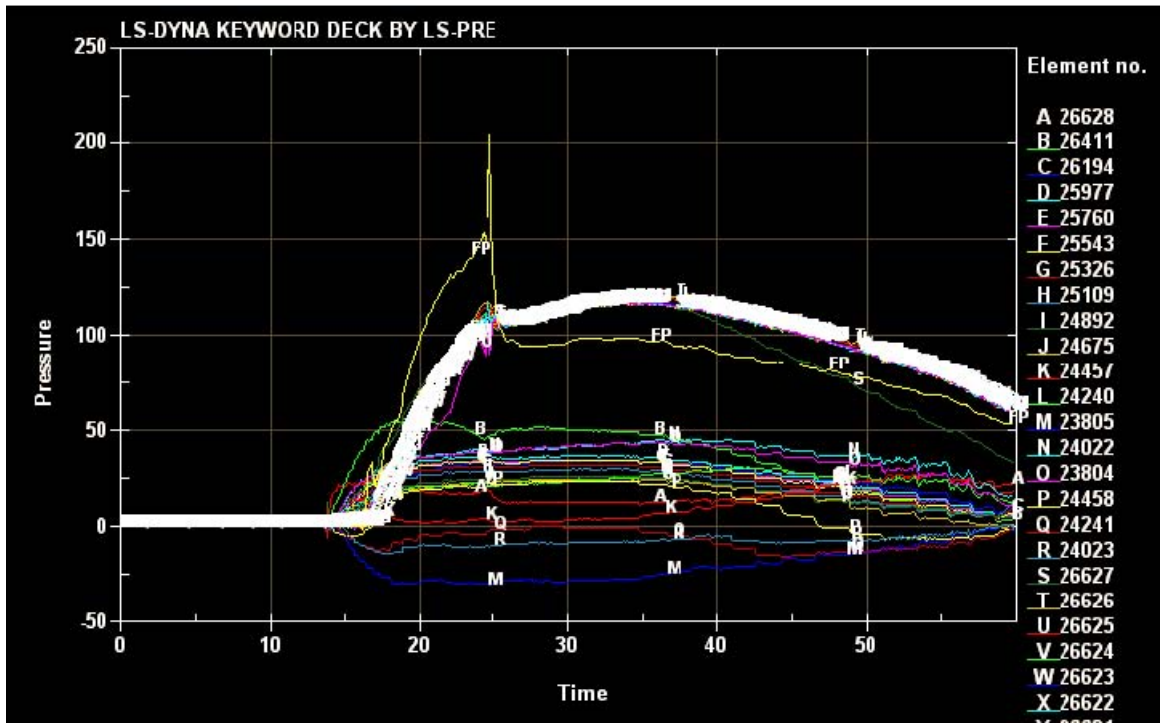


Figure 41. FVWAVE model: The plot of the pressures (in psi) including both the front and bottom face of the bridge deck; the white line corresponds to several elements on bottom face having same magnitude of pressure.

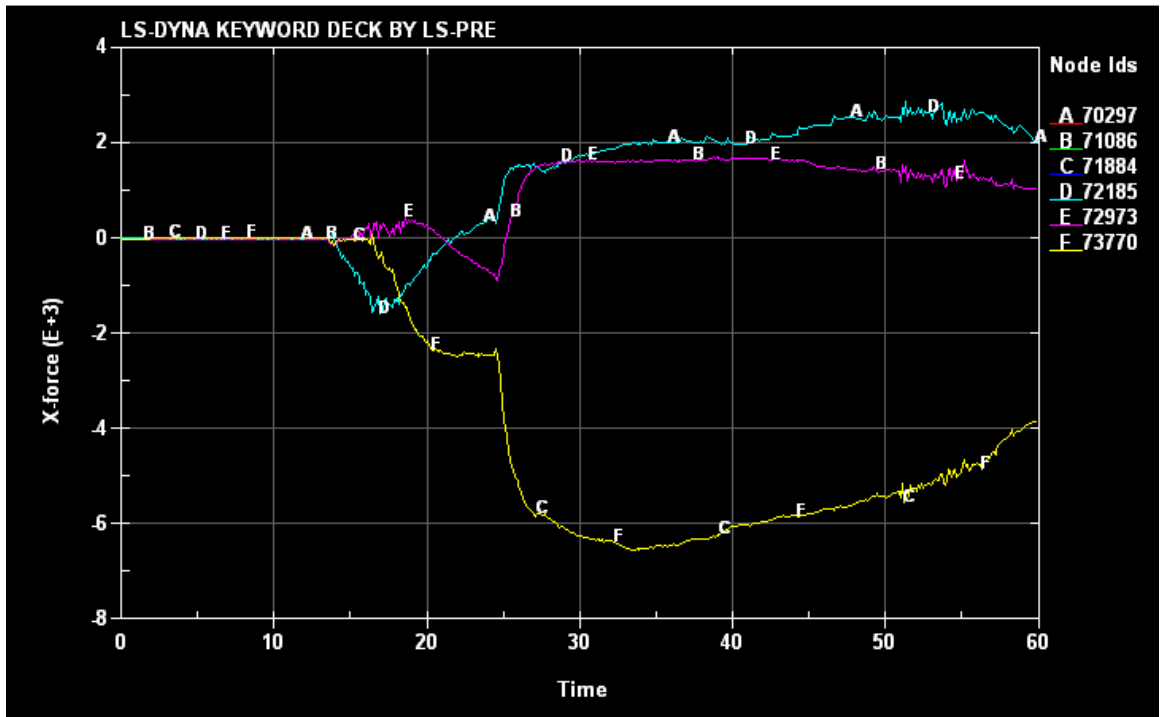


Figure 42. FVWAVE model: Support reactions (lb(f) per 3 inch sectional thickness) in X-direction.

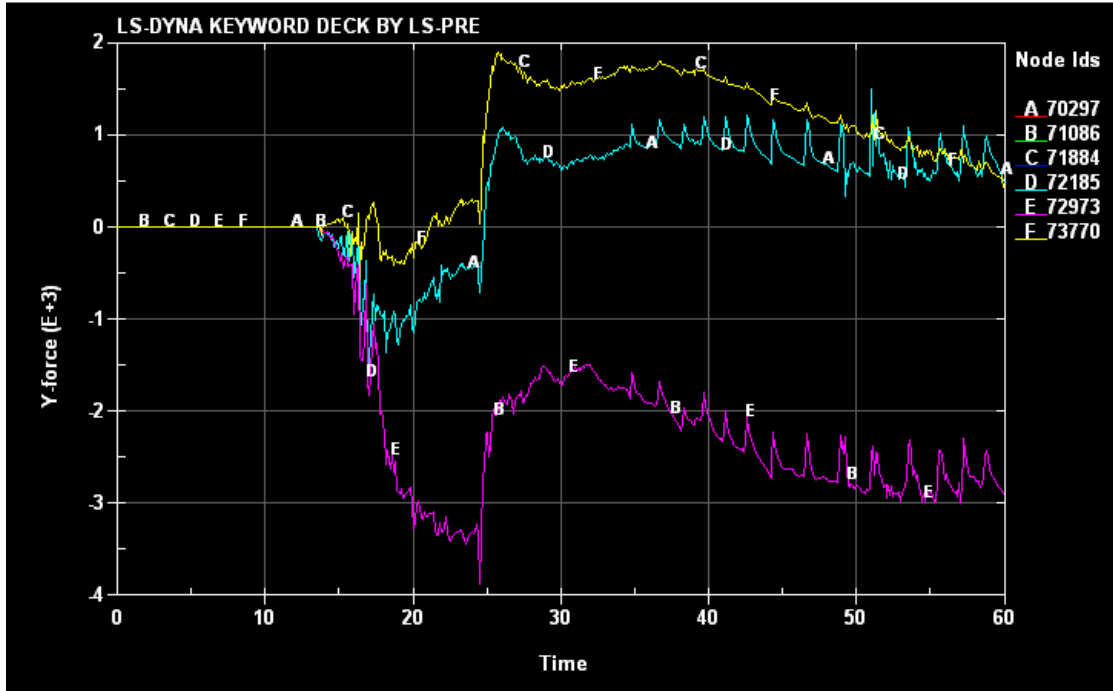


Figure 43. FVWAVE model: Support reactions (lb(f) per 3 inch sectional thickness) in Y-direction.

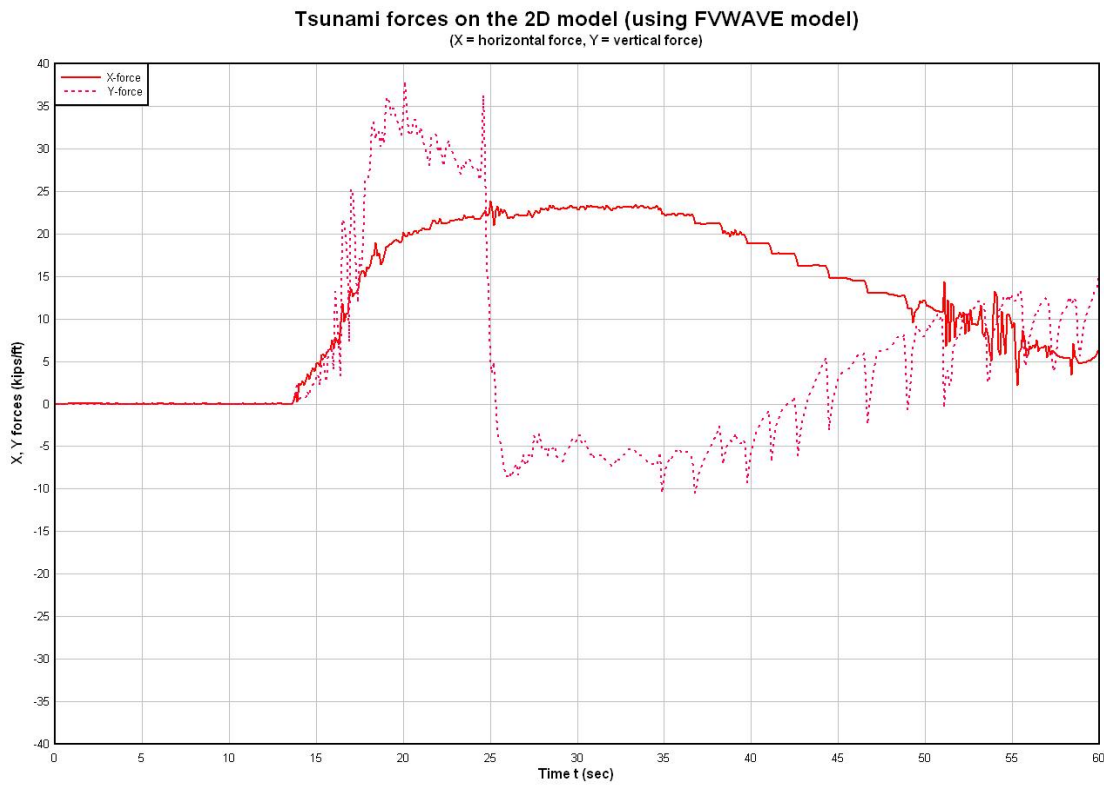


Figure 44. FVWAVE model: Tsunami forces (kips/ft) on the deck in both horizontal & vertical directions

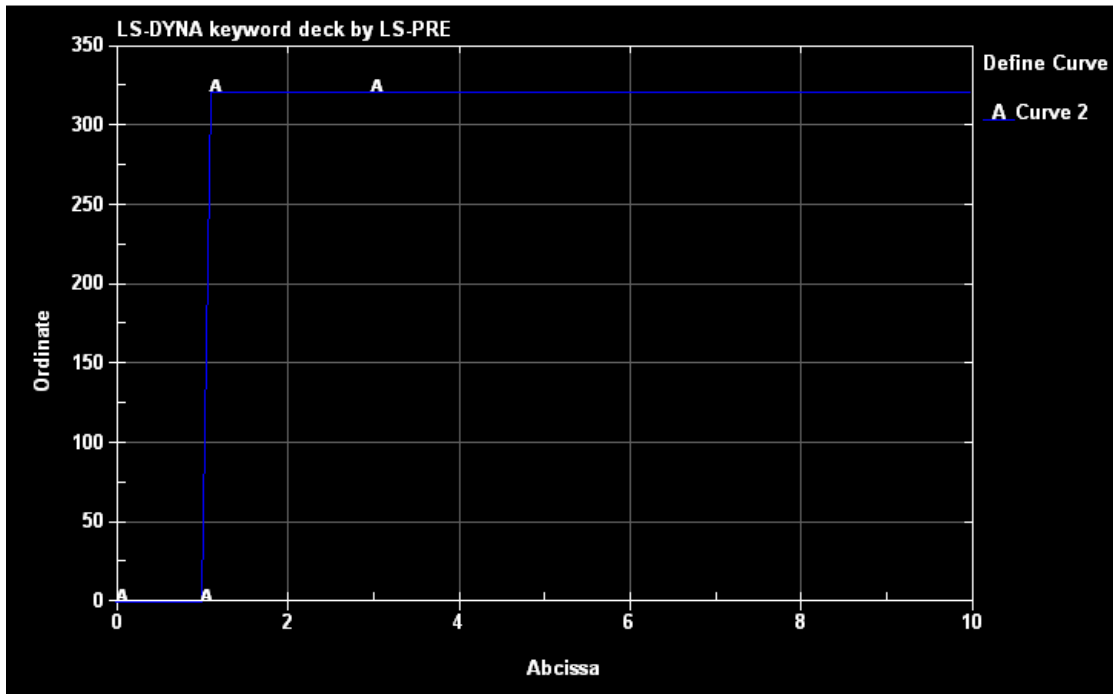


Figure 45. FVWAVE model (3D): Time history of the input velocity (ordinate is u in in/sec, abscissa is time t in sec).

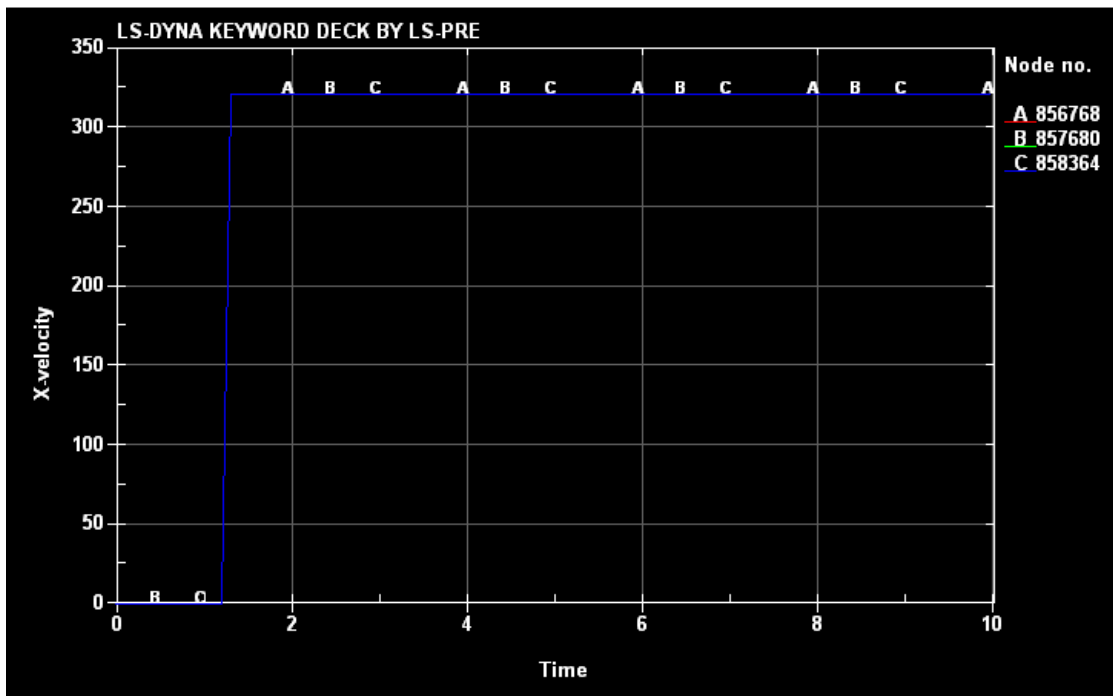


Figure 46. FVWAVE model (3D): Confirmation of the input velocity u (ordinate is u in in/sec, abscissa is t in sec) from post-processing.



Figure 47. FVWAVE model: screen shot at t=1.9 sec.



Figure 48. FVWAVE model: screen shot at t=2.2 sec.



Figure 49. FVWAVE model: screen shot at t=3 sec.

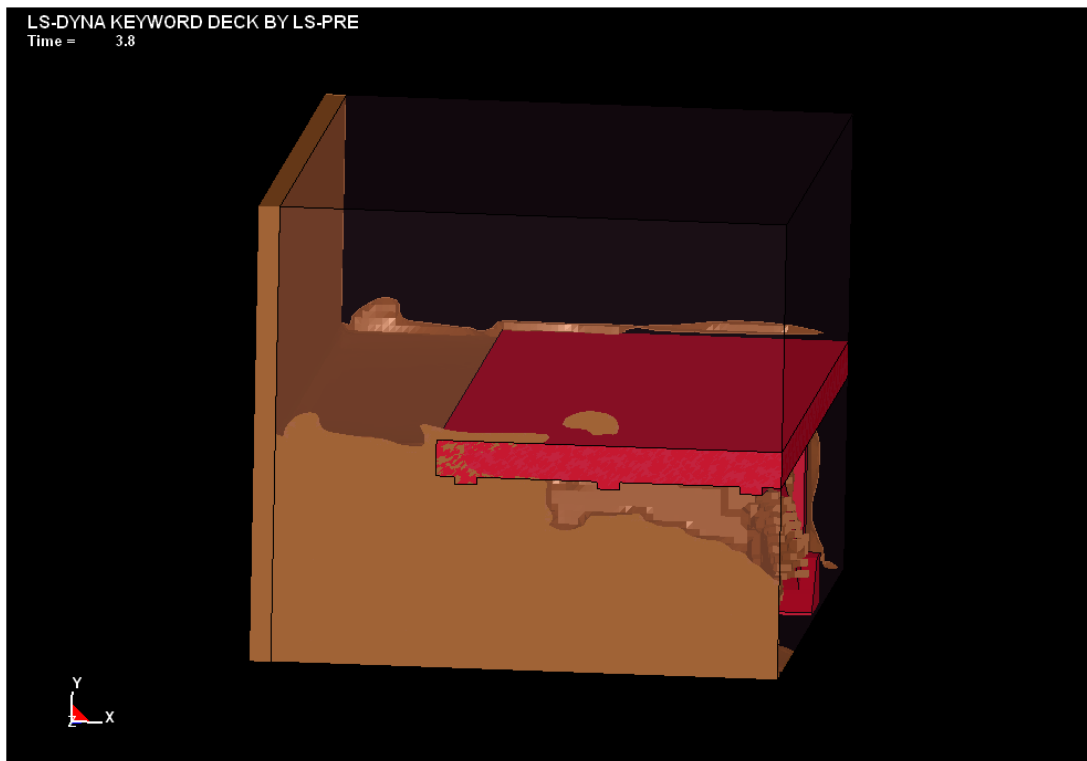


Figure 50. FVWAVE model: screen shot at t=3.8 sec.

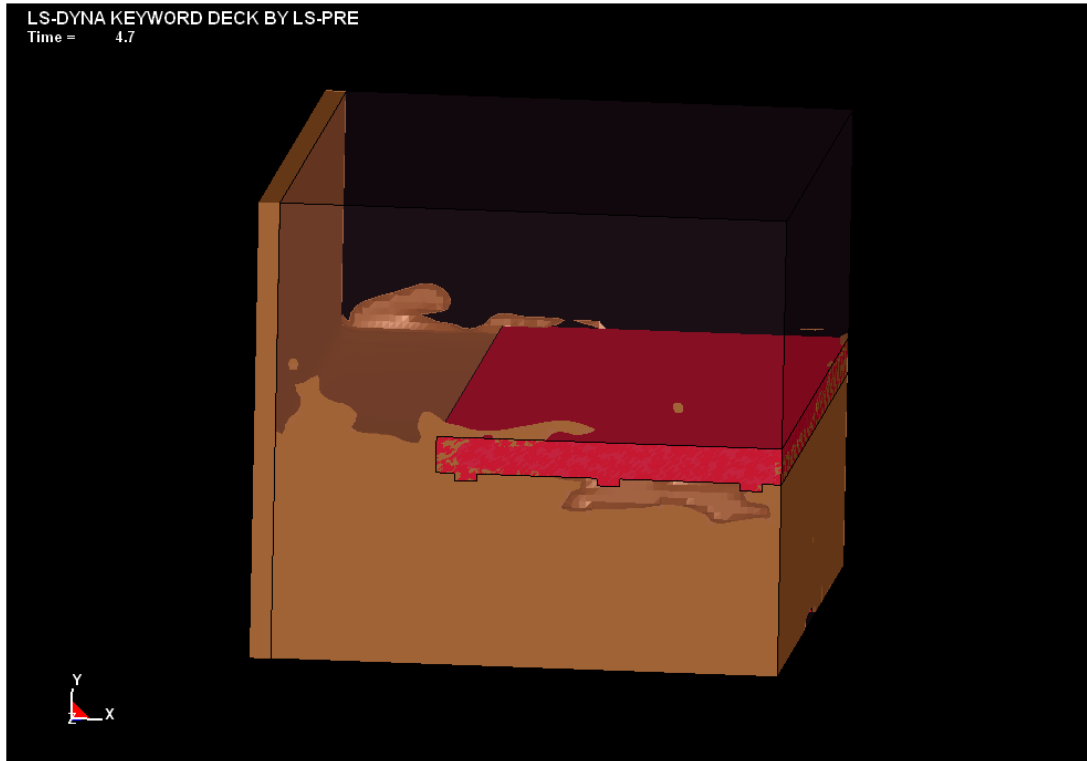


Figure 51. FVWAVE model: screen shot at t=4.7 sec.

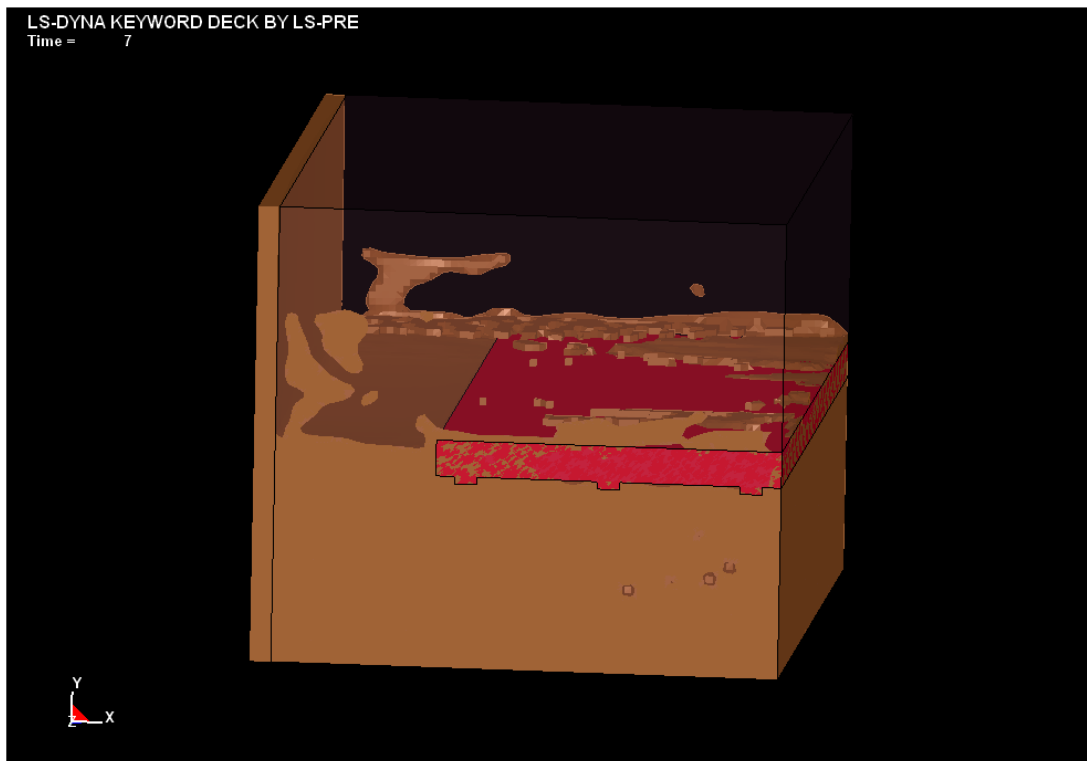


Figure 52. FVWAVE model: screen shot at t=7 sec.

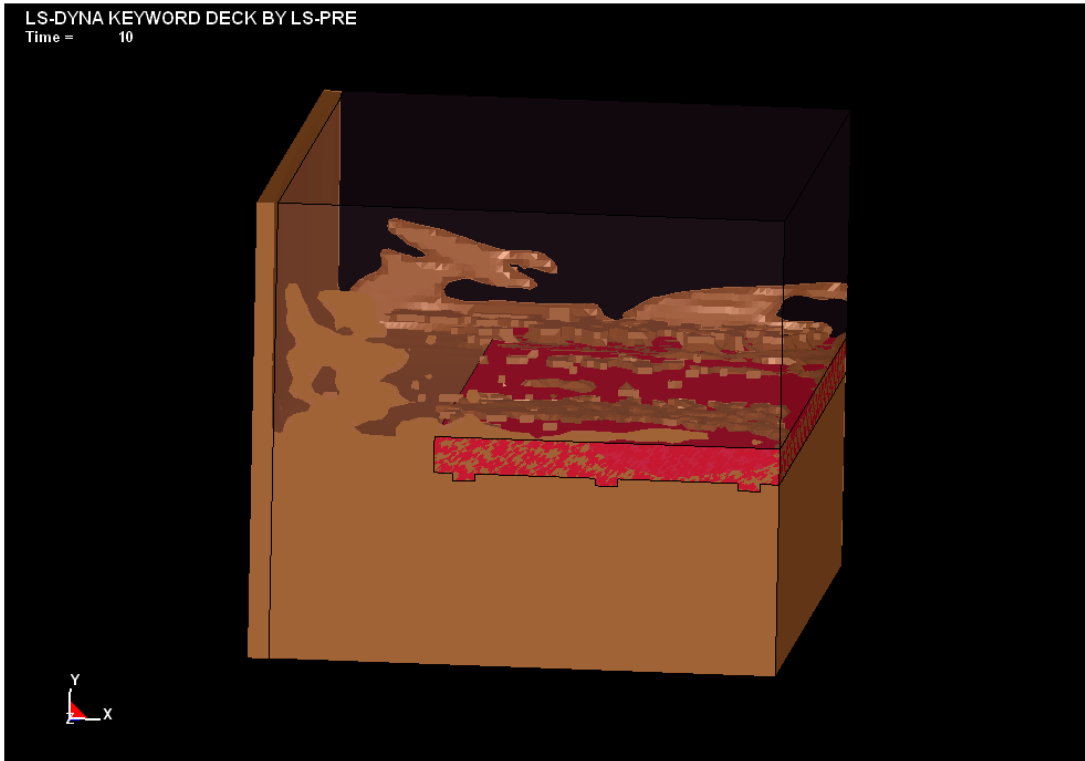
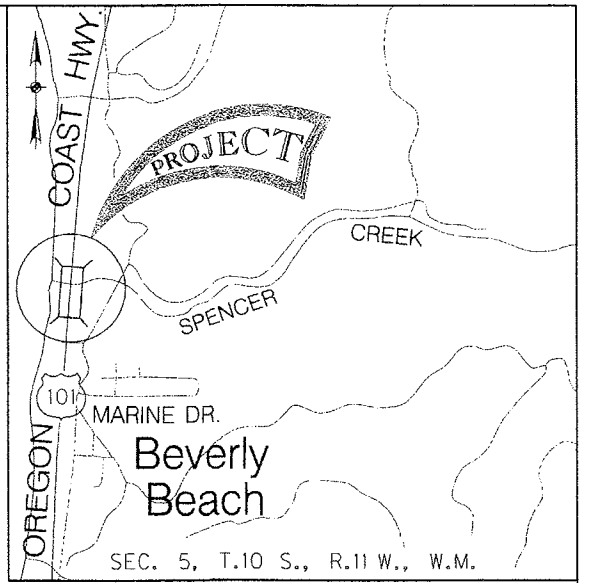
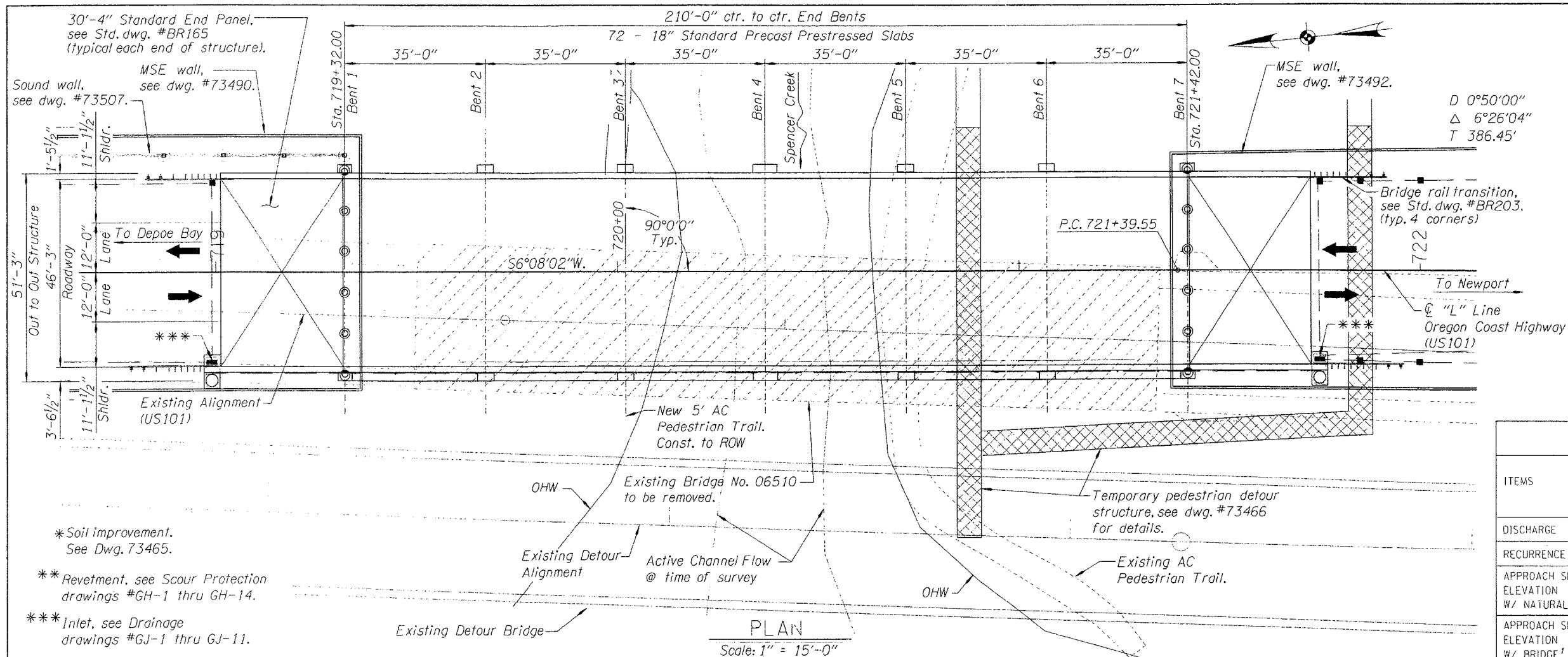


Figure 53. FVWAVE model: screen shot at t=10 sec.

Appendix-A



LOCATION MAP
No Scale

HYDRAULIC DATA						
ITEMS	(UNITS)	DESIGN FLOOD	BASE FLOOD	500 YEAR FLOOD	AVERAGE ANNUAL FLOOD	ORDINARY HIGH WATER ⁵
DISCHARGE	(ft ³ /s)	1300	1300	1600	430	430
RECURRENCE INTERVAL	(YRS.)	100	100	500	2	-
APPROACH SECTION H.W. ELEVATION W/ NATURAL CHANNEL ¹	(ft.)	19.6	19.6	20.4	16.7 (16.7)	-
APPROACH SECTION H.W. ELEVATION W/ BRIDGE ¹	(ft.)	19.6	19.6	20.4	16.7 (16.7)	21.3
BACKWATER	(ft.)	0.0	0.0	0.0	0.0	-
H.W. ELEV. AT UPSTREAM FACE OF BRIDGE ²	(ft.)	19.7	19.7	20.5	16.7 (16.7)	-
H.W. ELEV. AT DOWNSTREAM FACE OF BRIDGE ³	(ft.)	17.2	17.2	17.8	15.2 (15.7)	21.3
WATERWAY AREA AT DOWNSTREAM FACE OF BRIDGE ⁴	(ft ²)	120	120	150	51 (69)	-
AVERAGE VELOCITY AT DOWNSTREAM FACE OF BRIDGE	(ft/s)	11	11	11	8.4 (6.2)	-

¹ Approach section is one waterway opening width upstream from upstream face of bridge. Hydraulic grade line.

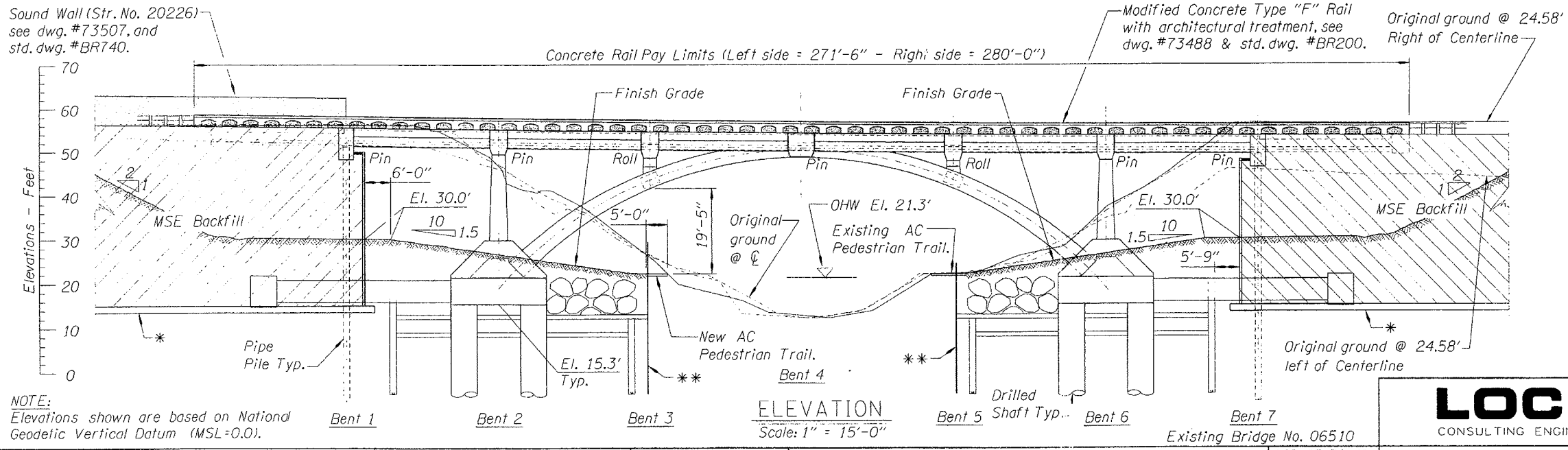
² Located at upstream face of bridge along the embankment. Energy grade line.

³ Located at downstream face of bridge opening. Hydraulic grade line.

⁴ Area normal to channel centerline. Waterway opening is unskewed.

⁵ Elevation includes wave runoff.

Elevations during the extreme winter check storm are in parenthesis.

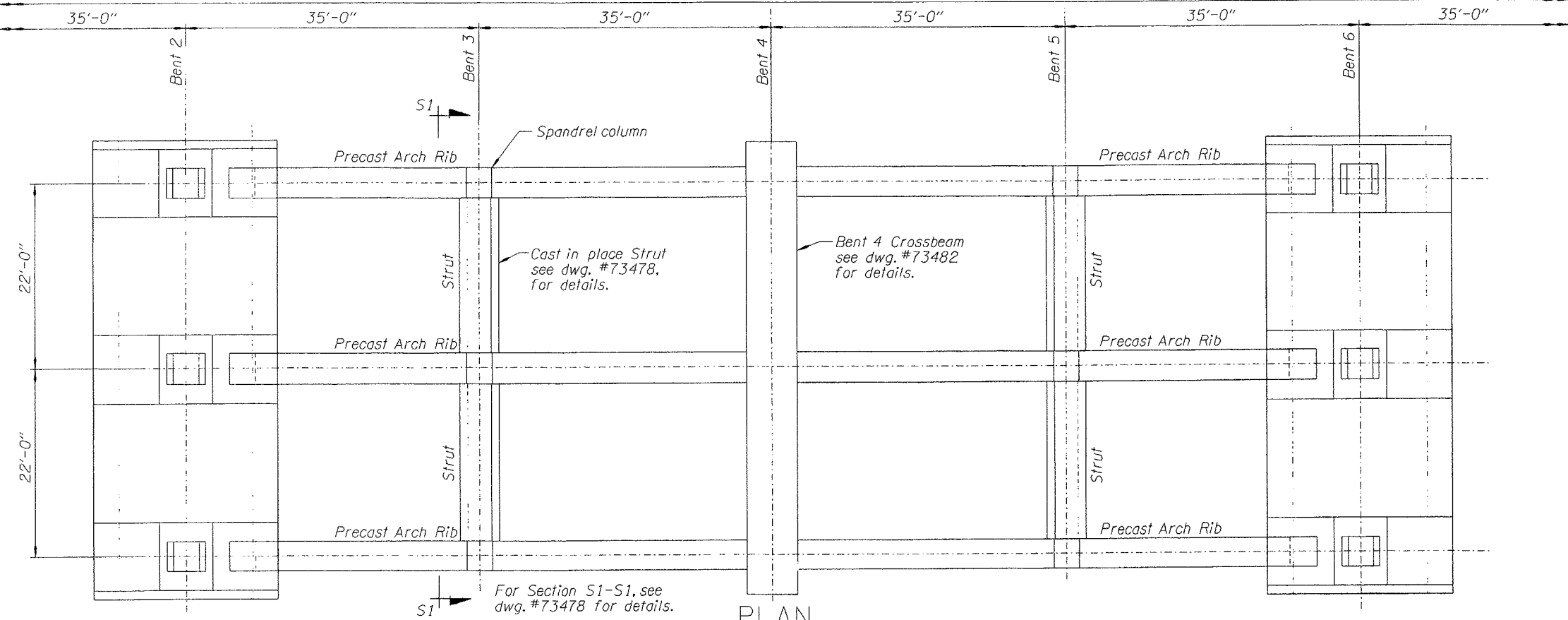


LOCHNER
CONSULTING ENGINEERS AND PLANNERS

2001 Front St. NE, Suite 120
Salem, Oregon 97303
(503) 586-0100 - Phone
(503) 589-9538 - FAX

DATE	REVISION	BY	DRAFTER: Sergio Chernishoff	CHECKER: Dan Minturn	DESIGNER: B. Koru / T. Potisuk	REVIEWER: Daniel J. McIntire	STRUCTURE NO. 20198	DATE 15-JUN-2006	CA.C. BOOK 5341	US101: SPENCER CREEK BRIDGE SEC. OREGON COAST HIGHWAY LINCOLN COUNTY	PLAN AND ELEVATION	SHEET 1 OF 46	DRAWING NO. 73462
------	----------	----	-----------------------------	----------------------	--------------------------------	------------------------------	---------------------	------------------	-----------------	--	--------------------	---------------	-------------------

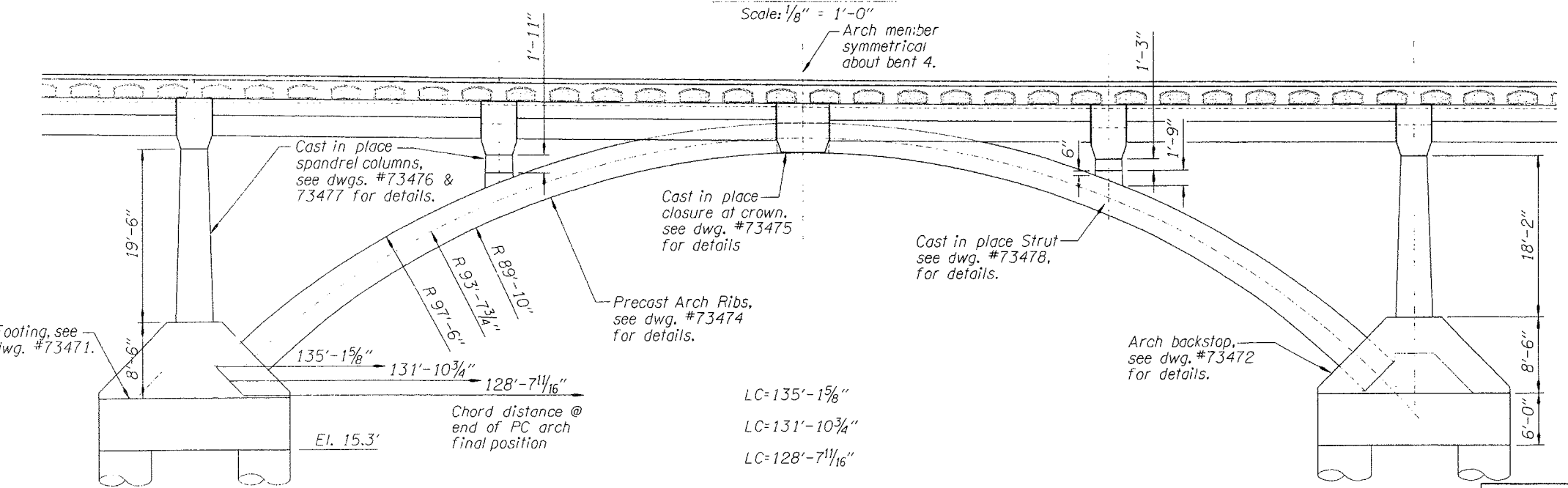
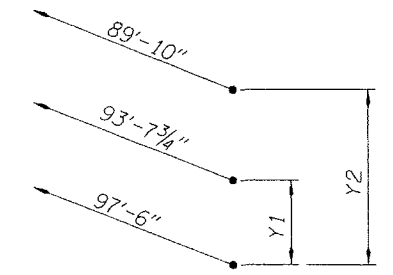
210'-0" ctr. to ctr. End Bents



ARCH GEOMETRY			
Location	Radius	Relative	
		X	Y
Top	97'-6"	0	0
℄	93'-7 ³ / ₄ "	0	2'-2"
Bottom	89'-10"	0	4'-4"

PLAN

Scale: 1/8" = 1'-0"



ELEVATION

Scale: 1/8" = 1'-0"

LOCHNER
CONSULTING ENGINEERS AND PLANNERS

2001 Front St. NE, Suite 120
Salem, Oregon 97303
(503) 586-0100 - Phone
(503) 589-9538 - FAX

DATE	REVISION	BY
		DRAFTER: <i>Sergie Chernishoff</i> Sergie Chernishoff
		CHECKER: <i>Dan Minturn</i> Dan Minturn
		DESIGNER: <i>B. Koru / T. Potisuk</i> B. Koru / T. Potisuk

REVIEWER

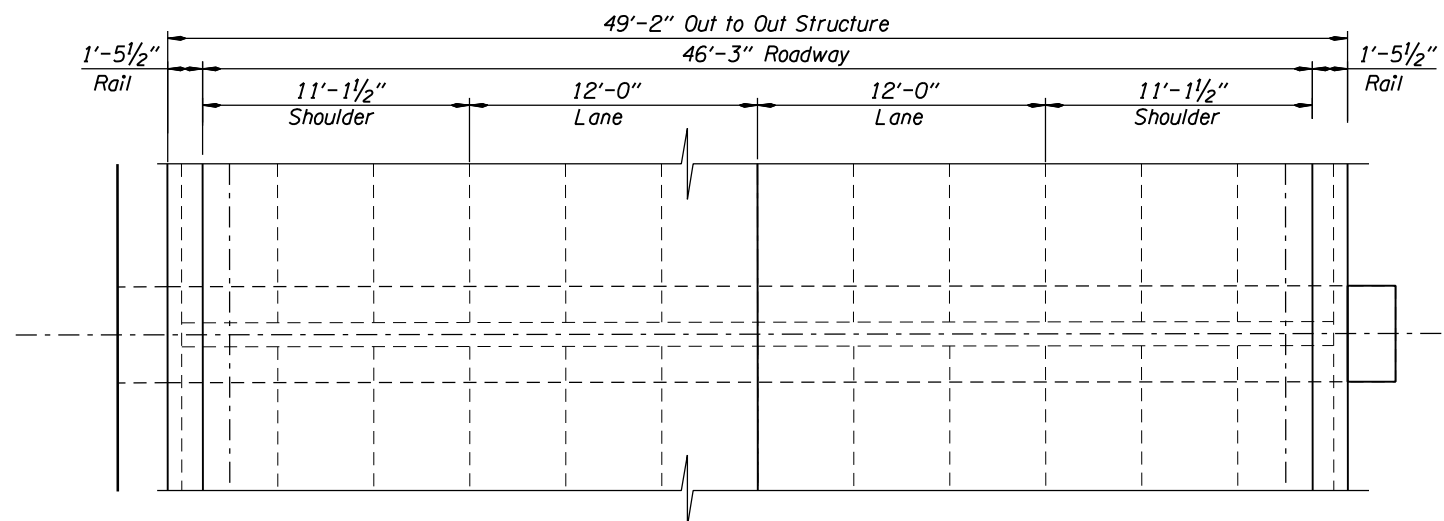
 DANIEL J. MCINTIRE
 EXPIRES: 12/31/06

OREGON DEPARTMENT OF TRANSPORTATION
 BRIDGE ENGINEERING

STRUCTURE NO. 20198
DATE 15-JUN-2006
CA: C. 300A 5341

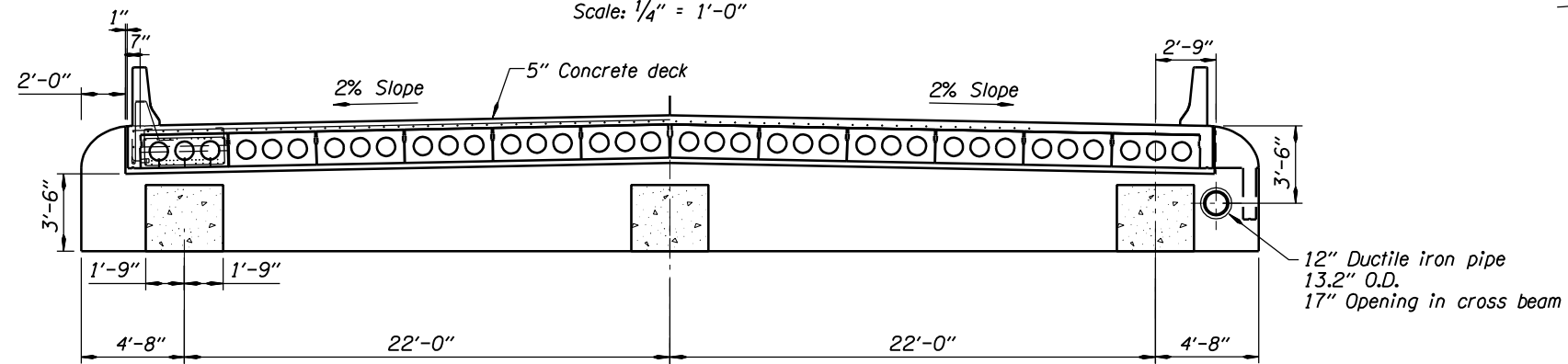
US101: SPENCER CREEK BRIDGE SEC.
ARCH: PLAN AND ELEVATION

SHEET 13 OF 46
DRAWING NO. 73473



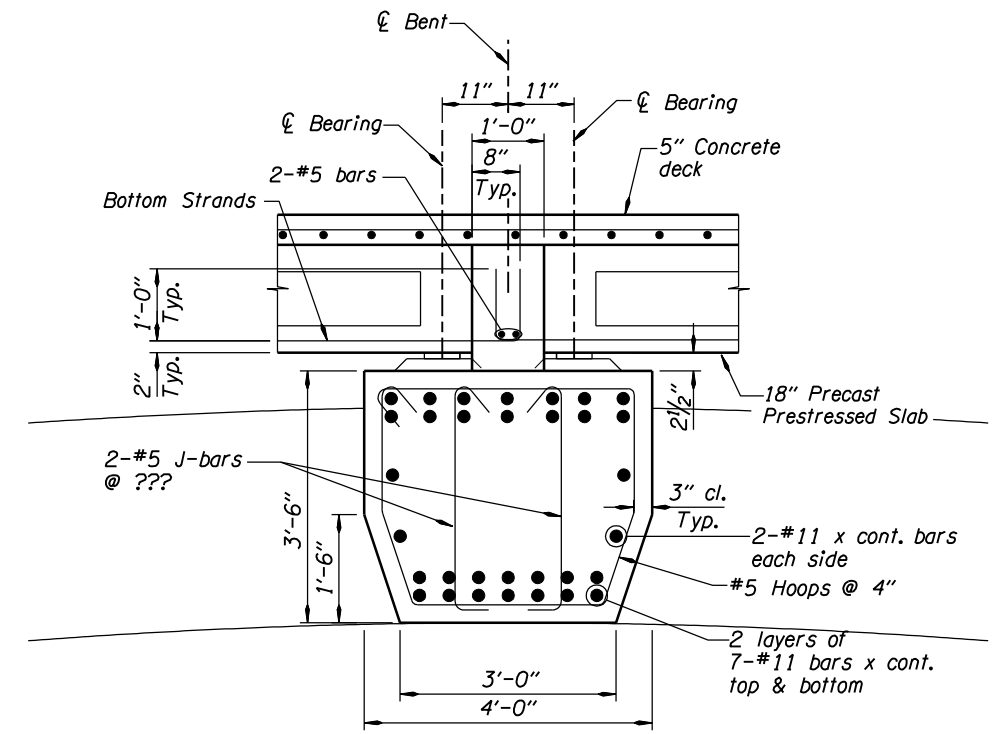
PLAN - BENT 4

Scale: 1/4" = 1'-0"



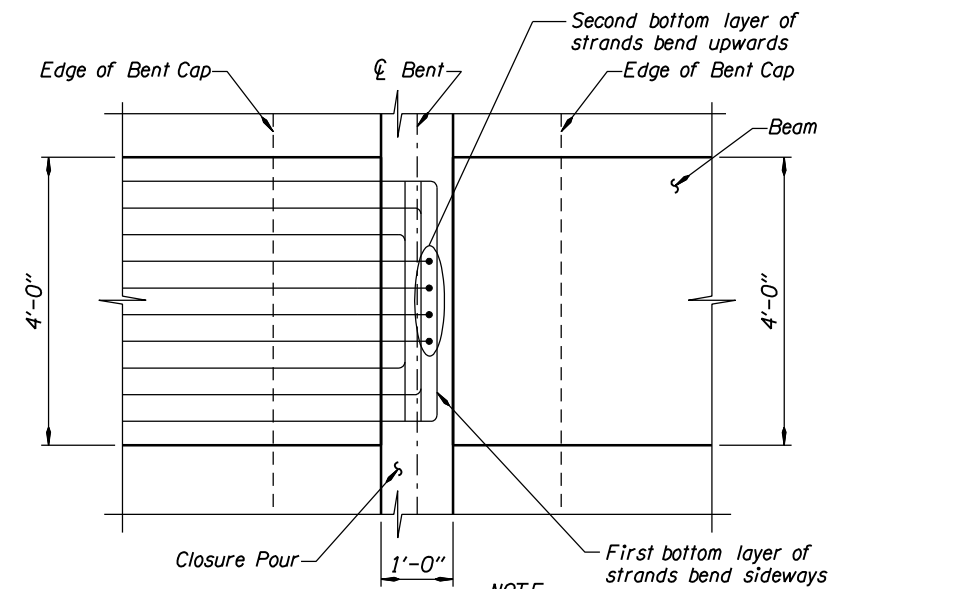
ELEVATION - BENT 4

Scale: 1/4" = 1'-0"



SECTION - BENT 4

Scale: 3/4" = 1'-0"



END STRAND PLACEMENT

Scale: 3/4" = 1'-0"

NOTE: Corresponding beam end strand placement are not shown for clarity.

LOCHNER
CONSULTING ENGINEERS AND PLANNERS

2001 Front St. NE, Suite 120
Salem, Oregon 97303
(503) 586-0100 - Phone
(503) 589-9538 - FAX

DATE	REVISION	BY

DRAFTER: *Sergie Chernishoff*
Sergie Chernishoff
CHECKER: Dan Minturn
DESIGNER: B. Koru / T. Potisuk

REVIEWER
REGISTERED PROFESSIONAL ENGINEER
74106PE
OREGON
JANUARY 13, 2004
DANIEL J. MCINTYRE
EXPIRES: 12/31/06

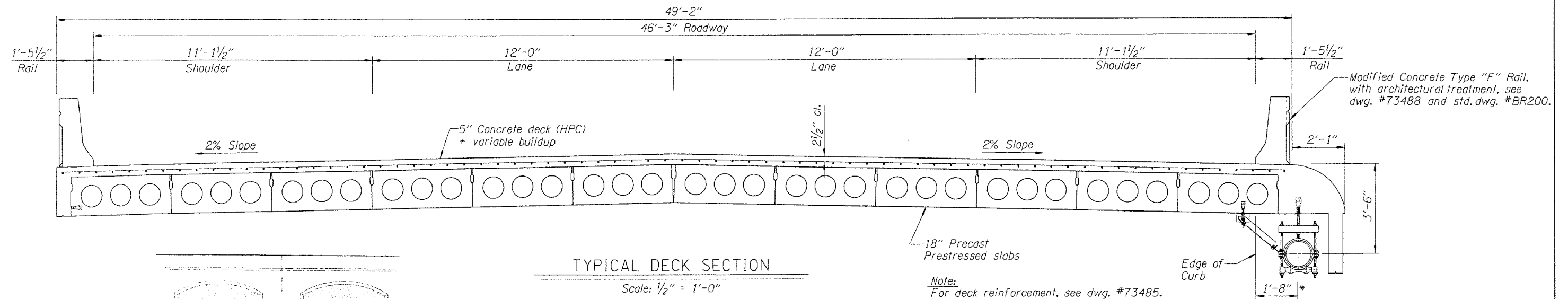
OREGON DEPARTMENT OF TRANSPORTATION
BRIDGE ENGINEERING

STRUCTURE NO.
20198
DATE
--DEC-2005
CALC. BOOK

SPENCER CREEK, HWY 9
BENT 4

SHEET
OF
DRAWING NO.
00000

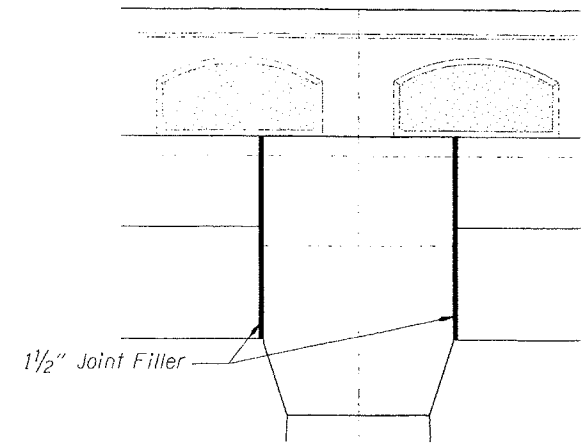
1/4" = 1'-0" - [BT4]



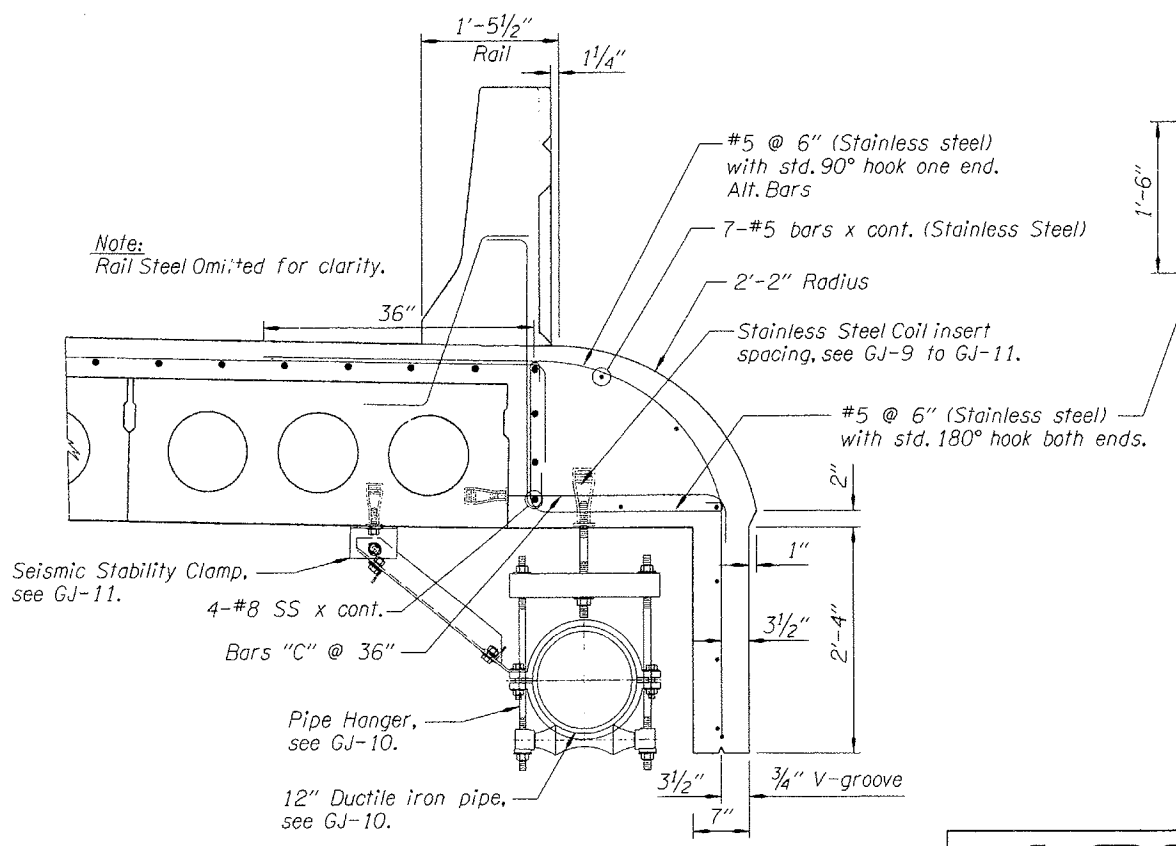
TYPICAL DECK SECTION
Scale: 1/2" = 1'-0"

Note:
For deck reinforcement, see dwg. #73485.

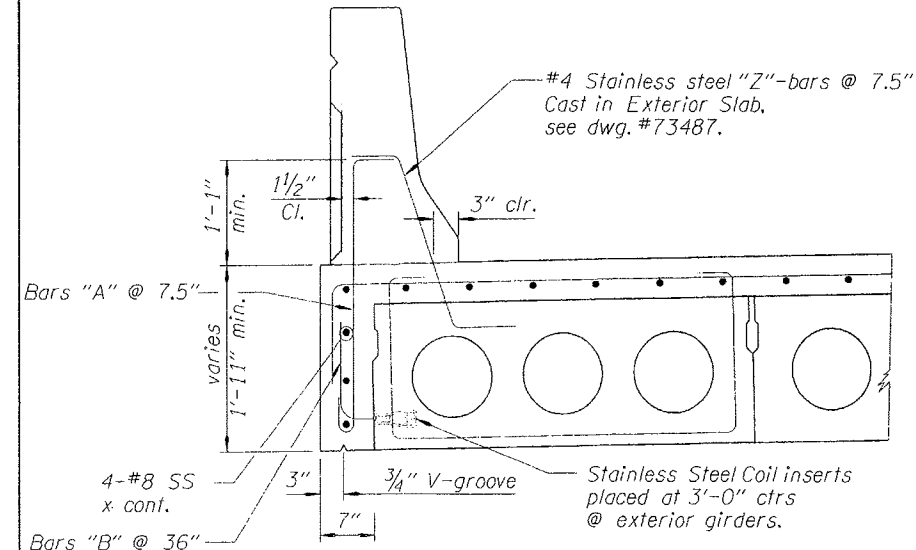
* Verify Location
w/ sheets GJ-1 to GJ-11



WEST EXTERIOR DECK @ CAP
No Scale



WEST - EXTERIOR DECK SECTION
Scale: 1" = 1'-0"



EAST - EXTERIOR DECK SECTION
Scale: 1" = 1'-0"

LOCHNER
CONSULTING ENGINEERS AND PLANNERS
2001 Front St. NE, Suite 120
Salem, Oregon 97303
(503) 586-0100 - Phone
(503) 589-9538 - FAX

DATE	REVISION	BY
		DRAFTER: <i>Sergie Chernishoff</i> Sergie Chernishoff
		CHECKER: <i>Dan Minturn</i> Dan Minturn
		DESIGNER: <i>B. Koru / T. Polisuk</i> B. Koru / T. Polisuk

REVIEWER
Daniel J. McInerney
REGISTERED PROFESSIONAL ENGINEER
EXPIRES: 12/31/06

OREGON DEPARTMENT OF TRANSPORTATION
BRIDGE ENGINEERING

STRUCTURE NO. 20198
DATE 15-JUN-2006
CALC. BOOK 5341

US101: SPENCER CREEK BRIDGE SEC.
TYPICAL DECK SECTION

SHEET 26 OF 46
DRAWING NO. 73486

1/2" = 1'-0" - EDS